Factors controlling fracture characteristics in Chalk Formations in the Dutch Offshore:

Results from a study based on Seismic Attributes

R.M. Nederveen

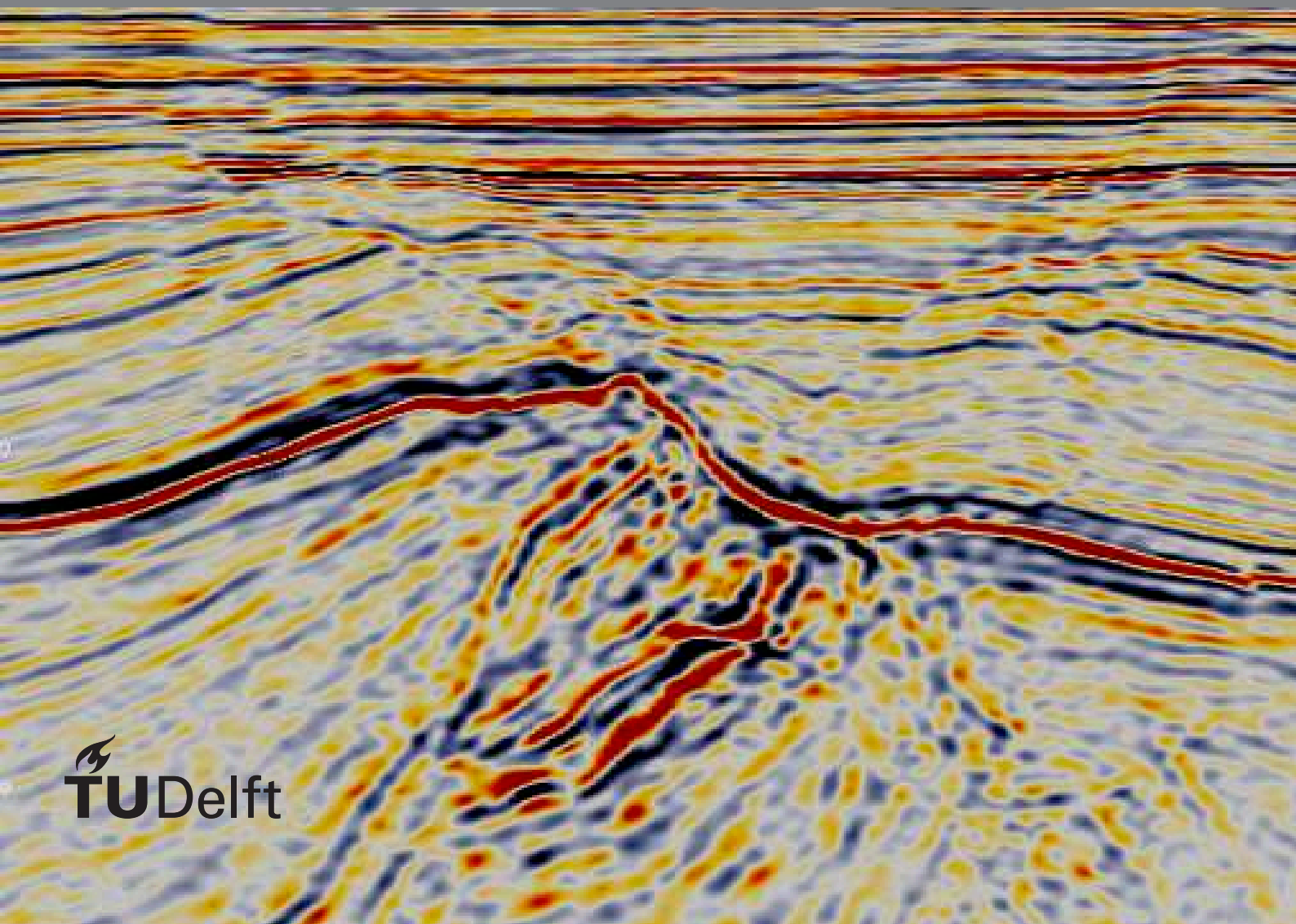

TU Delft

Factors controlling fracture characteristics in Chalk Formations in the Dutch Offshore:

Results from a study based on Seismic Attributes

by

R.M. Nederveen

to obtain the degree of Master of Science
at the Delft University of Technology,
to be defended publicly on Monday June 11, 2018 at 02:00 PM.

Student number:	4177002	
Project duration:	March 31, 2017 – June 11, 2018	
Thesis committee:	Prof. Dr. G. Bertotti,	TU Delft, Supervisor
	Dr. A. Barnhoorn,	TU Delft
	Drs. J.C. Blom,	TU Delft

An electronic version of this thesis is available at http://repository.tudelft.nl/.

TU Delft

Abstract

Faults can both improve producibility and fluid flow in hydrocarbon reservoirs, and cause leakage and instabilities in sealing layers. For this reason it is of importance to create a multiscale understanding of the drivers behind deformation, and how deformation is accommodated. Carbonates have always been of interest to the oil and gas industry as carbonates house some of the world's largest oil and gas reserves. Understanding, and maybe predicting the geometries and fracture types could therefore be of integral importance to the E&P industry. For that reason two seismic datasets were provided for analysis on both a Fault Network Scale (faults over >1km in length) and a Small Seismic Scale (faults <1km in length). For the Fault Network Scale Petrel was used for seismic interpretation of the faults, as only the largest faults were interpreted in both seismic datasets. For the Small Seismic Scale OpendTect was used for enhanced seismic interpretation. OpendTect's fracture enhancing attributes and filters provide seismic images with a high level of detail. These attributes were applied to 5 generated steering-cubes, to display even the smallest faults. The results on the Fault Network Scale show that most faults are caused by regional tectonics. However in areas where salt is underlying the chalks of the Chalk Group, halokinesis is the main driver of deformation. On the Small Seismic Scale drivers behind deformation differ more, fluid expulsion drives polygonal faulting patterns in areas where salt tectonics or far field extensional tectonics are absent. Towards halokinesis structures salt tectonics will be the main driver behind deformation. In areas where salt is absent, far field tectonics can still influence chalks forming fractures either parallel or perpendicular to the major surrounding faults.

Acknowledgements

First of all, I would like to thank my thesis supervisor Prof. Dr. Giovanni Bertotti for all his advice, guidance and patience. The door to Prof. Bertotti's office was always open whenever I had a question about my research. And he would always give me the freedom to decide where to go and how to get there, but would also steer me back on track when needed. This approach was of integral importance for me to get through the process of writing a thesis.

Thanks to Dr. Nico Hardebol for his help in the early stages of this thesis. Discussing the project with him provided me to get an early sense of direction regarding the thesis. He also was of importance in arranging the needed software packages, and providing me with the initial knowledge of OpendTect.

I would like to express gratitude to Dr. Auke Barnhoorn and Drs. Jan-Kees Blom for being part of my defence committee. Your knowledge and experience will be of invaluable importance during my thesis defence. Thank you for taking the time out of your schedules for this part of the thesis.

Sincere Gratitude to Total E&P UK/NL for providing one of the datasets and for sharing their knowledge. Without them this project would not be what it is today. Special thanks Bertrand Gauthier, Leon Barens, Arjen Confurius and Paul Segers for their geological know-how and for their motivation to increase the quality of this research.

Many thanks to Gerhard Diephuis who helped me setting up the seismic datasets without hesitation, despite living on the other side of the country. Gerhard is a passionate and inspiring man, and very skilled when it comes to Geophysics. This thesis would have been much harder without his help.

I would like to thank all my classmates, most of whom have scattered back all over the world, for their kind words of motivation and for their uninterested help when needed. You guys made the last three years fly by in the blink of an eye.

I would like to thank my parents and my sister for their unconditional support. And lastly I would like to express my sincerest gratitude to Sophie van Doeveren. She was the only motivation I needed to get through the hard times.

Ruud Nederveen
Delft, June 2018

Contents

List of Figures

List of Tables

1

Introduction

Carbonates have always been of interest in the oil and gas Exploration and Production (E&P) Industry. Not only do carbonates show enormous potential as hydrocarbon reservoirs by harbouring some of the world's largest oil and gas reserves, but carbonates also have the ability to function as a seal in the case of tight chalks. Fractures and faults could for this reason be seen as a double bladed sword when it comes to chalks. Fractures and faults can improve both producibility and fluid flow in reservoirs, however fracturing can also cause leakage and instabilities in sealing layers. Fracturing occurs all over the world, both naturally and induced. However when fracturing occurs unexpectedly, and in places where they should not occur things can become problematic.

An example of such 'mechanical problems' is the leakage at [redacted] on [redacted]th, [redacted] According to reports of [redacted], gas from the low permeability/high pressure [redacted] interval, overlying the primary reservoir in the Jurassic [redacted] Formation, entered the annulus of the [redacted] well when fracturing occurred due to a change in the geomechanical regime. The fractures caused the gas to escape into the atmosphere, which resulted in the full evacuation from the [redacted] production platform and the adjacent drilling rig. Thorough investigations showed that the permeability of the [redacted] Formation increased due to fracturing, caused by production related compaction of the underlying sandstones of the [redacted] Formation. This underlines the importance of understanding fracturing in chalks, and the driving mechanisms behind it.

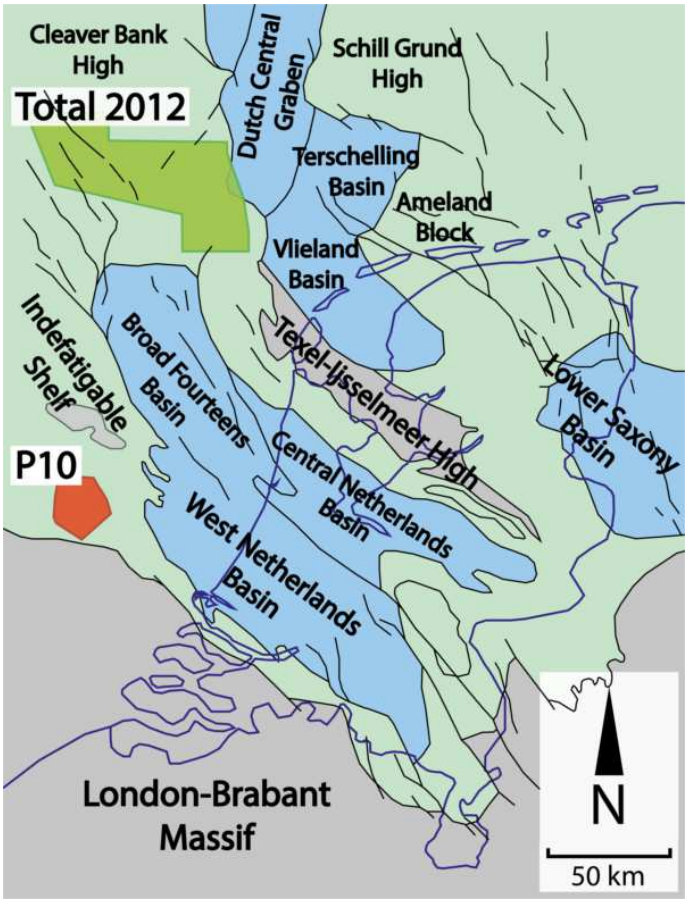

Figure 1.1: *A Map displaying all the different geological structures in the Dutch on- and offshore. The Late Jurassic to Early Cretaceous rift-basins in the Dutch onshore and offshore in blue, structural highs in grey, and platforms in light-green. Also displayed are the seismic surveys used in this research: in green the area of the Total 2012 seismic survey, and in red the area of the P10 seismic survey. Modified after de Jager, 2003.*

Faults and fractures form due to the exertion of stress on brittle layers such as chalks. Different mechanisms can be the driving force behind the exertion of these stresses such as tectonics, salt-tectonics, water escape or differential loading. These stresses can work on different scales. Faults can be kilometers long, and have throws of hundreds of meters or can be only centimeters long with throws of only millimeters. This forms the basis for this multiscale project: what are the origins and types of stress exerted, and how does that result in the present fracture geometries? To research this subject, thorough understanding of the behaviour of chalks on these scales is needed. This will be achieved by looking at two different seismic datasets in the Dutch offshore. One shot over the Cleaver Bank High, and the other shot over the Indefatigable Shelf (figure 1.1). By using new fracture enhancing attributes on these seismic datasets new insights have been gained into fractures. By using conventional seismic interpretation in Petrel, insights are gained on fracture patterns on a seismic scale by doing Fault Network Analysis. Fault Enhancing Attributes are then used to enhance the fractures of the seismic datasets to then create a better understanding of the mechanisms behind faulting on the reservoir scale just above the seismic resolution.

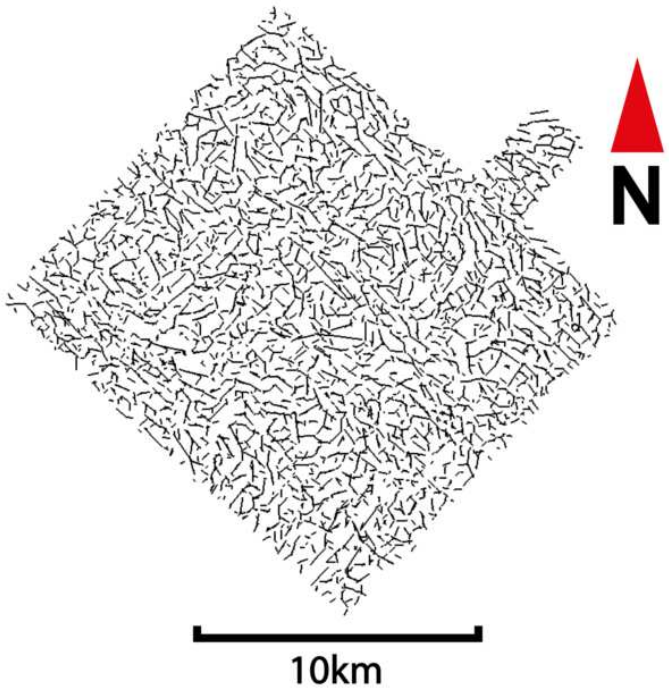

Figure 1.2: *A fracture map of the [redacted] area. Observable is the polygonal fracture pattern which was interpreted by [redacted] at the top of the Chalk Group, which is located at a depth of [redacted]m.*

According to [redacted] the fracturing at [redacted] has been related to a particular set of faults called: polygonal faulting. Figure 1.2 shows the fracture pattern present in the chalks at [redacted] which can be defined as a polygonal fault system (PFS). Polygonal faulting still is a relatively new subject, and over the last 20 years polygonal faulting has been observed in more, and more places. Currently PFS have been identified in more than 50 sedimentary basins worldwide (Cartwright, 2011). PFS consist of normal faults, normally with throws between 10-100m and fault trace lengths between 100-1000m, that are organized in a characteristic polygonal pattern without a regionally consistent preferred strike orientation (Cartwright et al., 2003)(Lonergan et al., 1998a). Polygonal faults are generally planar or gently listric, with dips between 30° and 70° (Goulty, 2008). However research done by Welch et al. (2015) and Hibsch et al. (2003) also shows that polygonal faulting occurs on a reservoir scale in outcrops of the UK and France. Polygonal Fault Systems are found exclusively in fine-grained sedimentary units, ranging from claystones (Cartwright and Lonergan, 1996)(Lonergan et al., 1998a)(Lonergan et al., 1998b) to chalks (Cartwright, 2011)(Hibsch et al., 2003), where there are negligible effects of tectonic extension or compression (Goulty, 2008).

Fault extraction and enhanced fault interpretation are relatively new topics, in which the most specialized tools are being used. One of the best known software packages for fault interpretation is Schlumberger's own seismic interpretation tool Petrel. But nowadays new, often free and open-source, softwares are being created, often with new interesting capabilities. One of these new softwares is OpendTect. OpendTect was created by dGB Earth Sciences as an open-source alternative to other seismic interpretation software packages. Due to OpendTect's open-source nature the software is constantly updated and equipped with new tools.

One of the most useful ones are the dip-steering capabilities and fault enhancing attributes. Nowadays these software packages are being used more often, and also in research people have been seeing their use to gain new insights in subsurface faults (Qayyum et al., 2010)(van Gent et al., 2010) (Brouwer and Huck, 2011)(Oppermann, 2012a)(Oppermann, 2012b)(Alai et al., 2014)(Zhang et al., 2014)(Jaglan et al., 2015). In this research a workflow proposed by Jaglan et al. (2015) will be followed.

To try and obtain the answers to the questions we ask ourselves in this research, multiple areas have been looked at with different parameters that could be of influence to the origination of the fracture patterns. As mentioned earlier, two different seismic datasets are used in this research. Both of the datasets were taken on platforms that have not been subject to tectonic inversion during the compressional phases of the Alpine Orogeny (figure 1.1). For the enhanced fracture interpretation in OpendTect, these two datasets were than used to produce five steering-cubes. These 'zoomed in' sections or 'seismic (out)crops', functioned as experiments to test variations in the different parameters mentioned above. Parameters such as thickness of the Chalk Group, the influence of salt-tectonics and the influence of nearby major faulting were looked at to try and make a predictive model of fracturing of chalks in the Dutch subsurface.

2

Geological Setting

This project focuses primarily on chalks found in the Dutch offshore. Throughout the Dutch offshore there is one interval containing mainly chalks: The Cretaceous Chalk Group. The Chalk Group is a succession often hundreds of meters in thickness, with ages ranging from the Cenomanian (100.5Ma - 93.9Ma), and locally even the Albian (113Ma - 100.5Ma), to the Maastrichtian (72.1Ma - 66Ma) (NAM, 1980)(van Adrichem Boogaert, 1993)(van Adrichem Boogaert and Kouwe, 1997). Even though the Chalk Group is primarily composed of white to light-grey, fine-grained chalky limestones, it also contains other lithologies such as marls, calcareous claystones and glauconitic sands (NAM, 1980)(van Adrichem Boogaert, 1993)(van Adrichem Boogaert and Kouwe, 1997).

The Chalk Group is present in large parts of the Dutch offshore. However the Chalk Group is often not present in the Late Jurassic basins in both the Dutch offshore and onshore such as the Broad Fourteens Basin (BFB), the West Netherlands Basin (WNB), the Roer Valley Graben (RVG), the Dutch Central Graben (DCG) and the Step Graben (SG). The absence of

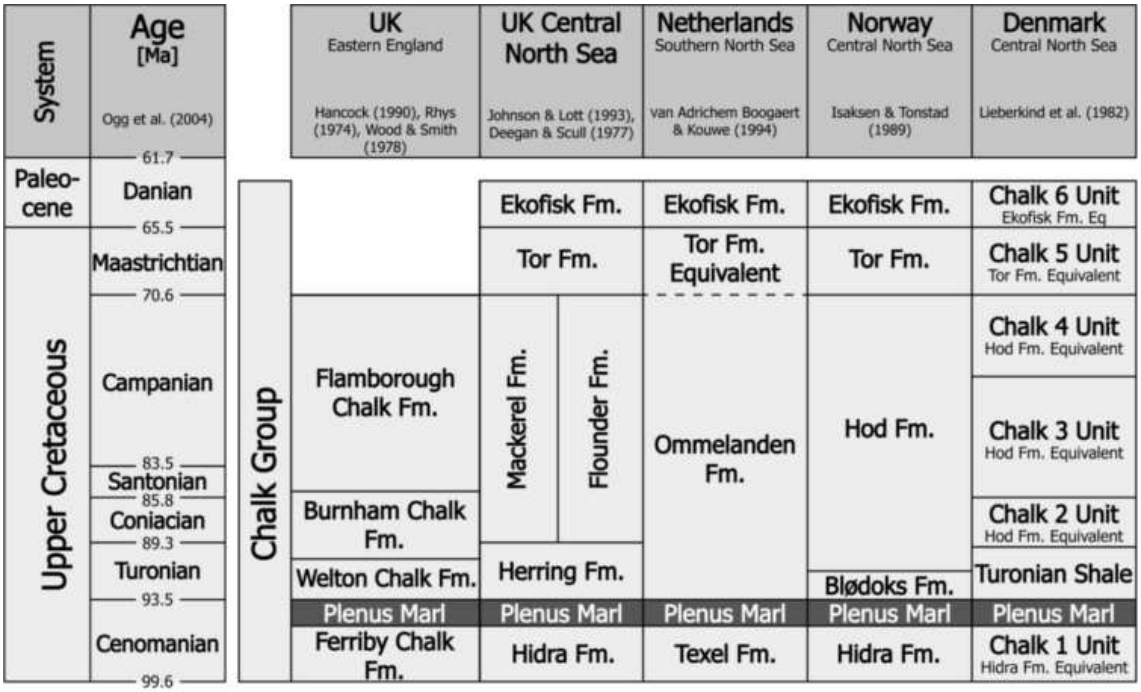

Figure 2.1: *The lithostratigraphy of the Chalk Group in the British, Dutch, Norwegian and Danish sectors of the North Sea. Modified after Mortimore et al. (2001) and van der Molen and Wong (2007).*

Cretaceous chalks in these basins is due to the tectonic inversion that took place during the Alpine Orogeny, during which these basins got uplifted, after which large portions of the Chalk Group got eroded. The carbonates of the Chalk Group were deposited widespread over the entire North Sea. Not only is the Chalk Group present in the Dutch off- and onshore, but also in other adjoining areas in the North Sea. Figure 2.1 explains how the Chalk Group is present and how the different formations are connected throughout the North Sea area. The different formations are often known by other formational names in different regions.

2.1. Geological History

The geological history of the research area - the Dutch offshore - starts in the Ordovician, ca. 450Ma, during the Caledonian Orogeny, during which the Laurentia and Baltica cratons converged and formed the Caledonian Fold Belt (figure 2.3A)(Wong et al., 2007). Around the same time the Gondwanaland-derived micro-continent of Avalonia, which includes the London-Brabant Massif, collided with the Baltica craton to form the North German-Polish Caledonides (Pharaoh et al., 1995). At this time the area of the Netherlands was located along the North German-Polish Caledonides, slightly East of the triple junction between the WNW-ESE running North German-Polish Caledonides and the NE-SW running Caledonian Fold Belt (Figure 2.3B) (Wong et al., 2007). Wong et al. (2007) states that accordingly 'two separate provinces may represent the basement of the Netherlands, namely the Gondwana-derived Avalonia, including the London-Brabant Massif, in the South, and the Caledonian Basement in the North. Even though the precise location of the suture between these provinces remains speculative, the general NW-SE trend, that is such a dominant structural feature in the southern half of the Dutch subsurface, may be related to this suture.' This implies that the regional NW-SE trend, which is often observed in the subsurface of the Dutch offshore, finds its roots in the Mid Paleozoic.

The Late Paleozoic marks the start of the convergence between Gondwanaland and Laurussia (Wong et al., 2007). The convergence between the two paleocontinents resulted in the forming of the Variscan Orogeny in the Early Carboniferous (Figure 2.3D) (Wong et al., 2007). In the Carboniferous, Gondwanaland continued to move in a northward direction, which pushed the front of the Variscan Fold Belt towards the area of the Netherlands (Wong et al., 2007). During this period, it is assumed that structural highs and fault zones, such as the Cleaver Bank High, Indefatigable Shelf and the Schill Grund High, formed shallow carbonate platforms (Figure 2.2) (Wong et al., 2007). These NW-SE trending platforms and basins (Figure 2.2) were likely bounded by faults, as was the case in the UK (Tubb et al.,

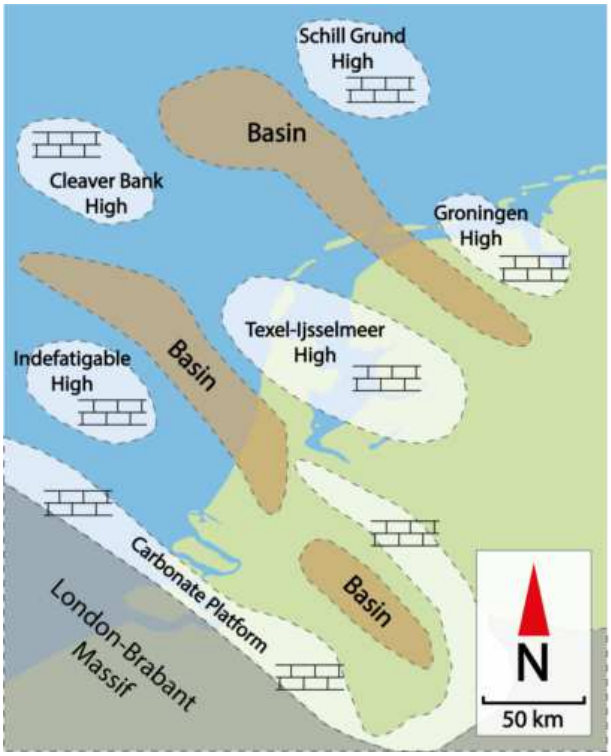

Figure 2.2: *Paleogeographic map of the research area in the Early Carboniferous showing presumed locations of carbonate platforms and intra-platform basins. Both the locations of the TEPNL dataset on the Cleaver Bank High and the P10 dataset on the Indefatigable Shelf have been a relative high in this area since the Early Carboniferous. Modified after Wong et al. (2007)*

1986), as well as E-W trending faults slightly North of the London-Brabant Massif (Vandenberghe, 1984). Currently the Variscan Fold Belt runs approximately in E-W direction through Belgium, just South of the area of the Netherlands (Ziegler, 1990). The research area became affected by Late Variscan post-orogenic tectonism at the end of the Carboniferous during the Permo-Carboniferous tectonic-magmatic event (Wong et al., 2007). The regional NW-SE trend that had been established in the Mid Paleozoic was reactivated during this period due to wrench-faulting in response to intrusive and extrusive magmatism, and thermal uplift (Ziegler, 1990). Decay of the thermal anomaly related to the Permo-Carboniferous tectonic-magmatic event resulted in regional subsidence during the Early Permian, and the forming of the E-W trending Southern Permian basin (van Wees et al., 2000). Degradation of both the Variscan Orogeny and the London Brabant Massif to the South, and the Mid North Sea and Ringkøbing-Fyn Highs to the North, lead to the deposition of the Rotliegend clastics into the basin (Wong et al., 2007). According to Wong et al. (2007) minor thickness variations in the Upper Rotliegend Group were formed by local syn-depositional normal faults, which were the forerunners of a.o. the Dutch Central Graben and the Broad Fourteens Basin.

Continuous degradation of the Variscan Orogeny and other surrounding highs decreased sedimentation rates, which resulted in the flooding of the Southern Permian Basin with saline water (Wong et al., 2007). Cyclic evaporation of the saline water deposited the salts of the Zechstein Sequence North of an imaginary E-W trending line slightly North of the Central Netherlands Basin, and through the center of the Broad Fourteens Basin (de Jager, 2003). The thickness of the deposited salt increased to the North to about 1500m in the axial zone of the Southern Permian Basin (Ziegler, 1988, 1990). In areas where the Zechstein salts were present the salt acted as a detachment level during multiple phases of tectonic deformation during the Mesozoic and the Cenozoic (de Jager, 2003). This detachment resulted in notable differences in structural style in the post-Permian sediments in areas where the Zechstein salts were present, and in areas where these salts were absent (de Jager, 2003). The Triassic marks the start of a new extensional phase and the break-up of the super-continent of Pangea. Rifting commenced in the North Atlantic between the present areas of Greenland and Scandinavia, and propagated southwards until it reached the area of the Southern North Sea in the Middle Triassic (Figure 2.3F) (Wong et al., 2007). Continued extension resulted in both the continental break-up of Pangea and the opening of the Central Atlantic Ocean in the Middle Jurassic (Figure 2.3G,H) (Wong et al., 2007). Rifting continued until the Early Cretaceous, when crustal separation was achieved in the North Atlantic Ocean (Wong et al., 2007)(Ziegler, 1988)(Ziegler, 1990). Around the same time rifting came to a halt in the Netherlands' area, whereas rifting continued more towards the North in the present areas of Greenland and Scandinavia, (Ziegler, 1988)(Ziegler, 1990), and in the Mediterranean until the Tethys Ocean was formed (Wong et al., 2007).

From the start of the Triassic until the Early Cretaceous the area of the Netherlands continuously moved northwards, from the arid climate zone to the sub-tropical latitudes of the northern hemisphere (Wong et al., 2007). During the Triassic and the Jurassic sedimentation took place under continuous thermal subsidence, interrupted locally only because of salt movement (Wong et al., 2007). During this period, there were small phases during which extensional faulting continued, in for example the Dutch Central Graben and the Broad Fourteens Basin, but generally accommodation space was created due to thermal subsidence (Wong et al., 2007). During the Middle Jurassic rifting accelerated again due to crustal separation in areas surrounding the Central Atlantic and Tethys Oceans (Wong et al., 2007). The North-South trend this East-West rifting phase entailed, terminated against the prominent NW-SE structural trend that had been formed already in the Mid Paleozoic (Wong et al., 2007). This caused NW-SE transtensional development of most of the basins in the Dutch on- and offshore areas such as the BFB, WNB, CNB and the RVG (Wong et al., 2007). This means that most of the basins and geological structures in the Dutch subsurface were formed during the Late Kimmerian rifting phase, from the Late Jurassic until the Early Cretaceous (Wong et al., 2007). Tectonic activity subsided in the area of the Netherlands in the

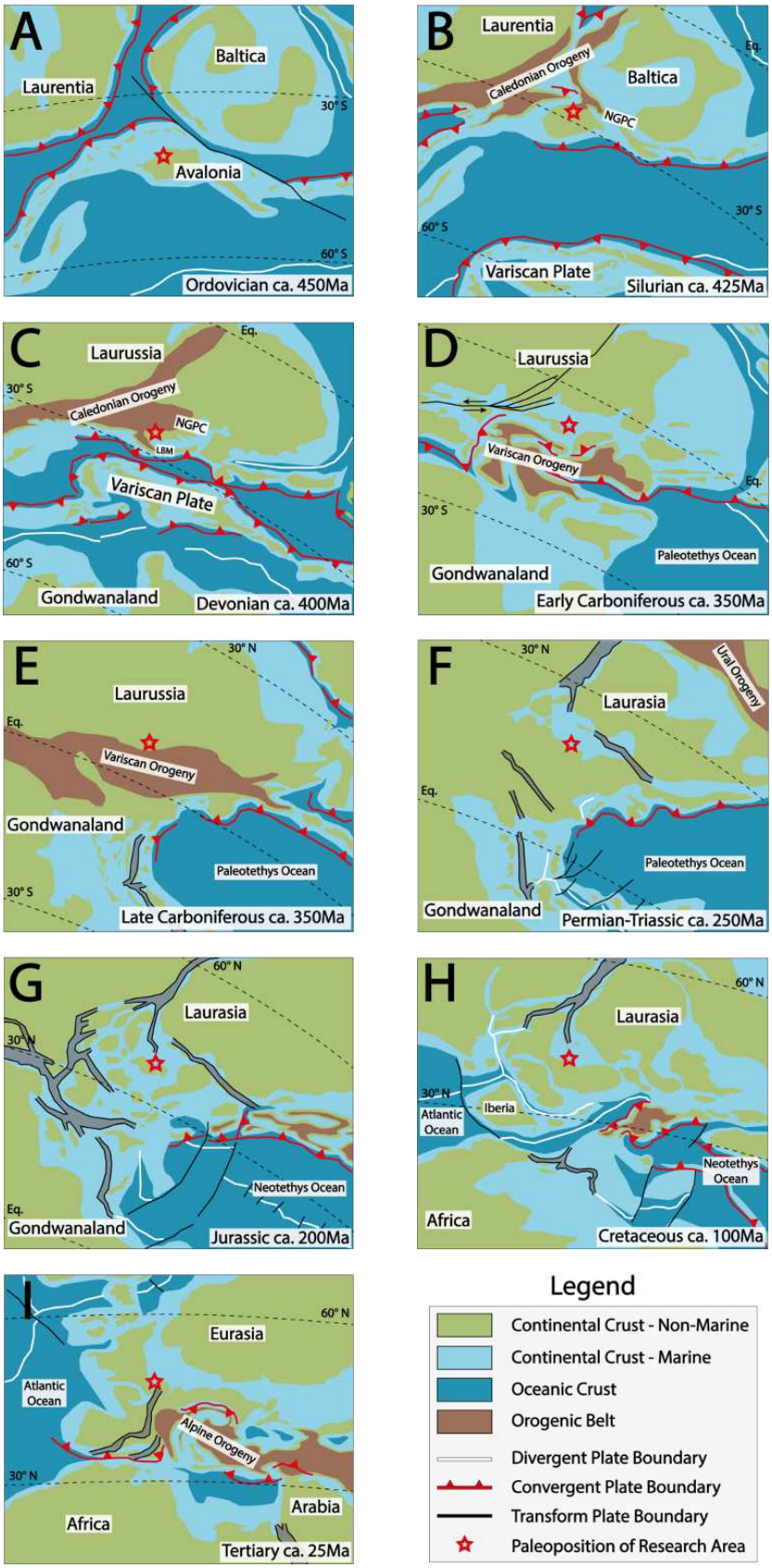

Figure 2.3: *Regional paleogeography maps of the research area from A. the Ordovician, B. the Silurian, C. the Devonian, D. Early Carboniferous, E. Late Carboniferous, F. the Permo-Triassic, G. the Jurassic, H. the Cretaceous to I. the Tertiary.*

Mid Cretaceous, which marked the end of the Late Kimmerian rifting phase (Ziegler, 1988)(Ziegler, 1990). Thermal subsidence and rising sea levels took over in the Late Cretaceous until the area of the Netherlands was completely covered by a shallow sea (Wong et al., 2007). This in combination with the sub-tropical latitudes the area of the Netherlands was in at this time formed an enormous carbonate factory which filled the shallow sea with chalks up to 2000m in thickness (Wong et al., 2007). Towards the end of the Late Cretaceous, the African-Arabian continent started to converge with Eurasia, until the Tethys Ocean closed and the Alpine Orogenic System was created (Figure 2.3I) (Wong et al., 2007). Increasing stresses exerted by the Alpine Orogeny caused the inversion of the Late Jurassic and Early Cretaceous extensional basins in the area of the Netherlands (Wong et al., 2007). Uplift caused by the tectonic inversion resulted in thinning and erosion of Upper Cretaceous and Lower Tertiary sediments in the Late Jurassic extensional basins (Wong et al., 2007). Tectonic inversion of the Late Jurassic and Early Cretaceous basins continued up until the Oligocene, after which subsidence increased and eventually the North Sea was formed (Wong et al., 2007).

2.2. The Chalk Group

The project focuses on the Cretaceous carbonates of the Chalk Group. In the Dutch Offshore area the Chalk Group can be subdivided in three formations:

- Ekofisk Formation
- Ommelanden Formation
- Texel Formation

2.2.1. Texel Formation

The Texel Formation is the oldest formation of the Chalk Group. It can be subdivided in three members: the Texel Greensand Member, the Texel Marlstone Member and the Plenus Marl Member.

Deposited during the Cenomanian Age (100.5Ma - 93.9Ma), the Texel Greensand Member is the oldest member of the Chalk Group. The Member generally is around 20m thick, and consists of greenish, glauconitic, calcareous sandstones with intercalated marls (NAM, 1980)(van Adrichem Boogaert, 1993)(van Adrichem Boogaert and Kouwe, 1997). Glauconitic greensands are typically formed in inner- to outer-neritic marine settings and can generally only be found in transgressive sand units. In the places where the Texel Greensand Member is present it conformably underlies the Texel Marlstone Member, and conformably overlies the Rijnland Group (NAM, 1980)(van Adrichem Boogaert, 1993)(van Adrichem Boogaert and Kouwe, 1997).The Texel Marlstone Member consists of white to light grey, locally pinkish, limestones and marly chalks. The member generally is around 20m - 100m in thickness, which is above seismic resolution, and is interpreted as sediments deposited in deep marine conditions during the Cenomanian Age (100.5Ma - 93.9Ma) (NAM, 1980)(van Adrichem Boogaert, 1993)(van Adrichem Boogaert and Kouwe, 1997). Generally the Texel Marlstone Member is conformably overlain by the Plenus Marl Member of the Texel Formation, however where the Plenus Marl Member is absent it is unconformably overlain by the Chalks of the Ommelanden Formation. In the places where the Texel Marlstone Member is overlain by the Ommelanden Formation the boundary between the two chalk formations can be hard to find, although the Texel Marlstone Member usually has a more irregular wire-line log pattern than the overlying Ommelanden Formation (NAM, 1980)(van Adrichem Boogaert, 1993)(van Adrichem Boogaert and Kouwe, 1997). The Plenus Marl Member consists of dark-grey to black, calcareous, laminated claystones, with a thickness often only up to a couple of meters (below seismic resolution). The Plenus Marl Member is very laterally distributed in both the Dutch on- and offshore and for this reason the Plenus Marl Member is often used as a marker-bed. The Plenus Marl

Member is interpreted as sediments deposited during an oceanic anoxic event which occurred due to a worldwide relative sea-level highstand combined with the rise of an oxygen minimum zone (NAM, 1980)(van Adrichem Boogaert, 1993)(van Adrichem Boogaert and Kouwe, 1997). The boundary with the overlying Ommelanden Formation can be clearly distinguished due to the high clay content present in the Plenus Marl Member, which causes much higher values in the Gamma Ray and acoustic wire-line logs (NAM, 1980)(van Adrichem Boogaert, 1993)(van Adrichem Boogaert and Kouwe, 1997).

2.2.2. Ommelanden Formation

The Ommelanden Formation generally is the most prominent and abundant Chalk Formation in the Dutch on- and offshore. The formation was deposited continuously from the Turonian (93.9Ma - 89.8Ma) to the Maastrichtian (72.1Ma - 66.0Ma) and consists of a succession of white, yellowish to light-grey, fine grained limestones, that are built up mostly of pelagic and biogenic remains. These pelagic and biogenic remains likely settled out of suspension, which means that the formation was likely deposited under relatively stable, low-energy conditions in carbonate shelf and upper bathyal conditions (NAM, 1980)(van Adrichem Boogaert, 1993)(van Adrichem Boogaert and Kouwe, 1997). The Ommelanden Formation consists primarily of thick layers of hard, dense limestones due to compaction and cementation over time, however towards the top of the formations the limestones tend to be softer and more chalky. Outside of the inverted Late Jurassic and Early Cretaceous basins thickness of the Ommelanden Formation may exceed 1500m, whereas within the boundaries of these basins the Ommelanden Formation can be only tens of meters thick or can be completely eroded. (NAM, 1980)(van Adrichem Boogaert, 1993)(van Adrichem Boogaert and Kouwe, 1997). Throughout the Dutch on- and offshore the Ommelanden Formation is generally unconformably overlain by tertiary sands and clays from the Lower and Middle North Sea Groups. This transition from Cretaceous chalks to Tertiary clastic sediments can often be easily observed on wire-line logs. In areas where the Ommelanden Formation is overlain by the Ekofisk Formation, this transition can be harder to observe, however the Gamma Ray logs of the Ekofisk Formation tend to show a slightly lower response and smoother pattern than the Chalks of the Ommelanden Formation (NAM, 1980)(van Adrichem Boogaert, 1993)(van Adrichem Boogaert and Kouwe, 1997).

2.2.3. Ekofisk Formation

The Ekofisk Formation consists of white, chalky limestones which generally have a higher porosity than the Ommelanden Formation, often increasing its potential as a hydrocarbon reservoir. The Ekofisk Formation was deposited in the Danian age (66.0Ma - 61.6Ma), and has a thickness ranging from 20m, barely above seismic resolution, up to 100m, depending on the location. The Ekofisk Formation often contains chert nodules and bedded chert layers, as well as clay laminae (NAM, 1980)(van Adrichem Boogaert, 1993)(van Adrichem Boogaert and Kouwe, 1997). In the Dutch on- and offshore the Ekofisk Formation is only limitedly present. The formation only occurs locally in the northern and southern areas of the North Sea and the Dutch onshore due to it being deposited post Alpine inversion. The Ekofisk Formation was deposited in a similar way as the Ommelanden Formation, which means that it consists generally of pelagic remains, and was deposited under stable, low-energy conditions in carbonate shelf and upper bathyal conditions (NAM, 1980)(van Adrichem Boogaert, 1993)(van Adrichem Boogaert and Kouwe, 1997). In the northern sector of the Dutch offshore where the formation might have been deposited in deeper water, redeposition by gravitational mass flows occurred, which is backed up by typical brecciated microstructures present in these chalks(NAM, 1980)(van Adrichem Boogaert, 1993)(van Adrichem Boogaert and Kouwe, 1997). The Ekofisk Formation is overlain by the sands and clays of the Tertiary Lower and Middle North Sea Groups. The transition between the two formations is clearly visible on wire-line logs, where the sands and clays show a higher Gamma Ray response than the Ekofisk chalks (NAM, 1980)(van Adrichem Boogaert, 1993)(van Adrichem Boogaert and Kouwe, 1997).

3

Data

3.1. Seismic Data

For this project two different seismic datasets have been made available. One has been made kindly available by Total E&P NL, whereas the other dataset has been provided by TNO's Dinoloket. These datasets have been chosen for their specific location, and the characteristics of the chalks in the respective areas. Logs for well correlation were obtained through TNO's Dinoloket, as well as the needed coordinates and deviation profiles to place the wells as accurately as possible. Checkshot and velocity data was also obtained to support the well-to-seismic matching, and the building of a velocity model.

3.1.1. TEPNL 2012 Data

This PSDM seismic survey was shot in 2012, and was provided by TEPNL. It is located in the North Sea, approximately 100km Northeast of the Island of Texel, NL. The block is about 105km across in an E-W direction, and about 65km across in a N-S direction. Table 3.1 displays other details of this dataset.

This survey was chosen for this project for its location on the Cleaver Bank High (CBH). The CBH has not been subject to as much tectonic inversion as other surrounding basins such as the WNB or the BFB. Due to the absence of major tectonic inversion, the Chalk Group is still largely present in the subsurface in this area. Figure 3.1 shows an example of a well in this area. As can be observed the Chalk Group generally has a thickness of more than 1500m in the TEPNL 2012 survey. Also the chalks are generally buried at a depth of more than 1000m. Figure 3.1 also shows that in this area all three formations of the Chalk Group are present in this area: Ekofisk, Ommelanden and Texel Formations.

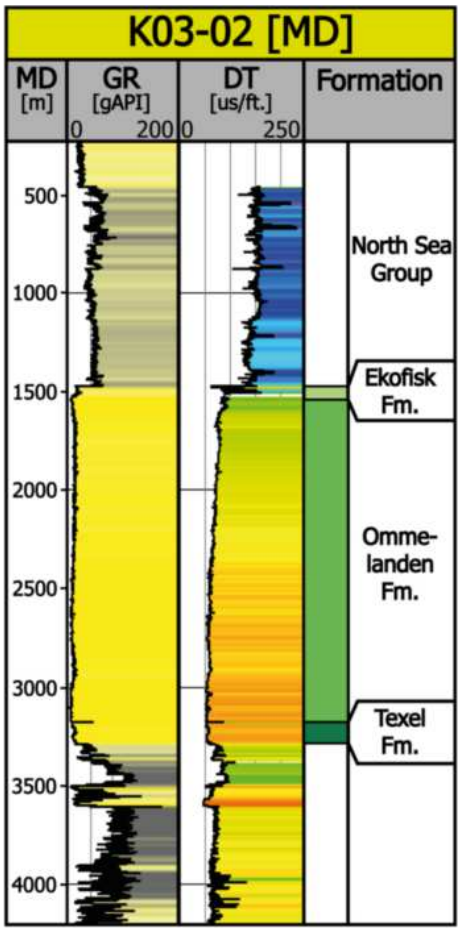

Figure 3.1: *An example of a well in the TEPNL 2012 dataset. Note the thickness of the Chalk Group in this area, which is around 1700m, and the presence of all 3 formations of the Chalk Group: Ekofisk, Ommelanden and Texel Formations.*

3.1.2. P10 Data

The P10 Block was shot in 1999, and has been provided by TNO. The PSTM survey was shot in the North Sea, approximately 100km West of Amsterdam, NL. The block is approximately 25km across in an E-W direction, and about 30km in a N-S direction. Other details regarding the P10 seismic survey can be found in Table 3.1.

The P10 block was chosen for this project for its location on the Indefatigable Shelf (IS). Like the CBH, the IS has not been subject to as much tectonic inversion as other surrounding Late Jurassic basins such as the WNB, or the BFB. Due to the lack of inversion tectonics, the Chalk Group has not been eroded, and is still largely present in the subsurface. Figure 3.2 shows an example of a well in this area. As can be observed the thickness of the Chalk Group is smaller when compared to the Chalk Group in the TEPNL 2012 survey. The Chalk Group is generally around 350m thick in this area, and is commonly buried at a depth of around 750m. Figure 3.2 also shows that in this area all three formations of the Chalk Group are present in this area.

The sediments in this area are not underlain by layers of salt as is the case in the TEPNL 2012 survey. However here the sediments are underlain by a heavily faulted basement of Permian clay- and sandstones.

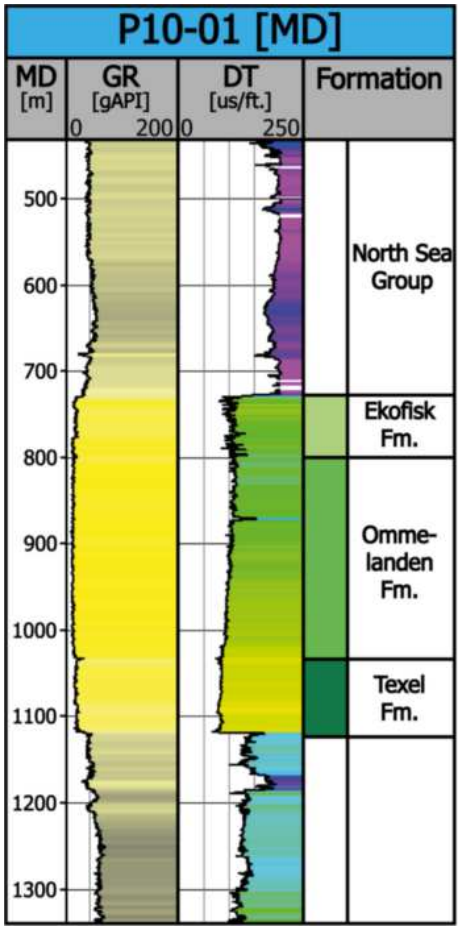

Figure 3.2: *An example of a well in the P10 dataset. Note the thickness of the Chalk Group in this area, which is around 400m, and the presence of all 3 formations of the Chalk Group: Ekofisk, Ommelanden and Texel Formations.*

3.2. Well Data

Multiple wells and their respective logs were used to determine the positions of the different formations of the Chalk Group in the seismic surveys, as well as to create a velocity model. These wells were chosen on the completeness of the logs (as the logs should cover the Chalk Group), the presence of formation well tops, and the presence of checkshots and velocity data. Checkshot and velocity data was sometimes taken from well or drilling reports, for wells that did not have checkshot data. For the TEPNL 2012 dataset a total of 43 wells were used, and for the P10 dataset a number of 8 wells were used, see figure 3.3 for an overview of the well positions. Appendix A shows a table containing all the wells used, and the different logs present in the dataset.

	TEPNL 2012 Data	P10 Block Data
X - Coordinates	354928.75 - 460166.25	499336.30 - 530226.30
Inline Length [m]	105225.00	25625.70
Y - Coordinates	5924351.75 - 5988989.25	5788757.80 - 5822441.35
Crossline Length [m]	64625.00	28016.35
Time [ms]	0 - 3800	0 - 5500
Nr. of Inlines	5171	2251
Nr. of Crosslines	8419	2051
In-/Crossline Spacing [m]	12.50	12.50
Inline Range	5657 - 10827	1950 - 4200
Crossline Range	2553 - 10971	1350 - 3400

Table 3.1: *Details of both the TEPNL 2012 and the P10 seismic surveys.*

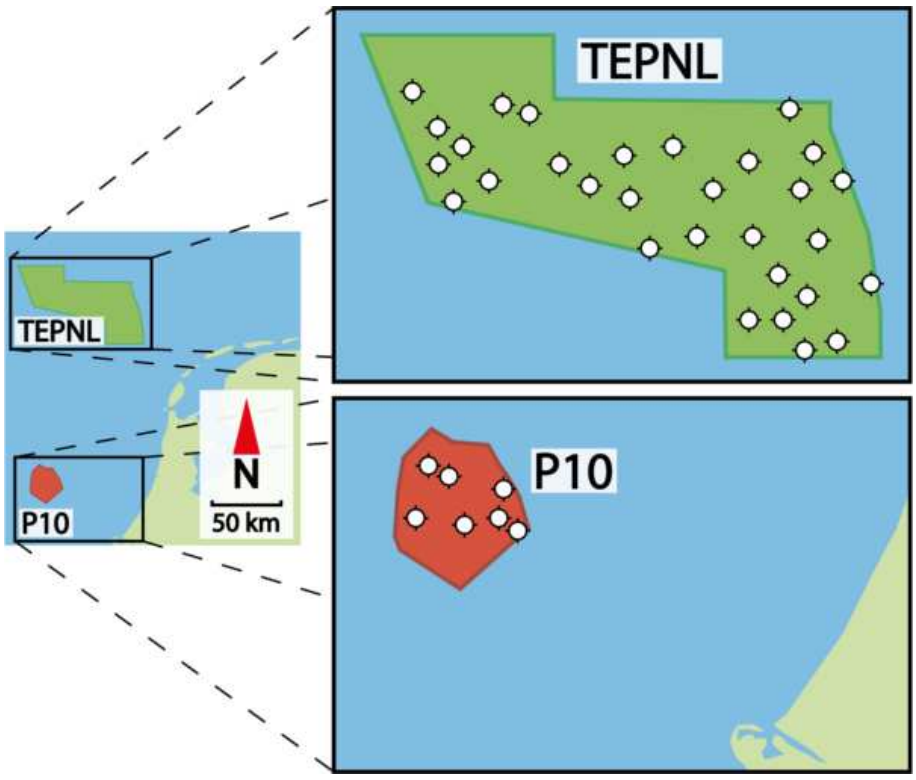

Figure 3.3: *A map showing all wells of both the TEPNL and the P10 datasets (on the exception of some wells deviating from the same platform, for that reason in the TEPNL map only 30 wells are shown, and in the P10 map only 7 wells are shown).*

4

Methods

For this research we would like to create a complete understanding of fractures in chalks, what their trigger mechanisms are and how this creates the patterns we see in the present subsurface. For large fault networks conventional seismic interpretation can already be a helpful tool, as these fault generally have throws exceeding seismic resolution (20-30m). However for faults with throws approaching seismic resolution regular seismic interpretation will not be sufficient, and other methods have to be used to visualize these faults. For that reason this research can be divided into two sections: (Large-scaled) Fault Network Analysis, and Analysis on the Small Seismic Scale.

4.1. Fault Network Analysis

For both datasets the Fault Network Analysis has a similar workflow. The first step is to determine at what positions the different Chalk horizons can be found in the seismic survey. This was achieved by plotting wells and their respective logs in Petrel. All wells contain formation well tops, however these are in depth, like the TEPNL dataset, whereas the P10 seismic dataset is in time. For this reason well-to-seismic matching had to be carried out for the P10 dataset. Well-to-seismic matching consists of two steps: Sonic Calibration and Synthetic Generation.

The Sonic Calibration process creates a Time-Depth Relationship (TDR) with the use of checkshots. Synthetics are generated from sonic and density logs from which the acoustic impedance is calculated. Acoustic impedance can then be used to calculate the primary reflectivity, by convolving it with a seismic wavelet to enable comparison with the seismic data. The seismic wavelet used in this research is the Butterworth Wavelet. After calculation of the synthetics of a certain well, this can be then be compared to the seismic data in the near region of this well. The synthetic seismogram and the seismic data will rarely be a perfect match, however usually a match can be made. Some wells used did not have complete sections of density logs. As these logs are often used to find hydrocarbons, the logs are usually only taken over sections of interest. The creation of synthetic seismograms needs both Density and Velocity logs, and for that reason incomplete density logs where filled with values that approximate the lithology to create synthetics. As we are focused on the chalks, the value used to extend the density logs was 2600 kg/m^3.

Once TDR's have been determined and wells have been matched to the seismic data, interpretation of the seismic data can commence. The TEPNL dataset was made available with Top and Bottom Chalk Horizons. For the P10 dataset these horizons had to be manually interpreted and generated. Once all horizons were interpreted and generated the faults could be interpreted. For this section of the thesis only large faults were interpreted that did not

need filters or attributes to be observable. These seismic scale fault networks were interpreted in both datasets in the Chalk Group interval.

The next step was to migrate the interpreted horizons and faults from the time domain, to the depth domain. This was done by creating a velocity model. This velocity model was based on a simple layer-cake model, where every stratigraphic unit has a specific, constant, interval velocity. In our case this interval velocity was taken from checkshot data which also contained velocity data. Input to create a velocity model consists of the generated horizons, and well markers. Once the velocity model was created, all horizons and faults were migrated to the depth domain, after which a fault model was created. Fault data was then extracted from the model, and used as input in an excel file to calculate parameters such as length and orientation.

4.2. Small Seismic Scale

As mentioned earlier, for the small seismic scale, seismic interpretation is not as straightforward as it is for the large seismic scale. As we approach smaller structures and smaller faults, differences between data and noise can get harder to observe. For that reason attributes and filters, present in most seismic interpretation softwares, were created. By applying such filters random noise gets filtered out, which makes it easier to spot discontinuities in the seismic data.

As we zoom into the seismic data for this section, the faults we observe become smaller. As the faults we observe get smaller, so does our Representative Elementary Volume, or, REV. The REV is the smallest volume over which a measurement can be made that will return a value representative of the total volume (Hill, 1963). As the size of the background faults was not deemed larger than a few 100s of meters, our REV was specified at around 1.25km. For that, and for computability reasons, we decided to crop sections of the seismic datasets to zoom into the small scaled structures. From the TEPNL dataset 3 crops were taken, and from the P10 dataset 2 crops were taken (table 4.1).

Crop Nr.	Dataset	Inline Range	Crossline Range	(-)Z [ms]	Area [km^2]
1	TEPNL	8020 - 8120	9370 - 9470	638 - 3454	1.56
2	TEPNL	3520 - 3620	8770 - 8870	346 - 2102	1.56
3	TEPNL	8750 - 8950	7000 - 7250	246 - 3002	7.81
4	P10	2850 - 2950	3000 - 3100	446 - 1750	1.56
5	P10	1650 - 1750	2850 - 2950	298 - 1302	1.56

Table 4.1: *Details of the crops generated for enhanced fracture characterization for both the TEPNL and P10 datasets.*

4.2.1. OpendTect

OpendTect is the world's only open source seismic interpretation system, created by dGB Earth Sciences. The open source platform encourages third-party developers to create new plug-ins to enhance OpendTect's abilities for seismic interpretation and analysis. OpendTect is used more and more due to its useful fault enhancing attributes and filters such as the Similarity Attribute, Thinned Fault Likelihood Attribute and the Fault Enhancement Filter. For the process of enhancing the seismic data in the 5 seismic crops, the workflows proposed by Jaglan et al. (2015) and Brouwer and Huck (2011) were used (figure 4.1). This workflow can be roughly divided in three steps (Brouwer and Huck, 2011):

1. The conditioning of the seismic data through dip-steering and the application of filters.
2. The application of attributes, and the optimization of the input parameters of said attributes.
3. The post-processing application of enhancing filters, or additional application of attributes on generated images.

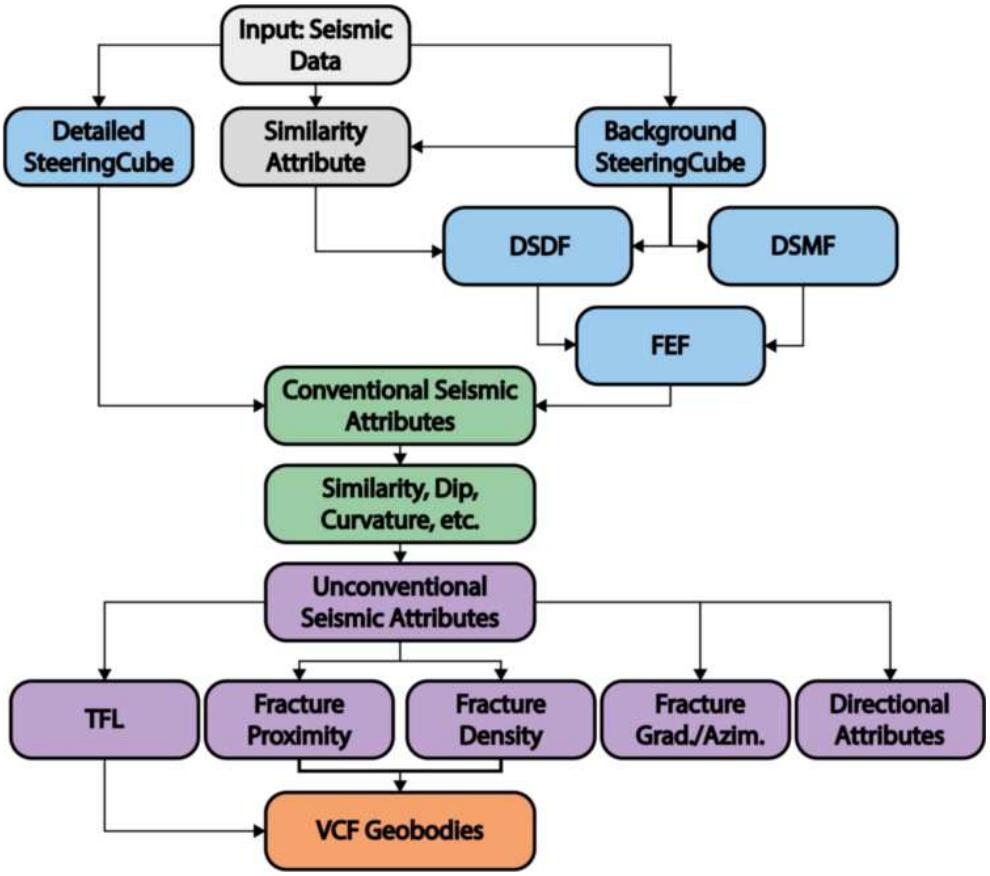

Figure 4.1: *The workflow proposed by Jaglan et al. (2015) in which different filters and attributes are used to create unconventional fracture attributes from seismic data for enhanced fracture interpretation.*

The first step in generating attributes and filters for enhanced fault interpretation in OpendTect is the generation of steering-cubes. A steering-cube is a seismic volume which contains the dip and azimuth of seismic events in inline and crossline directions at every sample point (Jaglan et al., 2015). A seismic volume can be dip-steered in two ways:

- Background Steering-cube
- Detailed Steering-cube

The difference between these cubes lies in the different algorithms used to calculate the volumes, and the amount of filtering used during the calculation. The Detailed steering-cube is either unfiltered, or slightly filtered, and thus

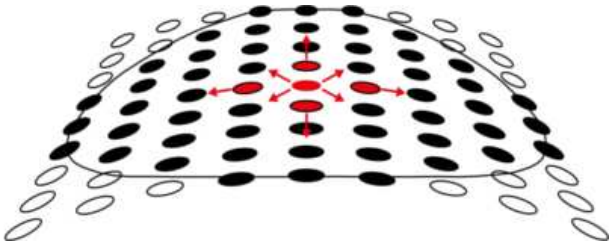

Figure 4.2: *An illustration displaying the dip-steering process in a schematical way. Starting from a central point, the process follows a three-dimensional surface on which the seismic phase is constant. (de Groot et al., 2008)*

still contains many details (and also respectively more noise). Detailed steering-cubes preserve more detail in a lateral direction and are generally used for stratigraphic and sedimentary features. The Background steering-cube is more heavily filtered, and contains only structural dip. It is more smoothed in a lateral direction, thereby preserving more background information, and emphasizing details on a local level. For this reason the Background steering-cube is used for all OpendTect work in this research.

Once a steering-cube is prepared, conventional attributes can be customized and applied along the dip and azimuth information (Jaglan et al., 2015). Dip-steered attributes are preferred over non-steered attributes as noise and artefacts have mostly been filtered out, and only geological pictures remain (Jaglan et al., 2015).

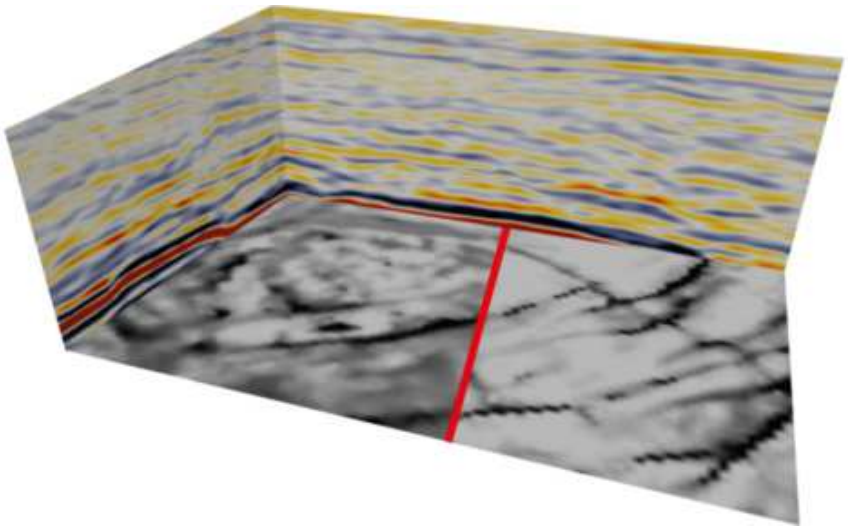

Figure 4.3: *A combined image comparing non-steered similarity (left side of Z-slice) to similarity applied on a Background steering-cube (right side of Z-slice). Note that the dip-steered image has higher contrast, resolution and is generally smoother.*

The next step was working towards the Fault Enhancement Filter, or FEF. The FEF is a useful tool in enhanced fault interpretation as it slightly roughs discontinuities in the seismic volume, thereby highlighting faults. The FEF requires two other filters as input: the Dip-Steered Median Filter and the Dip-Steered Diffusion Filter. By applying a minimum similarity filter on the raw seismic data, continuity of the seismic reflectors is enhanced. The FEF then utilizes a cut-off value which corresponds to the continuity of these seismic reflectors. Seismic reflections which show a continuity which corresponds to a value below the cut-off value will then be filtered with the DSMF, thereby reducing noise, and smoothing the seismic data. On the other hand seismic reflections which show discontinuity correspond to a value above the cut-off, and will be filtered with the DSDF, which enhances discontinuities and enhances faults and fractures. The Fault Enhancement Filter shows a sharper definition of faults, and improves the visualization and interpretation of faults (Jaglan et al., 2015).

The Dip-Steered Median Filter, or DSMF, is one of the two filters used as input for the FEF, and is a statistical filter that is applied to the seismic data with the use of a pre-processed steering-cube (Jaglan et al., 2015). The DSMF uses median statistics on the seismic amplitudes by following the dip and azimuth information from the steering-cube (Jaglan et al., 2015). This process removes background noise and improves the continuity of the seismic reflectors which results in a smoothed seismic volume (Jaglan et al., 2015). However the DSMF will also enhance the continuity of fault zones, and for this reason the DSMF is combined with the DSDF in the FEF.

The Dip-Steered Diffusion Filter, or DSDF, is an intermediate filter that is used to improve the sharpness of discontinuities (Jaglan et al., 2015). The DSDF evaluates the quality of the seismic data in a dip-steered circle, in which the central amplitude is replaced by the amplitude where the quality is regarded best (Jaglan et al., 2015). Near a fault zone, the effect is such that good quality seismic data is moved towards the fault plane from either side of the faults, thereby increasing the sharpness of the fault.

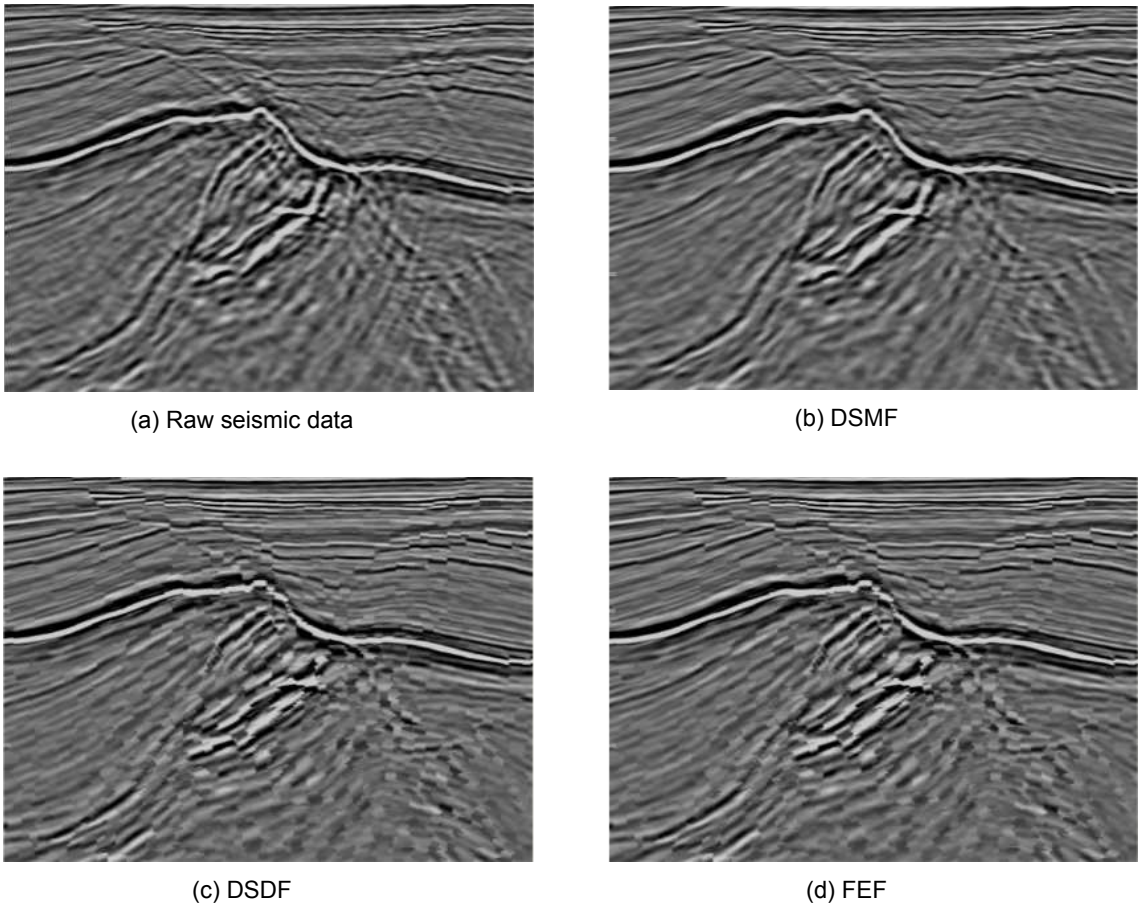

(a) Raw seismic data

(b) DSMF

(c) DSDF

(d) FEF

Figure 4.4: *Examples from Crop 3 of the TEPNL Dataset, to show the effects of the different filters: a) raw seismic data, b) Dip-Steered Median Filter, c) Dip-Steered Diffusion Filter and d) Fault Enhancement Filter*

When the FEF is created, it can be used as input for the Similarity attribute. Jaglan et al. (2015) states that the Similarity attribute can be explained as such: *"The lateral correlation between waveforms along a given reflection can be measured by computing the euclidean distance between the amplitude vectors representing the waveform. This operator is often referred to as a similarity measurement. Its computation provides a direct measurement of lateral discontinuities in the waveform."* The Similarity attribute is very sensitive to phase changes, which makes it very useful for fault interpretation. The Similarity attribute displays correlation strength between waveforms in three dimensions (Jaglan et al., 2015). If the correlation strength is 100%, it suggests that the traces are similar in the response, thereby being continuous (Jaglan et al., 2015). If the strength is below 60% it means that the traces do no correlate properly, which suggests discontinuities or, faults (Jaglan et al., 2015). The Similarity attribute can be used with all filters or (dip-steered) volumes. However it functions best when combined with the FEF to create even better distinction between fault and reflector.

Eventually the use of filters and attributes leads to the latest step used to drastically enhance the visualization of faults. The Thinned Fault Likelihood attribute, or TFL, is a semblance-based algorithm which is defined as a power of semblance (1 - semblance^n). It is similar to the Similarity algorithm which uses the ratio of the energy of the component traces to measure how similar a particular trace is compared to a group of traces. Similarity only compares individual traces, one trace at a time. TFL scans the range of fault dips and strikes to identify maximum likelihood for the delineated faults or fractures in the region of interest. The values calculated ranges between 0 and 1. This produces faults with true dips and strikes. The TFL's output is a razor sharp fault image that can be displayed either on horizontal or vertical slices.

4.2.2. Petrel

To test the abilities of OpendTect's fault enhancing attributes and filters it was decided to test OpendTect's abilities to Petrel, which has different, but similar attributes.

The workflow for applying filters and attributes is similar to OpendTect, however there are differences. The first major difference is that dip-steering is not supported in Petrel. Instead, the seismic crops first have to be realized. Realization of seismic data is a form of compressing seismic data to improve calculation speed and it enables Petrel to do calculations and conversions that it is unable to do directly on a raw seismic dataset.

Like in OpendTect the realized volume first has to be conditioned. This is done through the application of the Structural Smoothing Filter. The Structural Smoothing Filter is based on Gaussian weighted filter which delivers spatial smoothing, and it also contains an option for edge enhancement. It is used for smoothing the seismic data, thereby reducing background noise and increasing the continuity of seismic reflectors. For that reason it can be compared as an equivalent of OpendTect's FEF.

The next step in Petrel is the application of the Variance attribute. The Structural Smoothed seismic crop was used as input. The Variance attribute calculates the dissimilarity between seismic traces, rather than the similarity between traces, producing sharper and more distinct images. It is equivalent to OpendTect's Similarity attribute, however where the Similarity attribute uses similarity correlation, the Variance attribute uses dissimilarity correlation.

The last step in the Petrel workflow consists of applying the Ant-Tracking attribute. In practice this delivers similar results as OpendTect's TFL attribute, but it functions in a completely different way. The attribute is based on the swarm intelligence ants display in nature (Cox and Seitz, 2007). Ants use pheromone trails to direct other colony members to food they have found or to nests they have built (Cox and Seitz, 2007). Petrel 'translated' this into their Ant-Tracking attribute. The attribute when applied to seismic data releases 'digital ants' computed to follow discontinuities (Cox and Seitz, 2007). Like the pheromone trails in nature, the path which is most marked, will attract more ants, thereby identifying, tracking and sharpening faults (Cox and Seitz, 2007). The Ant-Tracking attribute uses the Variance attribute as input.

4.2.3. OpendTect Vs. Petrel

The output of enhanced seismic images are not always as 'true' as one might believe. An important issue is how many of the imaged objects and structures are real and how many are artifacts. To test the abilities of OpendTect's fault enhancing attributes and filters, and to see if artifacts can be recognized it was decided to test OpendTect's abilities to Petrel, which has different, but similar attributes. In this comparison all parameters regarding the data remained the same to make the comparison as good as possible. This means that the seismic crops have the exact same size, and that where possible the exact same parameters were used for generating the attributes.

Maybe the most useful attributes are the similarity and variance attributes. These attributes track (dis)continuities in seismic traces, and are therefore very useful for fracture interpretation. When comparing OpendTect's Similarity attribute to Petrel's Variance attribute it can be noted that the Similarity attribute displays a higher resolution and more detail than the Variance attribute (figure 4.5a,b). This can be seen above the blue z-slice line, where in figure 4.5a multiple fractures (small vertical black lines) are observable, and in figure 4.5b these discontinuities are not present, instead only bold black horizontal lines are observable. Differences in resolution such as the one mentioned above can be seen throughout figures 4.5a,b. These differences are highlighted in figures 4.5c,d which display the TFL and Ant-Tracking attributes. These attributes use Similarity and Variance as input and therefore highlight discontinuities slightly better than the discontinuity attributes.

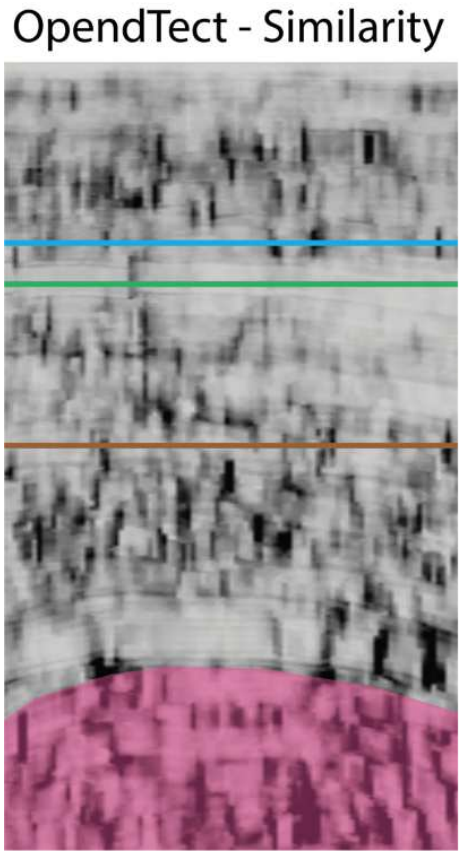

(a) OpendTect Similarity Attribute

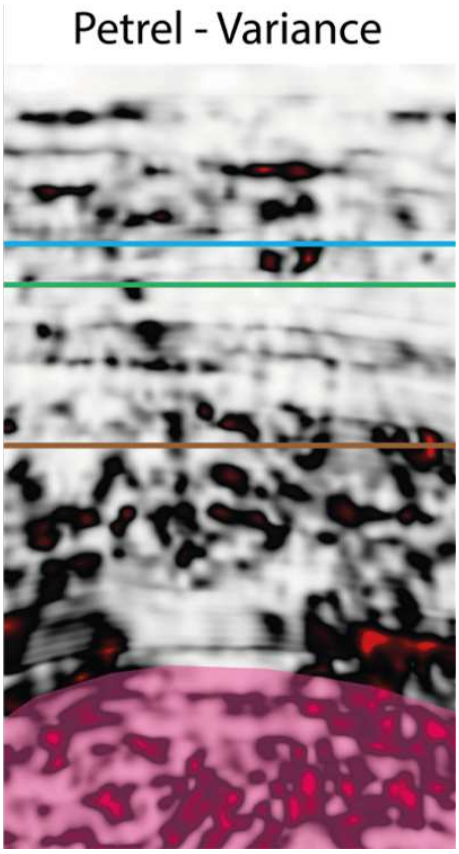

(b) Petrel Variance Attribute

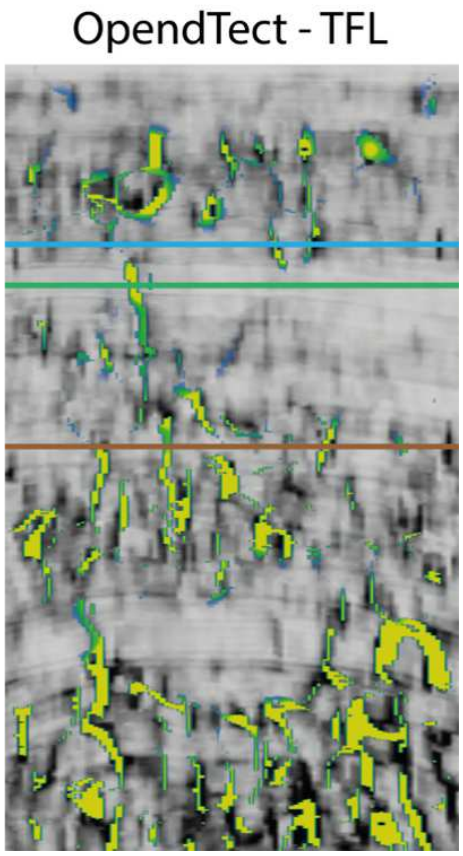

(c) OpendTect TFL Attribute

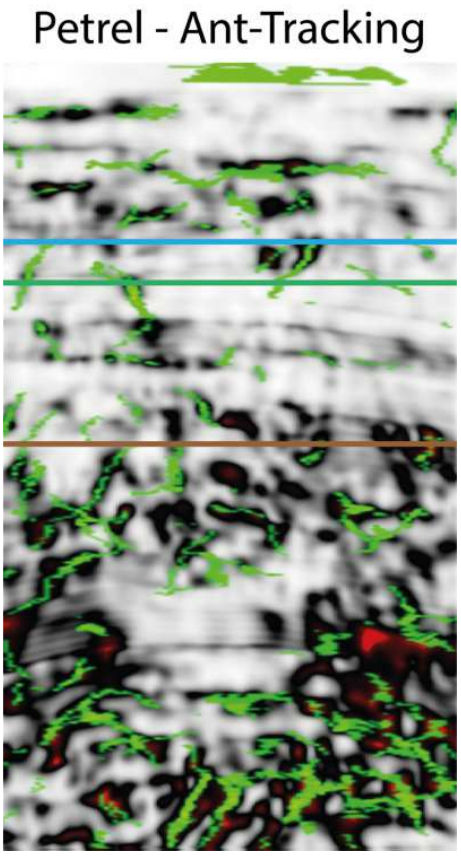

(d) Petrel Ant-Tracking Attribute

Figure 4.5: *These images display inline 8820 of seismic crop 2, comparing made the used attributes of OpendTect and Petrel. Displayed are also the positions of the Z-slices displayed in figure 4.6: Blue: -780ms, green: -865ms and brown: -1200ms. The pink overlay on figures 4.5a and 4.5b displays salt in the salt present in this seismic crop.*

When looking above the blue z-slice line in the same area as mentioned above, we can see that the differences in resolution between the two attributes are even better observable. The TFL attribute tracks the discontinuities and highlights the faults of which the attribute is most certain. Observable are now about 10 fractures, whereas the Ant-Tracking attribute only tracks the bold horizontal lines (the bedding planes), thereby not imaging any faults. Throughout figures 4.5c,d more examples can be found in which the Similarity and TFL attributes locate discontinuities, and where the Variance and Ant-Tracking attributes don't. When looking at the underlying salt in figures 4.5 we see all attributes have trouble making distinctions between fractures and salt. Salt is usually highly transparent on seismic data. Apparently this transparency is easily mistaken for fractured rock by these attributes.

Figure 4.6 shows three Z-slices of seismic crop 2. The positions of these Z-slices can be found in figure 4.5. For every Z-slice the Similarity and TFL attributes are compared to Petrel's Variance and Ant-Tracking attributes. Figure 4.6a, b show the most shallow Z-slice at -780ms. When comparing the Similarity attribute to the Variance attribute we can see that, like in the comparisons on the vertical plane mentioned above, that the Similarity attribute shows higher resolution and more detail. Figure 4.6a shows many discontinuities, often in a polygonal pattern, and shows clear connectivity between faults. Figure 4.6b shows less detail. The biggest faults are easily observable as they are shown very boldly. However when comparing the bold black lines from figure 4.6b to 4.6a we see that often these faults are not just one fault, but consist of multiple faults. Also the Variance attribute often connects discontinuities where the Similarity attribute does not. This is often supported by the TFL attribute of figure 4.6a, which traces many small faults, and also displays a polygonal pattern in the faults. The Ant-Tracking attribute shows longer connected faults, whereas the TFL shows shorter more unconnected faults.

Figures 4.6c,d are relatively similar. Here the Ant-Tracking attribute actually displays more discontinuities than the TFL attribute. However as can be spotted on the right side of figure 4.6d, it also recognizes faults that are not supported by either OpendTect or by Petrel's Variance attribute. Again, OpendTect displays most faults, both short and long, whereas Petrel only images the longer, more connected faults.

When comparing figures 4.6e,f we see comparable results as between figures 4.6a,b. OpendTect's Similarity attribute displays high resolution and a lot of detail, whereas the Variance attribute lumps together many discontinuities, what results in the bold black lines observable in figure 4.6f. Figure 4.6e shows that the bold black discontinuities of figure 4.6f are interpreted as multiple connected smaller faults in OpendTect. This is supported by the TFL attributes which highlights many small faults, especially on the top and bottom of figure 4.6e. However when comparing to the Ant-Tracking attribute we see that many small faults either get skipped, or get lumped with larger faults. Also Petrel shows a lot of connectivity between faults whereas the higher resolution of the TFL attribute distincts multiple unconnected faults and different connectivities.

An important part of this research focuses on faults with throws just above seismic resolution. These faults are often not visible because of poor data quality, or they are seen as noise. Both OpendTect and Petrel posses fault enhancing attributes which reduce noise, and enhance data quality. However when comparing the attributes of both software packages, it is observable that the attributes of OpendTect increase the resolution and the amount of detail visible on the seismic data more so than the attributes of Petrel. For that reason OpendTect was chosen as the software package for this research.

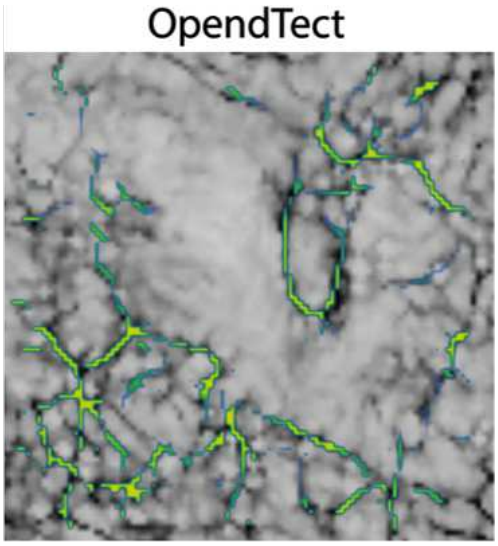

(a) Z = -780ms

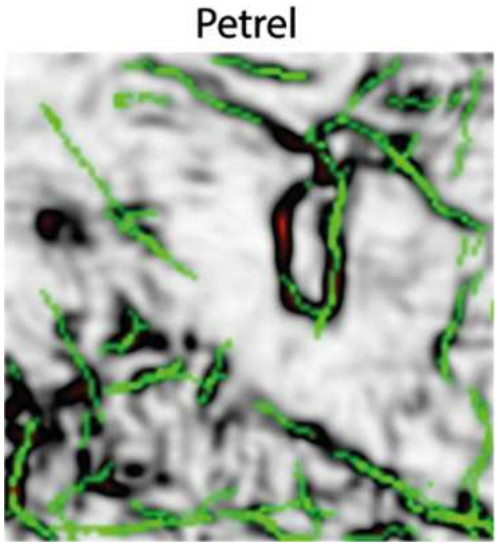

(b) Z = -780ms

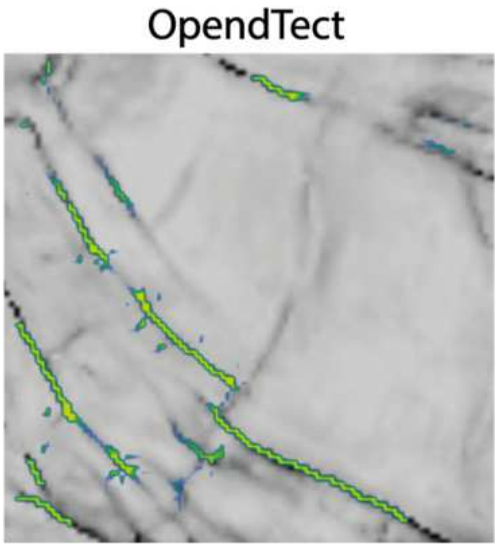

(c) Z = -865ms

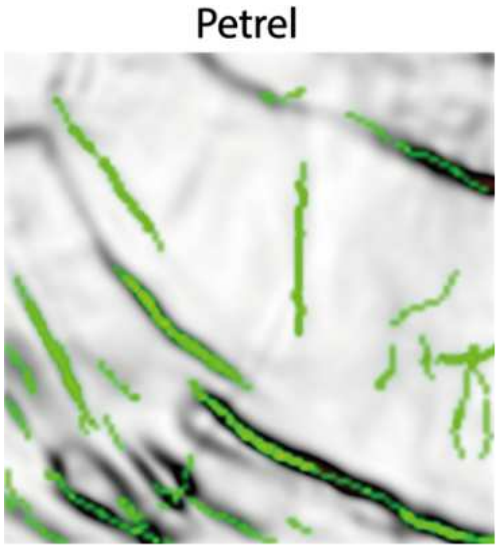

(d) Z = -865ms

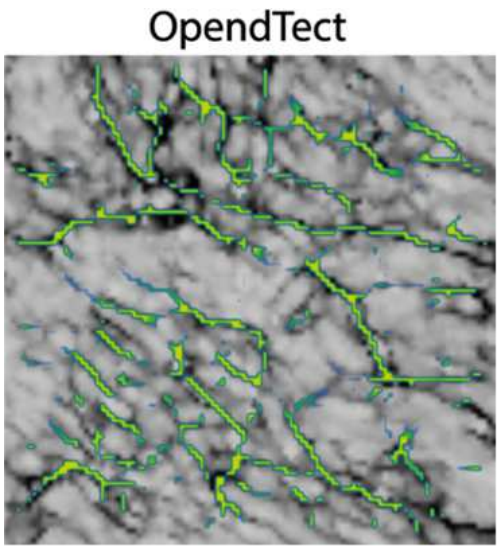

(e) Z = -1200ms

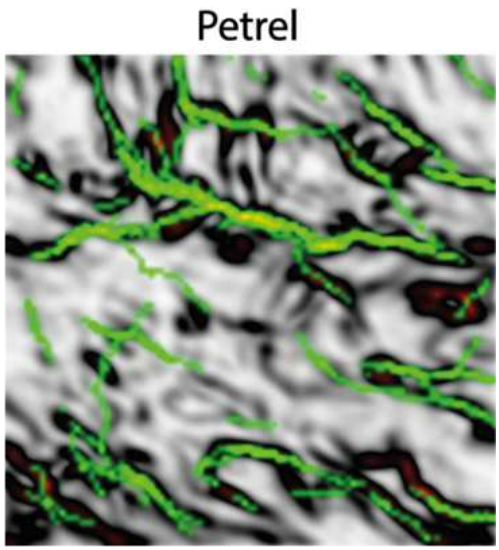

(f) Z = -1200ms

Figure 4.6: *These images display 3 Z-slices of seismic crop 2. The positions of these Z-slices can be found in figure 4.5. Images a,c & e have been generated in Opendtect and contain both Similarity and TFL attributes. Images b, d & f have been generated in Petrel and contain Variance and Ant-Tracking attributes.*

5

Fault Network Scale

For both datasets fault models were constructed that consist of the largest faults (>1000m) in each dataset. All faults used for this analysis were picked without the help of attributes and/or filters, and had to be present (partly) within the Chalk Formation. These faults were migrated from time to depth to accommodate for length and angle calculations, and were eventually used to construct fault models. For the P10 dataset this fault model consisted of 29 faults, and for the TEPNL dataset the model consisted of 45 faults. The Fault Network Scale analysis functioned as a base for the Small Seismic Scale analysis, as the positions of the seismic crops were chosen based on the results of the Fault Network Scale analysis. After construction of the fault models parameters such as P21, fault orientation, fault length and dip angle were extracted and analyzed. With these results we will try to answer questions like, what are trigger mechanisms behind faulting on a regional level? And when did faulting occur in this region?

5.1. P10 Dataset

The construction of the fault model in the P10 dataset resulted in a model consisting of 29 faults. Figure 5.1 displays an overview of the fault model, and it can be observed that generally the faults follow a NW-SE trend. This statement is supported by the rose diagram also displayed in figure 5.1, showing that the most frequent orientation of the faults is between 120° and 135°. Towards the West of the area faults can be observed with E-W, to almost NE-SW orientations, which

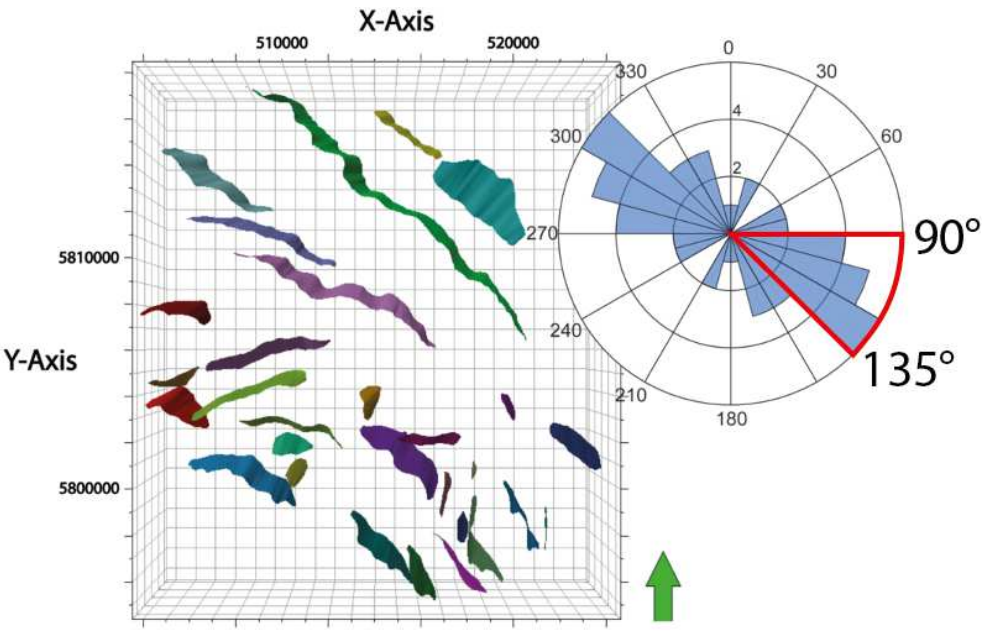

Figure 5.1: *The Fault Network Analysis fault model of the P10 dataset, displaying all 29 faults and a rose diagram of the fault orientations.*

is also supported by the rose diagram. As well as to the Southeast of the area where multiple faults with a N-S orientation can be found.

Figure 5.2 displays the positions of the three inlines highlighted in figure 5.3. Observable from figure 5.3 is that generally the Chalk Group thickens towards the Northeast. This thickening mainly occurs in the Ommelanden and Texel Formations, as the thickness of the Ekofisk Formation remains constant. The thickening of the Texel and Ommelanden Formations, in particular in the deeper parts of the area, could be indications of syntectonic deposition or onlapping on underlying sediments. In figure 5.3 faults are interpreted that both intersect with the Chalk Group, and faults that do not. Only the faults that intersect the Chalk Group have been included in the fault model, since these are the only faults that will affect fracture geometries within the Chalks.

Figure 5.3 displays three inlines through the P10 dataset fault model. Inline 2611 displays 5 faults through the most Northwestern part of the P10 area. It can be observed that there are no faults in this area that cross the complete chalk interval, and that all faults terminate either in the Texel Formation, or just after entering the Ommelanden Formation. The faults can be followed all the way past the Jurassic-Triassic Angular Unconformity, into the underlying Triassic and Permian Sediments. All faults are extensional in nature, except for the most Northeastern fault (the yellow fault). When observing this fault, we can see that in the lower sediments the fault can be seen to be extensional in nature. However above the Jurassic-Triassic angular unconformity, it can actually be seen to be compressional in regime.

Inline 3087 of figure 5.3 displays 6 faults, approximately through the middle of the area, from the Southwest to the Northeast. This inline is marked by two faults that cross all the way through the Ommelanden Formation to terminate against the Ekofisk Formation. The other three faults terminate within the Ommelanden Formation. All faults can be followed all the way into the underlying Triassic and Permian sediments. Except for the two Northernmost faults, all faults are extensional in nature. When observing the two Northernmost faults, it is observable that these faults have an extensional nature below the Jurassic-Triassic angular unconformity, whereas above this unconformity these faults exhibit compressional features, such as uplift in the hanging-wall.

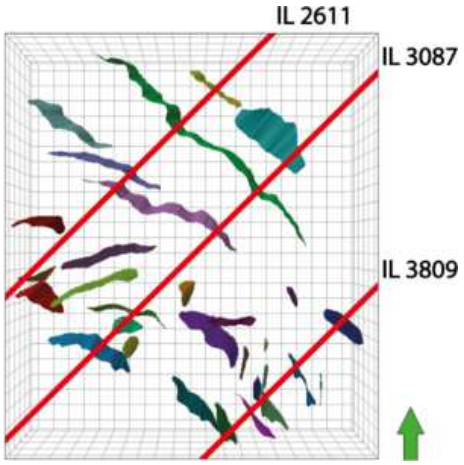

Figure 5.2: *The Fault Network Analysis fault model of the P10 dataset, displaying all 29 interpreted faults, as well as the positions of the inlines of figure 5.3.*

The third inline of figure 5.3, inline 3809, displays 5 faults in the Southeastern part of the P10 area. This inline is marked by one fault that cuts through the complete Chalk Group, to terminate in the overlying sediments of the North Sea Group. The other faults terminate in either the Texel Formation, or the Ommelanden Formation. As can be seen in the other inlines, all faults can be followed downward all the way into underlying Triassic and Permian sediments. All interpreted faults in this inline are extensional in nature.

Figure 5.4 displays three frequency distribution diagrams extracted from the P10 fault model. The frequency distribution on fault orientation shows, like the rose diagram in figure 5.1, that the faults of the fault model roughly have a NW-SE trend between 120° and 135°.

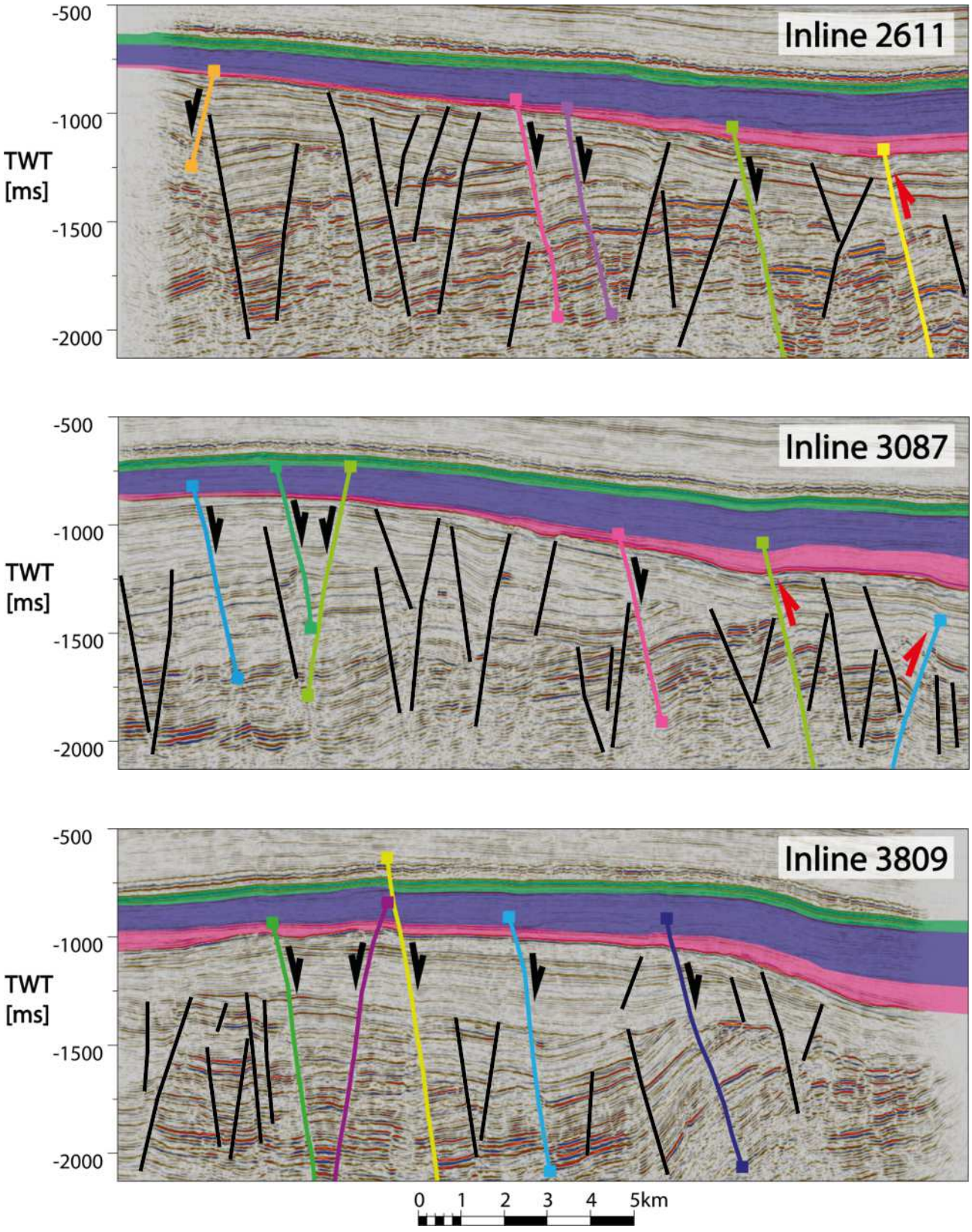

Figure 5.3: *These images display the three inlines shown on the overview of figure 5.2. The inlines display the interpreted faults of the fault model (colored faults) and the faults that do not intersect the Chalk Group (black faults). The different formations are highlighted in Green (Ekofisk Fm.), Blue (Ommelanden Fm.) and Pink (Texel Fm.).*

However also observable is that the range in orientations is also very wide, as there are only no fault interpreted between 30° and 60°.

A frequency distribution diagram on fault length is shown in figure 5.4b. Observable is that relatively short faults occur more than large ones, as out of 29 interpreted faults, only 2 are longer than 10km. Figure 5.4c displays a frequency distribution diagram on fault dip angle.

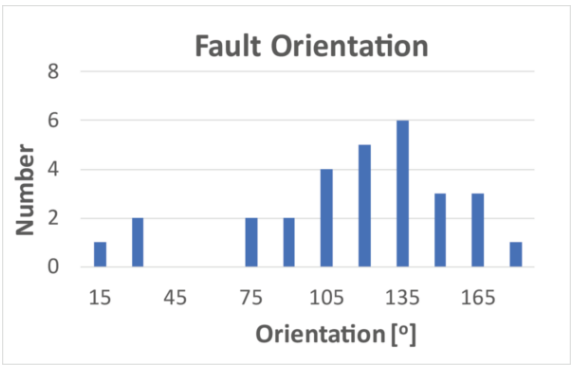

(a)

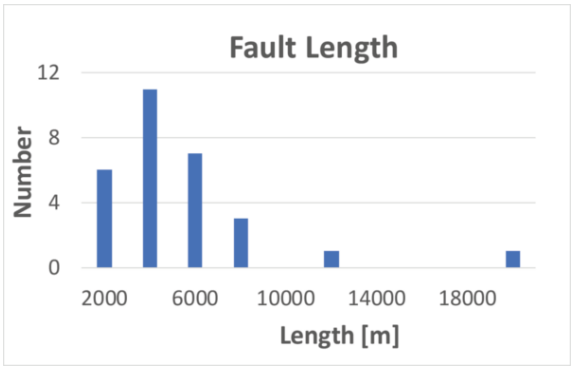

(b)

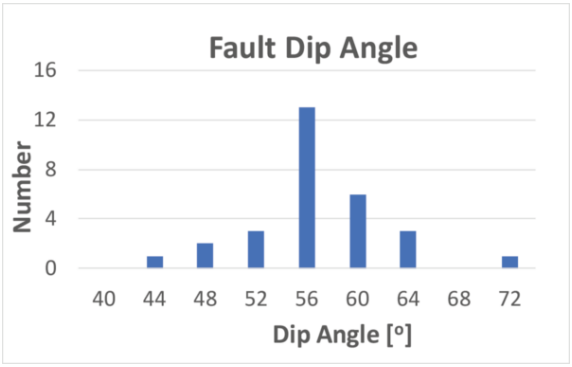

(c)

Figure 5.4: *The results extracted from the P10 fault model. These results consist of three frequency distribution diagrams: a) Fault Orientation, b) Fault Length and c) Fault Dip Angle. Only the faults that intersect the Chalk Group are used in these histograms.*

5.2. TEPNL Dataset

The construction of the fault model in the TEPNL dataset resulted in a model consisting of 45 faults. Figure 5.5 displays an overview of the fault model, and it can be observed that generally the faults follow a NW-SE trend. This statement is supported by the rose diagram also displayed in figure 5.5, showing that the most frequent orientation of the faults is between 135° and 165°.

Figure 5.6 displays the positions of the six inlines highlighted in figures 5.7 and 5.8. Observable from figures 5.7 and 5.8 is that this area is marked by large salt domes and diapirs. This locally affects the thickness of the Chalk Group. From figure 5.7 it is observable that the Chalk Group and its subformations have a more constant thickness in the Western part of the area. Whereas inlines 9572 and 7756 of figure 5.8 show that the thickness of the Chalk Group gets greatly reduced towards the East. Also observable in figure 5.8 is that the Ekofisk

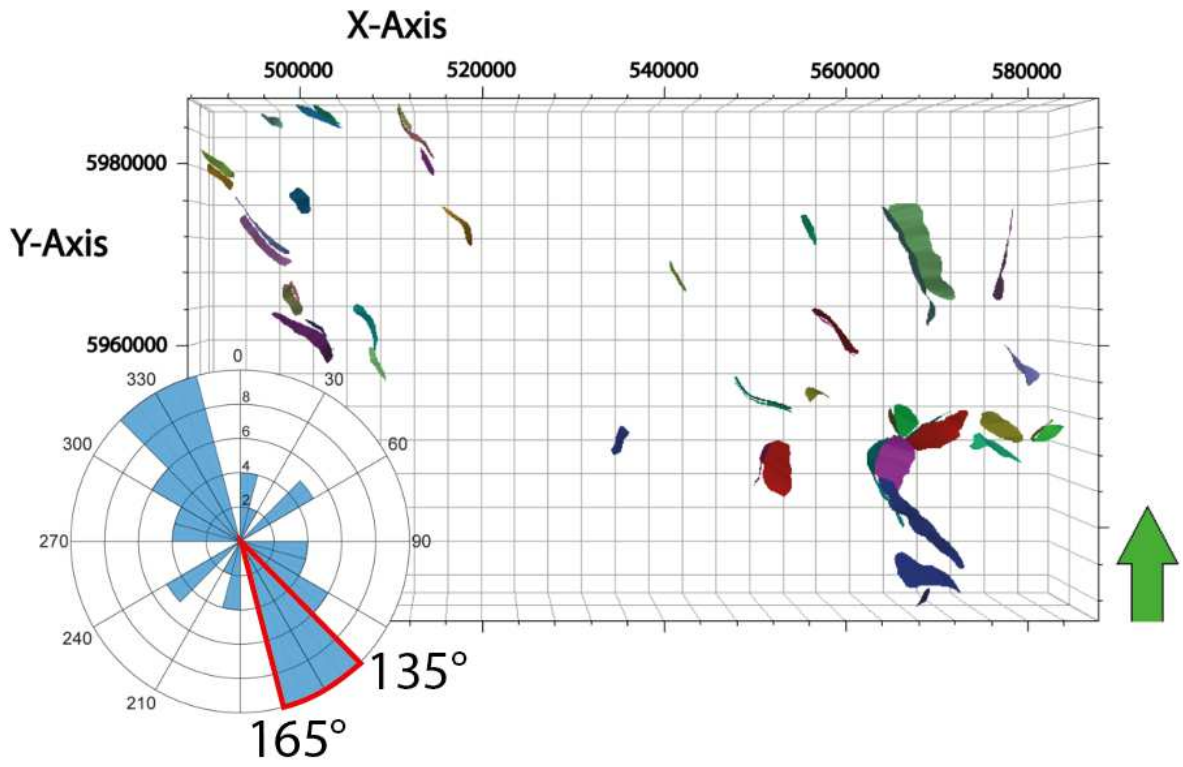

Figure 5.5: *The Fault Network Analysis fault model of the TEPNL dataset, displaying all 45 faults and a rose diagram of the fault orientations.*

thins towards the East until the point that is absent. Whereas the Ekofisk Formation pinches out to the East, and the Ommelanden Formation gets much thinner towards the East, the Texel Formation generally has a constant thickness throughout the area. The thinning of the Ekofisk and Ommelanden Formations could be indications of either syntectonic deposition, or slight onlapping on underlying sediments.

Figure 5.7 displays the three inlines on the Western side of the TEPNL dataset area. Inline 10756 displays 5 faults through the most Northwestern part of the TEPNL area. It can be observed that out of the five interpreted faults, two cut through the complete chalk interval and three cut through only partially. The most Western fault is a very steep one, and can be follow far down into the Zechstein salt, and can be seen terminating in the Ommelanden Formation. The other four faults are located on the top of NW-SE trending salt-ridges. The blue and green faults can both be followed down to the sediments underlying the Texel Formation, and up to the sediments of the overlying North Sea Group. The yellow and orange fault show a similar geometry, however both faults terminate in the Ekofisk Formation on the top, and the Ommelanden Formation on the bottom. All faults are extensional in nature.

Inline 9692 of figure 5.7 displays 3 faults through the Northwestern part of the TEPNL area. It can be observed that out of the three interpreted faults, all cut through the complete chalk interval. The two Western faults are located on the top of NW-SE trending salt-ridge, where the Chalk Group is thinnest. The pink and purple

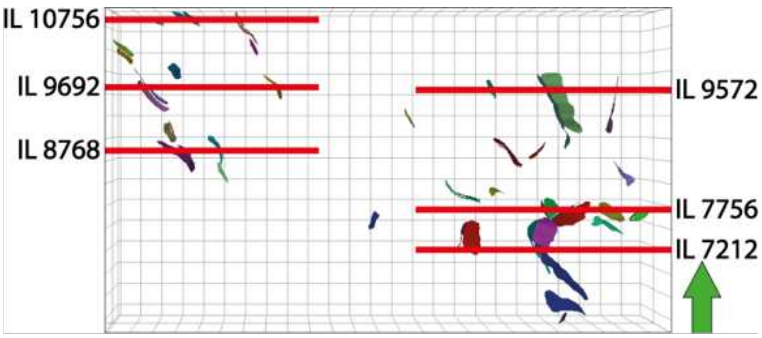

Figure 5.6: *The Fault Network Analysis fault model of the TEPNL dataset, displaying all 45 interpreted faults, as well as the positions of the six inlines of figure 5.7.*

faults can both be followed down to the underlying Zechstein salts, and can be seen terminating in the overlying sediments of the North Sea Group. The orange fault is also located on a salt high, on a place where the Chalk Group has a reduced thickness. It can be followed all the way down to the underlying salts of the Zechstein Group, and can be seen terminating in the overlying sediments of the Tertiary North Sea Group. All faults are extensional in nature.

Inline 8768 displays 3 faults through the Western part of the TEPNL dataset. It can be observed that out of three interpreted faults, all can be seen cross-cutting the complete chalk interval. The purple and dark-blue fault are located on a NW-SE trending salt-ridge, where the chalk interval is thinnest. Both these faults can be seen terminating in the overlying North Sea Group. Downwards it is observable that the purple fault can be followed all the way into the underlying Zechstein salts, whereas the dark-blue fault terminates against the purple fault. The light-blue fault on the Eastern side is also located on a salt-ridge. It can be observed terminating slightly under the Texel Formation, and on the top in the sediments of the North Sea Group. All faults are extensional in nature.

Inline 9572 of figure 5.8 displays 4 faults through the Northeastern part of the TEPNL dataset. It can be observed that out of four interpreted faults, three can be seen cross-cutting the complete chalk interval and one (the dark-green fault) can be seen terminating in the Ommelanden Formation on the top and downward into the Zechstein salt. This fault is very steep respective to the others, and can be seen dividing the Chalk Group in a thick part to the West, and a thinner part to the East. The blue, light-green and pink faults are located on a salt-ridges, where the chalk interval is thinnest. These faults can be seen terminating in the overlying Tertiary sediments. Downwards it is observable that these faults can be followed all the way into the underlying Zechstein salts. All faults are extensional in nature.

Inline 7756 of figure 5.8 displays 5 faults through the Eastern part of the TEPNL dataset. It can be observed that out of five interpreted faults, three (light-green, light-blue and red) can be seen cross-cutting the complete chalk interval. The two most Western faults are located on a salt-ridge where the Chalk Group is thinnest. This is similar for the red fault, which is located on a very thin part of the Ommelanden Formation on top of a salt-ridge. The dark-green fault can be seen terminating against the light-green fault, downwards of the Chalk Group,

and within the Ommelanden Formation towards the top of the fault. The yellow fault to the East terminates halfway into the Ommelanden Formation, and can be followed far into the overlying sediments of the North Sea Group. All faults are extensional in nature.

Inline 7212 of figure 5.8 displays 5 faults through the Southeastern part of the TEPNL dataset. It can be observed four out five interpreted faults cross-cut the complete chalk interval. The two most Western faults are located on a small salt-ridge, on a place where the Chalk Group is relatively thin. Both faults terminate high up in the overlying Tertiary sediments, and can be followed down into the Zechstein salts. Towards the East there are three faults located on a NW-SE trending salt anticline. Observable is that the Chalk Group is very thin at this location. Both the light-blue and purple faults cross-cut the complete chalk interval, whereas the dark-blue fault only cross-cuts the Ommelanden Formation. Both the dark-blue and purple faults can be seen terminating against the light-blue fault, which can be followed all the way down into the Zechstein salts. All faults are extensional in nature.

Figure 5.9 displays three frequency distribution diagrams extracted from the TEPNL fault model. The frequency distribution on fault orientation shows, like the rose diagram in figure 5.5, that the faults of the fault model roughly have a NW-SE trend between 120° and 165°. However also observable is that the range in orientations is also very wide, as there are only no fault interpreted between 30° and 45°, and between 60° and 90°. Figure 5.9a also shows that there are relatively many (5 interpretations) between 45° and 60°, which is perpendicular to the main NW-SE trend.

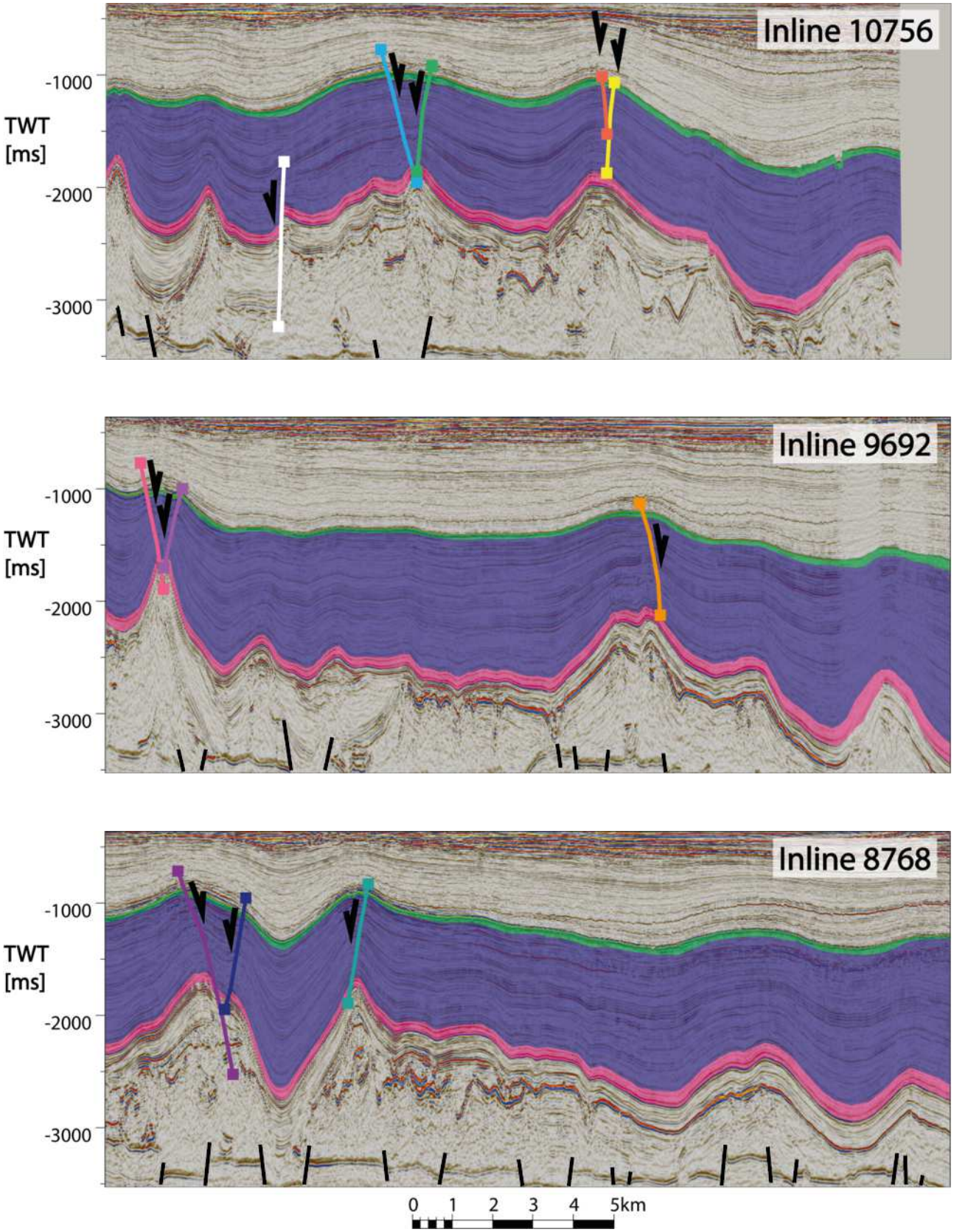

Figure 5.7: *These images display the most western three inlines of six shown on the overview of figure 5.5. The inlines display the interpreted faults of the fault model (colored faults) and the faults that do not intersect the Chalk Group (black faults). The different formations are highlighted in Green (Ekofisk Fm.), Blue (Ommelanden Fm.) and Pink (Texel Fm.).*

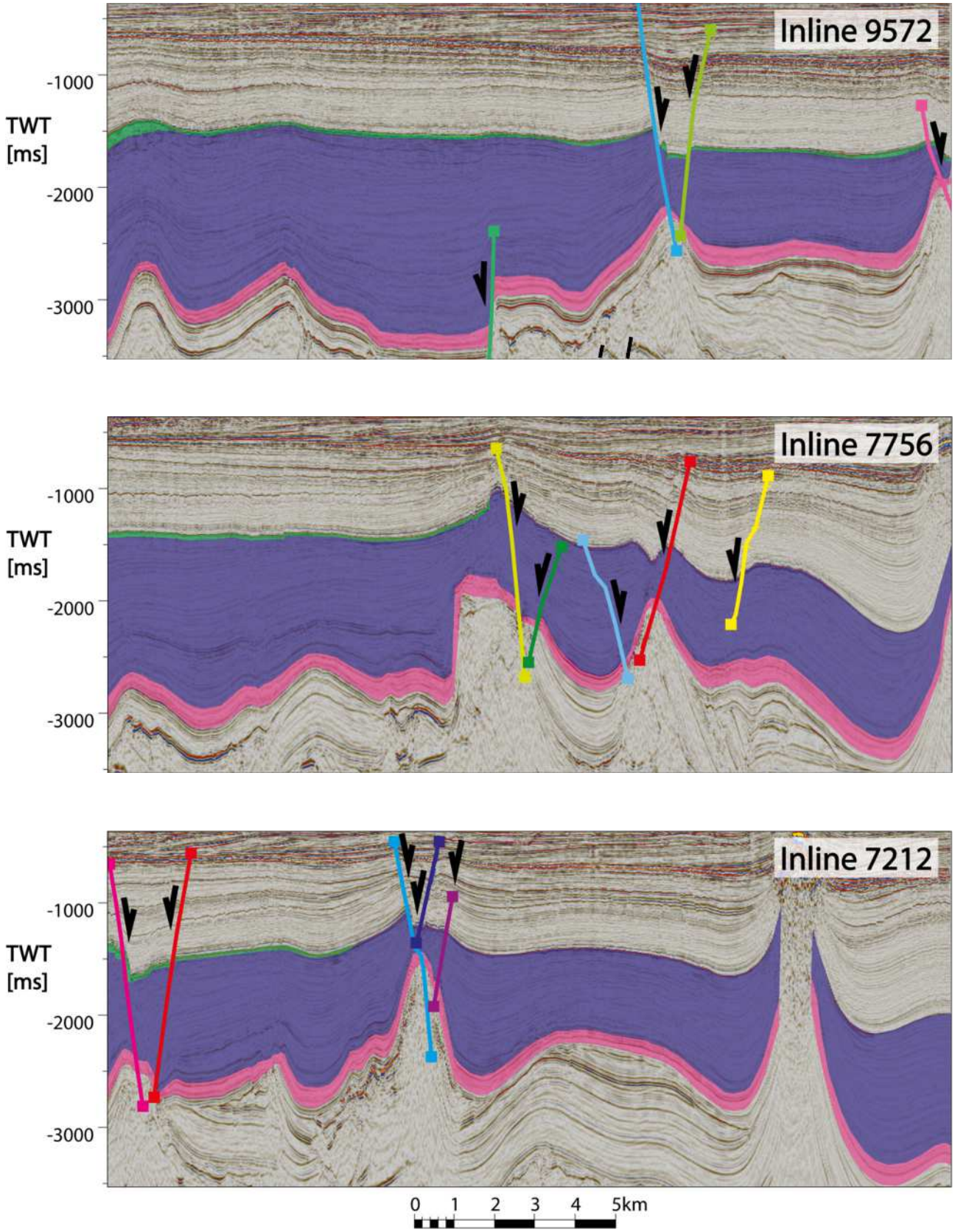

Figure 5.8: *These images display the most eastern three inlines of six shown on the overview of figure 5.5. The inlines display the interpreted faults of the fault model (colored faults) and the faults that do not intersect the Chalk Group (black faults). The different formations are highlighted in Green (Ekofisk Fm.), Blue (Ommelanden Fm.) and Pink (Texel Fm.).*

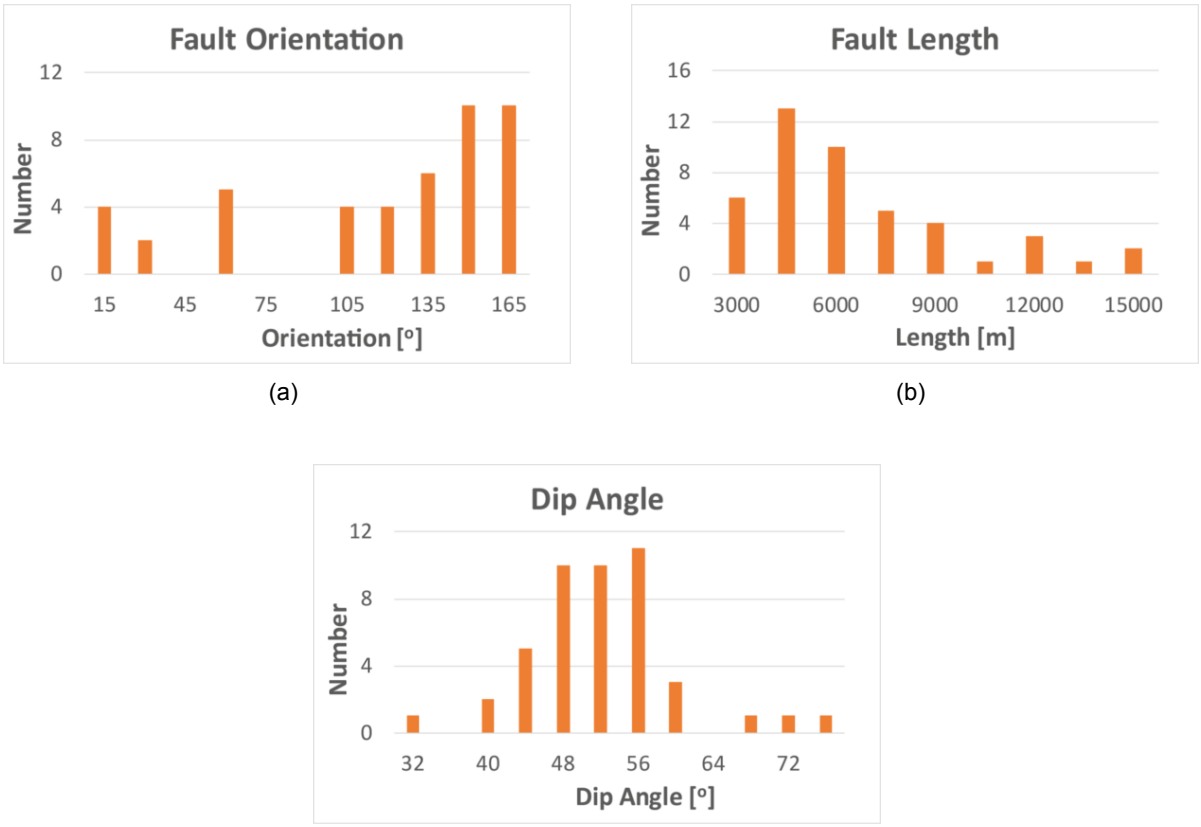

Figure 5.9: *The results extracted from the TEPNL fault model. These results consist of three frequency distribution diagrams: a) Fault Orientation, b) Fault Length and c) Fault Dip Angle. Only the faults that intersect the Chalk Group are used in these histograms.*

A frequency distribution diagram on fault length is shown in figure 5.9b. Observable is that relatively short faults occur more than large ones, as out of 45 interpreted faults, only 7 are longer than 10km.

Figure 5.9c displays a frequency distribution diagram on fault dip angle. Expected in an extensional regime, most interpreted faults dip at an angle of around 60°. Out of 45 interpreted faults, 24 faults are between 48° of the 60° angle usually found in normal faults. Observable is that their are two faults with dip angles larger than 70°, as well as 8 faults with dips lower than 44°, which is are shallow dips for extensional regimes.

5.3. Discussion

Both the P10 dataset and the TEPNL dataset exhibit many deformational features. However both datasets show that the areas show that deformation was accommodated in different ways. The biggest difference we see between the datasets for Fault Network Analysis can be seen in table 5.1.

Property	**P10 Dataset**	**TEPNL Dataset**
Orientation [°]	WNW-ESE 90° - 135°	NW-SE 135° - 165°
Fault Length [m]	Most faults <8000m, 2 faults >8000m	Most faults <9000m, 7 faults >9000m
Fault Dip Angle [°]	Most faults 52° - 64°	Most faults 40° - 60°
Fault Shape	Straight Faults can be followed into basement	Slightly Listric Faults terminate at Zechstein Salt
Do the faults cross the Chalk Group?	Only the Texel Fm. and bottom of Ommelanden Fm.	Yes, the complete Chalk Group
Fault Spacing [m]	Even spacing – 1km	Uneven spacing Groups of faults sometimes kilometers apart

Table 5.1: This table displays the comparison between the various properties of both the P10 dataset and the TEPNL dataset.

In the P10 dataset the faults are oriented in a WNW-ESE direction, with most faults ranging in orientation between 90° and 135° (figure 5.1). Whereas the faults of the TEPNL dataset are oriented in a NW-SE orientation, with most interpreted faults between 135° and 160° (figure 5.5. Figure 1.1 shows that in the P10 area the main geological structures exhibit NW-SE orientations, whereas to the North the orientations become more oriented in a N-S orientation. This is in line with the orientations of the interpreted faults of both the P10 and TEPNL datasets, showing slightly more NNW-SSE structures in the TEPNL dataset, and WNW-ESE structures in the P10 dataset.

Figure 5.12 depicts a Z-slice of the TEPNL seismic dataset, displaying traces of the antiforms related to salt tectonics. The traces and the included rose diagram display that, like the faults depicted in figure 5.5, that there is a NW-SE trend in the salt antiforms, as well as in the interpreted faults. As displayed in the rose diagram, 8 out of 9 antiform traces have an orientation between 135° and 165°, which is exactly the same as the TEPNL dataset. As most of the faults in intersecting the Chalk Group show similar orientations as the antiforms created by salt movement, it is highly probable that most of the faults in the TEPNL dataset are affected by salt tectonics, rather than regional tectonics such is likely the case in the P10 dataset.

Figure 5.11 displays a comparison between the fault lengths of the interpreted faults of both the P10 dataset and the TEPNL dataset. Observable is that both datasets show a similar fault length distribution of the interpreted faults. Both datasets display relatively more interpreted faults with lengths between 0m and 6000m, and gradually less interpreted faults above 6000m in length, which is in line with a normal fault length distribution.

Figure 5.12 Displays a comparison made between the fault dip angles of the interpreted fault of both the P10 dataset as well as the TEPNL dataset. The figure displays that the

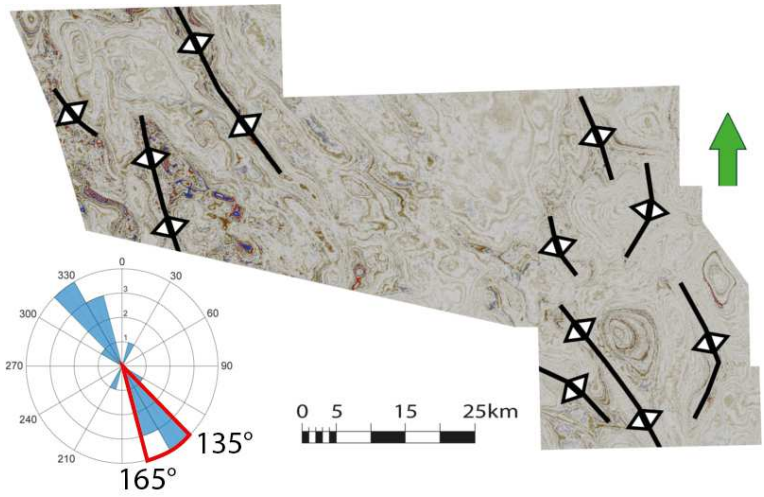

Figure 5.10: *A Z-slice from within the Chalk Group (Z=-2212ms) of the TEPNL Seismic Dataset, displaying traces of salt tectonic related antiforms. A rose diagram is added to quantify the results of the traces.*

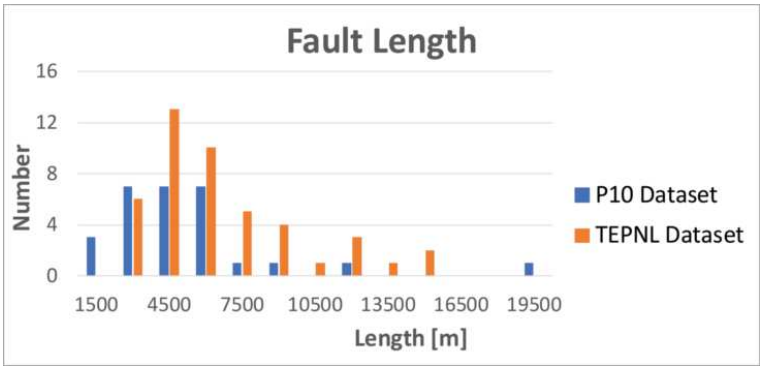

Figure 5.11: *A comparison between the Frequency Distributions on Fault Length of the P10 dataset (blue) and the TEPNL dataset (orange).*

P10 dataset contains slightly steeper faults when compared to the TEPNL dataset. For the P10 dataset most interpreted faults exhibit dips between 56° and 60°, whereas in the TEPNL dataset most faults range between 44° and 56°. The dip angles for both datasets are in line with what one would expect in an extensional tectonic regime.

When looking at the shapes of the faults it is observable that it in the P10 dataset the interpreted faults exhibit steep, straight faults that can be followed all the way into the underlying basement rocks. This indicates that the extensional faults were active before the Jurassic, since the throw of the faults decreases above the Triassic-Jurassic angular unconformity. This suggests that these faults were active long before those times. However this also suggests that these faults have been overprinted in later rifting phases. Another form of overprinting is observable in inlines 2611 and 3087 of figure 5.3 where two faults show signs of tectonic inversion. This enhances the probability that the P10 area is mostly affected by regional extensional tectonics. Figure 5.3 suggests that this inversion took place in the Tertiary since the Chalk Group and the visible overlying Tertiary sediments all display an anticlinal structure above the compressional pop-up structure. In the TEPNL dataset however, faults exhibit shallower, slightly listric shapes, with almost all faults intersecting the complete Chalk Interval, and terminating against the top of the Zechstein salts. These differences imply a different time-line. The fact that almost all faults intersect the entire Chalk Group suggest that these faults were active in a later stage than the faults of the P10 dataset.

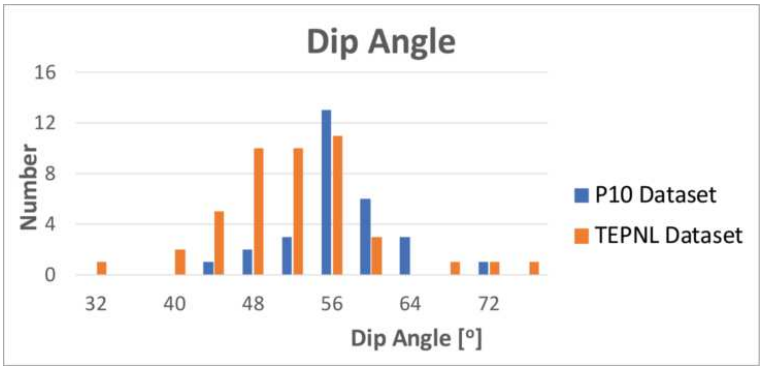

Figure 5.12: *A comparison between the Frequency Distributions on Fault Dip Angle of the P10 dataset (blue) and the TEPNL dataset (orange).*

In the P10 dataset both the Ommelanden and Ekofisk Formations display continuous thicknesses throughout the P10 area. This suggests that these formations were deposited post-tectonically. On the other hand the Texel Formation of the Chalk Group displays many thickness differences. The seismic cross-sections of figure 5.3 show that in the lower areas of the P10 dataset the chalks of the Texel Formation are much thicker than on the higher areas. This suggests that the chalks of the Texel Formation were deposited syn-tectonically, thereby depositing thicker chalk packages in lower areas, and thinner packages on higher areas. As rifting ceased in the Mid Cretaceous (Ziegler, 1988)(Ziegler, 1990) the syn-tectonic deposition of the Texel Formation also ceased, and thermal subsidence and rising sea-levels marked the deposition of the Ommelanden Formation. This explains why the overlying Ommelanden and Ekofisk Formations do not display large thickness variations. Faults are spaced evenly, which contributes to the case that the deformation in the P10 dataset is mainly accommodated by regional extensional tectonics.

When compared to the P10 area, instead of thickness differences in the Texel Formation, we see thickness variations in the Ommelanden and Ekofisk Formations in the TEPNL area, whereas the Texel Formation displays a continuous thickness throughout the area. The seismic cross-sections of figures 5.7 and 5.8 show that the Ekofisk Formation gets gradually thinner towards the Southeast until it is completely absent (figure 5.8). The Ommelanden Formation can be seen on inline 9572 of figure 5.8 to be syn-tectonic in nature. Inline 9572 displays a clear thickness variation in the Ommelanden Formation. Also in the seismic cross-sections of figure 5.8 we can see that the Ommelanden Formation is the only formation to be affected by salt-tectonics. The thickness variations above the salt-ridges in figure 5.8 suggest that the Ommelanden Formation was deposited syn-tectonically to the halokinesis of the Zechstein salts. Larger thickness variations of the Ommelanden Formation in the East of the TEPNL area, suggests that differential loading must have been higher than in the West where the Ommelanden Formation has a more constant thickness. The constant thickness of the Ommelanden Formation in the NW of the TEPNL area suggests that the halokinesis here started later, which is supported by the fact that we see the same anticlinal and synclinal structures in the Tertiary sediments as we see them in the Chalk Group. Due to differential loading the underlying salts start to flow towards areas that exert less pressure. In these areas the salt started to accumulate, forming salt-ridges and pillows. Above these areas the different layers will bend, and fracture to accommodate for the bending. For this reason faults are spaced much more unevenly in this dataset. It is observable that almost all faults are located on salt-ridges, or on other topographical highs related to halokinesis. Tectonically induced extensional faulting seems to be absent here, whereas most faulting is related to halokinesis.

6

Small Seismic Scale

After constructing fault models in Petrel for both datasets, locations were chosen to produce seismic crops. The locations of these seismic crops were chosen with different parameters in mind; thickness of the Chalk Group, nearby major faulting and the presence of salt. These seismic crops were than used as input for the workflow introduced in chapter 4, which consisted of the generation of steering-cubes and the application of various filters and attributes. The most optimized and enhanced images were then used as input for enhanced fault interpretation, during which even the smallest faults above seismic resolution were interpreted. For all seismic crops, except for seismic crop 3, three Z-slices were interpreted: 1 North Sea Group, 1 in the Ekofisk Formation and 1 in the Ommelanden Formation. It was chosen to make Z-Slices in the sediments of the North Sea Group to see how fractures behave above the Chalks, and to see if there are any connections between the layers. After interpretation the data of the generated fault models could be extracted, and used for calculations on Fault Density, Fault Orientation and Fault Length. These results help us understand what the main drivers are behind deformation on a local level, and how this deformation is accommodated.

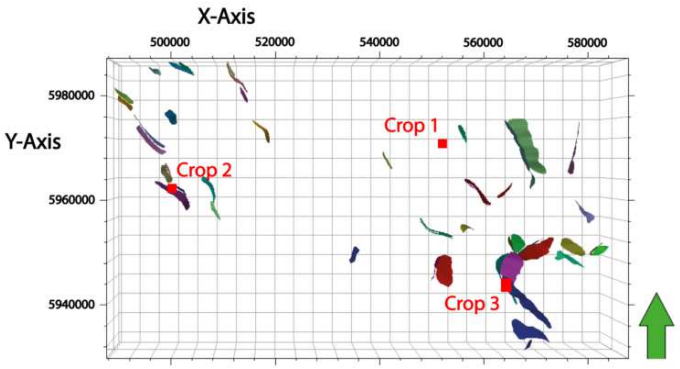

Figure 6.1: *An overview of the TEPNL dataset and fault model, with the displayed locations of the three seismic crops.*

6.1. TEPNL

Three seismic crops, or steering-cubes, were generated from the TEPNL dataset. Figure 6.1 shows the locations of the three crops. Table 6.1 displays the practical information regarding the three seismic crops of the TEPNL dataset, and the reasoning behind their respective locations. The location of Seismic Crop 1 was chosen for it being away from major faulting and at this location the Chalk Group is at its thickest within the entire dataset. As can be see in figure 6.1 there are almost no major faults surrounding this crop, making it easier to look at background structures, instead of looking at effects caused by either salt tectonics or regional extensional tectonics. The location of Seismic Crop 2 was chosen for it being placed on the top of a NW-SE trending salt-ridge. The Chalk Group is much thinner at this location compared to seismic crop 1. Whereas at the location of Seismic Crop 3, which is also located

on a salt-ridge, the Chalk Group is even thinner, and effects of major faults on a local level can be observed.

	Seismic Crop 1	**Seismic Crop 2**	**Seismic Crop 3**
Area [km^2]	1.56	1.56	7.81
Avg. Thickness of Chalk Group [m]	1904	781	597
Location	Located away from major faults, in an area where the Chalk Group is thickest.	Located on a salt-ridge, in an area where the Chalk Group is thinner.	Located on a salt-ridge, in an area where the Chalk Group is very thin, and where major faults are present.
Focus point	Background faulting	Influence of salt tectonics	Influence of salt tectonics, and major faulting

Table 6.1: This table displays the practical information regarding the three seismic crops of the TEPNL dataset. It also shows on what basis the locations of the seismic crops were chosen and with what reasoning.

6.1.1. Seismic Crop 1

Figure 6.2 displays the 3 Z-Slices, with both the original image consisting of OpendTect's Similarity Attribute with a Thinned Fault Likelihood overlay, and the interpreted fault networks as an overlay on the Similarity attribute with additional rose diagrams. As can be seen in figure 6.2 and table 6.2 the Z-Slices were taken at different depths. One at 1400m depth within the sediments of the Lower North Sea Group. One is located at a depth of 1555m, which means its located within the Ekofisk Formation. And one Z-Slice was taken at a depth of 2050m, located within the Ommelanden Formation of the Chalk Group.

Z-Slice 1: Lower North Sea Group

Table 6.2 displays an overview of the results of Z-Slice 1. A total of 77 faults were interpreted in this Z-Slice which results in a Fracture Density of 9.69km/km^2. Figure 6.2a displays the image that was enhanced in OpendTect. Figure 6.2b displays the fault interpretation made using figure 6.2a as input. When looking at figure 6.2b and its respective rose diagram it can be observed that there is not one dominant orientation present in the fault network. The rose diagram shows that there are 3 directions that were more interpreted that other orientations, which is also highlighted in table 6.2. The absence of a clear trend in this Z-Slice also comes forward when looking at the fault interpretations themselves. Faulting displays a polygonal pattern, and the fault network consists of mostly short faults.

Figure 6.3 display Frequency Distributions made from the extracted data of the interpreted fault model of Z-Slice 1 in orange. The Fault Length Frequency Distribution of Figure 6.3a, shows a normal distribution. Which means that smaller faults are distributed more, than larger faults. 70 out of an interpreted 77 faults are below 400m in length. Figure 6.3b displays the Frequency Distribution on Dip Angle of the interpreted faults. Observable is that the area has a wide range of fault dips; between 57° and vertical dips. However most interpreted faults display very steep dips with angles above 75°.

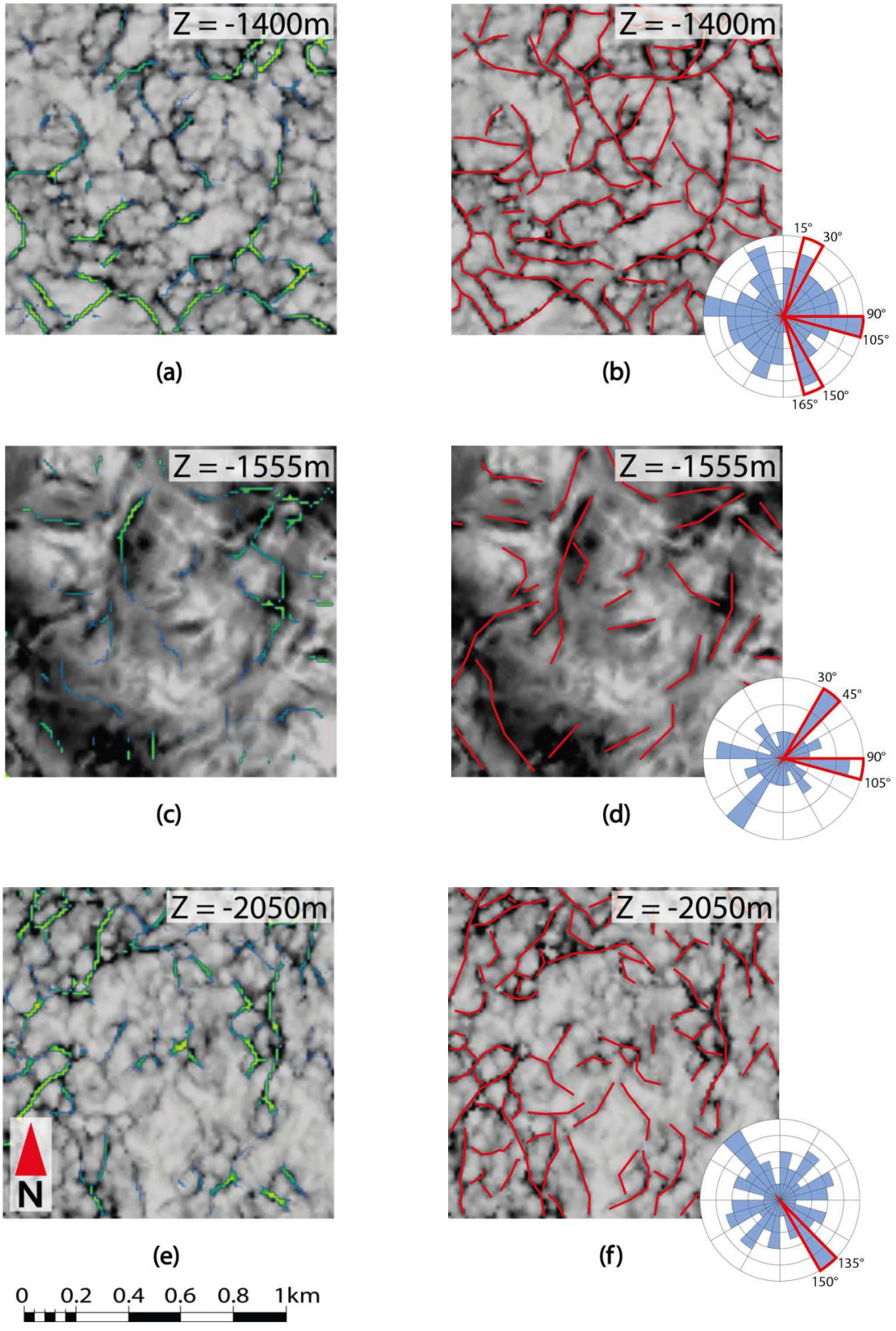

Figure 6.2: *These images display 3 Z-slices of seismic crop 1 extracted from the TEPNL dataset. The left side displays the original generated images (a, c and e), and the right side displays the images with interpreted faults and the corresponding rose diagrams (b, d and f).*

	Z-Slice 1	**Z-Slice 2**	**Z-Slice 3**
Depth [m]	1400	1555	2050
Formation	North Sea Gp.	Ekofisk Fm.	Ommelanden Fm.
Nr. of Faults Interpreted	77	31	65
P21 (Fracture Density) [km/km^2]	9.69	4.04	7.08
Fault Orientation [°]	3 dominant orientations: 15° - 30° 90° - 105° 150° - 165°	2 dominant orientations: 30° - 45° 90° - 105°	1 dominant orientation: 135° - 150° other orientations interpreted evenly
Fault Length [m]	Almost all faults <300m	Almost all faults <300m	Almost all faults <300m
Fault Dip Angle [°]	Wide distribution: Most faults 78° - 84°	Wide distribution: Most faults >75°	Wide distribution: Most faults >69°
Fault Geometry	Polygonal	Polygonal	Polygonal

Table 6.2: This table compares the various results of the three Z-Slices taken in Seismic Crop 1.

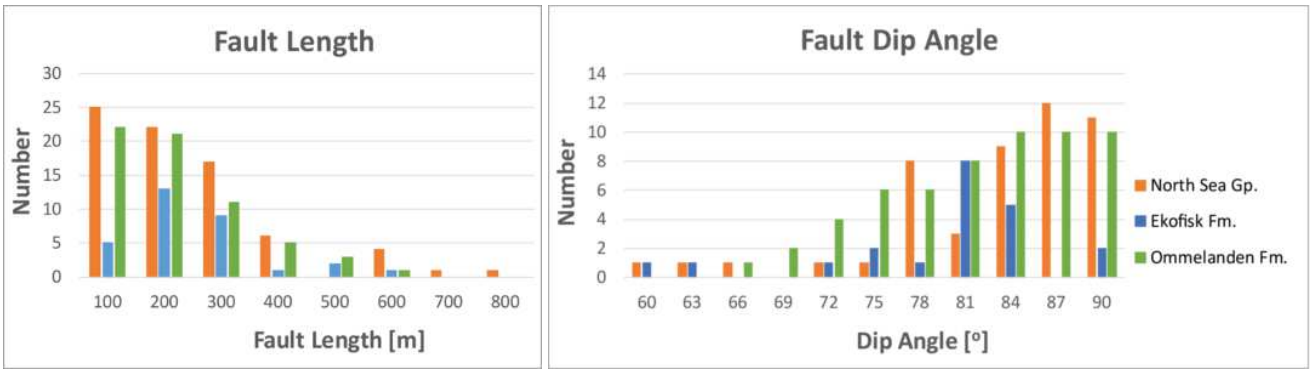

(a) (b)

Figure 6.3: *These images display Frequency Distribution diagrams extracted from the interpreted Z-Slices of Seismic Crop 1. Figure (a) displays a Frequency Distribution on Fault Length, whereas (b) displays a Frequency Distribution on Fault Dip Angle. All three Formations are shown: the North Sea Group in orange, the Ekofisk Formation in blue and the Ommelanden Formation in green.*

Z-Slice 2: Ekofisk Formation

An overview of the results of Z-Slice 2 are displayed in table 6.2. It shows that a total of 31 faults were interpreted, which resulted in a P21 of 4.04km/km^2. Figure 6.2c displays the output from OpendTect's seismic enhancing attributes, and figure 6.2d displays the fault interpretation based on OpendTect's output. When looking at figure 6.2c, it is observable that the image was not as clear as figure 6.2a, and that fault interpretation was slightly more challenging. When looking at figure 6.2d it is observable that there are not as many faults present as in figure 6.2a,b. The rose diagram shows that there are two dominant directions, which is also displayed in table 6.2. The faults display less connectivity than the faults of Z-Slice 1, and display a polygonal pattern.

Figure 6.3 display Frequency Distributions made from the extracted data of the interpreted fault model of Z-Slice 2 in blue. The Fault Length Frequency Distribution of Figure 6.3a, shows a slightly skewed distribution. Meaning that instead of the smallest fault being interpreted most, they are actually interpreted only a few times. Whereas slightly larger faults were interpreted more times. Faults in this area are short, as 27 out of 31 interpreted faults are smaller than 300m. Figure 6.3b displays a Frequency Distribution on Dip Angle of the interpreted faults. Observable is that the area has a wide range of fault dips; between 57° and vertical dips. However most interpreted faults display very steep dips with angles above 78°.

Z-Slice 3: Ommelanden Formation

Table 6.2 displays that in Z-Slice 3 a total of 65 faults were interpreted, resulting in a Fracture Density of 7.08km/km^2. Figure 6.2e displays the output consisting of the Similarity and TFL attributes, and figure 6.2f displays the fault interpretation based on the enhanced seismic image. Figure 6.2e displays a similar image to figure 6.2a. When looking at figure 6.2e it is observable that many faults have been interpreted with many different orientations. The rose diagram shows that there is one dominant direction between 135° and 150°, and that all the other orientations have been interpreted similar amount of times. This is observable as a polygonal fault pattern in the Z-Slices.

The Fault Length Frequency Distribution of figure 6.3a, shows a normal distribution. Out of an interpreted 65 faults 56 are below 300m in length, making this area very populated with short faults. Figure 6.3b displays a Frequency Distribution on Dip Angle of the interpreted faults. Observable is that the area has a wide range of fault dips; between 63° and vertical dips. However most interpreted faults display very steep dips with angles above 69°.

6.1.2. Seismic Crop 2

Figure 6.4 displays the 3 Z-Slices, with the original generated images from OpendTect on the left side, and the images with the interpreted fault models and rose diagrams on the right side. As can be seen in figure 6.4 and in table 6.3 the Z-Slices were taken at different depths. One at 780m depth, which is located within the sediments of the Lower North Sea Group. One is located within the Ekofisk Formation at a depth of 865m. And one Z-Slice was taken within the Ommelanden Formation of the Chalk Group at a depth of 1200m.

Z-Slice 1: Lower North Sea Group

Table 6.3 displays an overview of the results of Z-Slice 1. A total of 96 faults were interpreted in this Z-Slice which results in a P21 of 9.23km/km^2. When looking at figure 6.4b and as highlighted in table 6.3, it can be observed that there is one dominant orientation present in the fault network with a WNW-ESE orientation. Other orientations were interpreted roughly similar amount of times. When looking at the fault interpretation of figure 6.4b, the WNW-ESE trend is not clearly observable from the faults, however it is observable that a section of +-300m wide cuts the area roughly NW-SE in which faulting is absent. The faulting that was interpreted in the area displays polygonal patterns, and the fault network consists of mostly short, interconnected faults.

Figure 6.5 displays Frequency Distributions made from the extracted data of the interpreted fault model of Z-Slice 1 in orange. The Fault Length Frequency Distribution of Figure 6.5a, shows a normal distribution. Out of an interpreted 96 faults 87 are below 300m in length, making this area very populated with short faults. Figure 6.5b displays a Frequency Distribution on Dip Angle of the interpreted faults. Observable is that the area has a wide range of fault dips; between 66° and vertical dips. However most interpreted faults display very steep dips with angles above 78°.

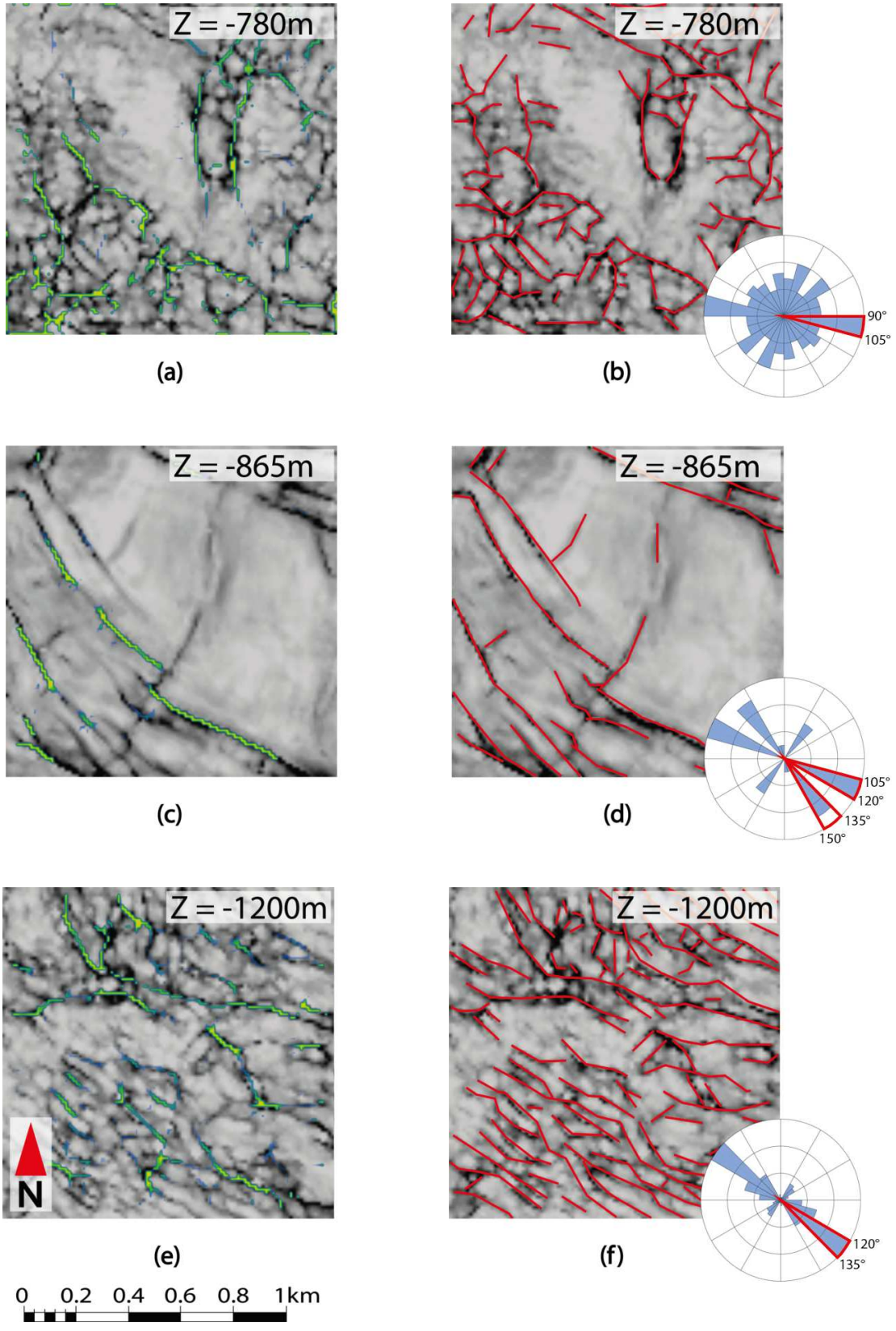

Figure 6.4: *These images display 3 Z-slices of seismic crop 2 extracted from the TEPNL dataset. The left side displays the original generated images (a, c and e), and the right side displays the images with interpreted faults and the corresponding rose diagrams (b, d and f).*

	Z-Slice 1	**Z-Slice 2**	**Z-Slice 3**
Depth [m]	780	865	1200
Formation	North Sea Gp.	Ekofisk Fm.	Ommelanden Fm.
Nr. of Faults Interpreted	96	17	86
P21 (Fracture Density) [km/km^2]	9.23	4.24	11.27
Fault Orientation [°]	1 dominant orientation: 90° - 105° other orientations interpreted evenly	2 dominant orientations: 105° - 120° 135° - 150°	1 dominant orientation: 120° - 135°
Fault Length [m]	Almost all faults <300m	Almost all faults 100m - 900m	Almost all faults <300m
Fault Dip Angle [°]	Wide distribution: Most faults >78°	Wide distribution: Most faults 75° - 84°	Wide distribution: Most faults 69° - 75° and >81°
Fault Geometry	Polygonal	Straight	Fracture Zone

Table 6.3: This table compares the various results of the three Z-Slices taken in Seismic Crop 2.

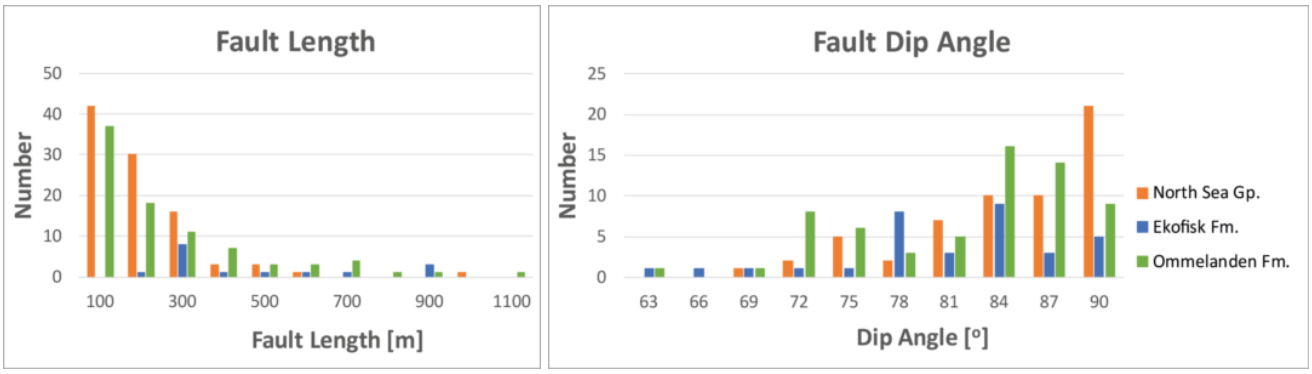

(a) (b)

Figure 6.5: *These images display Frequency Distribution diagrams extracted from the interpreted Z-Slices of Seismic Crop 2. Figure (a) displays a Frequency Distribution on Fault Length, whereas (b) displays a Frequency Distribution on Fault Dip Angle. All three Formations are shown: the North Sea Group in orange, the Ekofisk Formation in blue and the Ommelanden Formation in green.*

Z-Slice 2: Ekofisk Formation

An overview of the results of Z-Slice 2 are displayed in table 6.3. It shows that a total of 17 faults were interpreted, resulting in a Fracture Density of 4.24km/km^2. When looking at figure 6.4c, it is observable that faults in this section are generally longer and present in smaller numbers. Faults are generally straight, and cross-cut almost through the entire area. When looking at figure 6.4d it is observable that there are not as much faults present as in figure 6.4a,b. The rose diagram shows that there are two dominant directions between 105° and 120°, and between 135° and 150°. There is also one direction slightly less dominant perpendicular to the main dominant directions between 30° and 45°.

Figure 6.5 displays Frequency Distributions made from the extracted data of the interpreted fault model of Z-Slice 2 in Blue. The Fault Length Frequency Distribution of Figure 6.5a, shows a skewed distribution, where faults between 200m and 300m were interpreted the most. However this skewness could also be an effect of the small amount of 17 interpreted faults. Figure 6.5b displays a Frequency Distribution on Dip Angle of the interpreted faults. Observable is that the area has a wide range of fault dips; between 60° and vertical dips. However most interpreted faults display very steep dips with angles between 75° and 84°.

Z-Slice 3: Ommelanden Formation

Table 6.3 displays that in Z-Slice 3 a total of 86 faults were interpreted, which results in a P21 of 11.27km/km^2. Figure 6.4e displays the output consisting of the Similarity and TFL attributes, and figure 6.4f displays the fault interpretation based on the enhanced seismic image. Both the Similarity and TFL attributes interpret many faults with a dominant NW-SE orientation. The interpreted fault model of figure 6.4f and its respective rose diagram both show the same. The faults in this area have one clear dominant trend, resembling a fracture zone.

Figure 6.5 displays Frequency Distributions made from the extracted data of the interpreted fault model of Z-Slice 3 in Green. The Fault Length Frequency Distribution of Figure 6.5a, shows a normal distribution, where faults below 400m were interpreted the most. Out of a total of 86 faults, 71 interpreted faults have a length below 400m. Figure 6.5b displays a Frequency Distribution on Dip Angle of the interpreted faults. Observable is that the area has a wide range of fault dips; between 60° and vertical dips. However most interpreted faults display very steep dips with angles above 81°, which is very steep even for extensional faults.

6.1.3. Seismic Crop 3

Figure 6.6 displays the 2 Z-Slices that were taken at this location. The original generated images from OpendTect on the left side, and the images with the interpreted fault models as overlay on the right side. As can be seen in figure 6.6 and highlighted in table 6.4, Z-Slice 1 was taken at a depth of 730m in the sediments of the North Sea Group. The sedimentary layers presently are organized in an anticlinal structure. For that reason this area can not be treated as a layer-cake model. Only 1 Z-Slice was taken within the Chalk Group. The Z-Slice solely displays the Ommelanden Formation as the Ekofisk Formation is absent in this area (see inline 7212 of figure 5.8. The sections NE and SW of the interpreted area were left uninterpreted as they fell outside of the Chalk Group due to the anticlinal structure of the sediments in this area.

Z-Slice 1: North Sea Group

Table 6.4 displays an overview of the results of Z-Slice 1. A total of 184 faults were interpreted in this Z-Slice which results in a Fracture Density of 7.26km/km^2. When looking at figure 6.6b and its respective rose diagram it can be observed that there is one dominant orientation present in the fault network with a NW-SE orientation. Both in the rose diagram as in the interpreted faults a second, much less dominant, direction is found perpendicular to the NW-SE trend. These faults are observable SW and NE of the NW-SE trending faults in the center, and have an orientation between 30° and 75°. When looking at the fault interpretation of figure 6.6b, the NW-SE trend is clearly observable from the faults. The faulting that was interpreted in the area is directional, and consists of both long and short faults. When looking at the center of the antiform, the fracture patterns look similar to those of figure 6.4f.

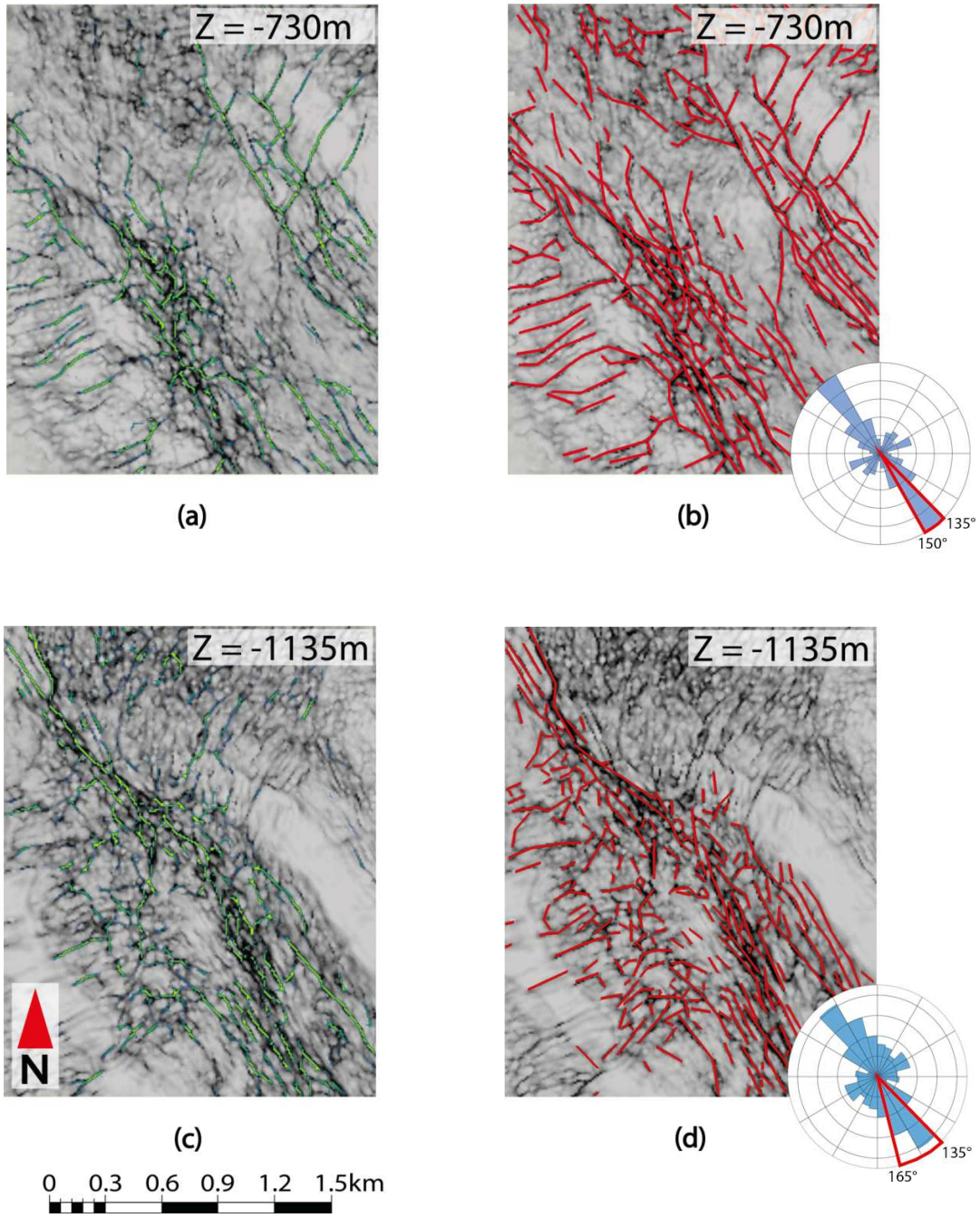

Figure 6.6: *These images display 1 Z-slice of seismic crop 3, located on the top of a salt-ridge, extracted from the TEPNL dataset. The left side displays the original generated image (a), and the right side displays the image with interpreted faults and the corresponding rose diagram (b).*

Whereas the perpendicular faults that are visible to the NE and SW of the NW-SE fracture zone, show more resemblance to the perpendicular faults of figure 6.4d. Figure 6.7 displays Frequency Distributions made from the extracted data of the interpreted fault model of Z-Slice 1 in orange. The Fault Length Frequency Distribution of Figure 6.7a, shows a normal distribution, where faults below 600m were interpreted the most. Figure 6.7b displays a Frequency Distribution on Dip Angle of the interpreted faults. Observable is that the area has a wide range of fault dips; between 60° and vertical dips. However most interpreted faults display very steep dips with angles above 72°.

	Z-Slice 1	**Z-Slice 2**
Depth [m]	730	1135
Formation	North Sea Gp.	Ommelanden Fm.
Nr. of Faults Interpreted	184	216
P21 (Fracture Density) [km/km^2]	7.26	5.03
Fault Orientation [°]	1 dominant orientation: 135° - 150°	1 dominant orientation: 135° - 165°
Fault Length [m]	Almost all faults <600m	Almost all faults <600m
Fault Dip Angle [°]	Wide distribution: Most faults >72°	Wide distribution: Most faults >69°
Fault Geometry	Fracture Zone	Fracture Zone

Table 6.4: This table compares the various results of the two Z-Slices taken in Seismic Crop 3.

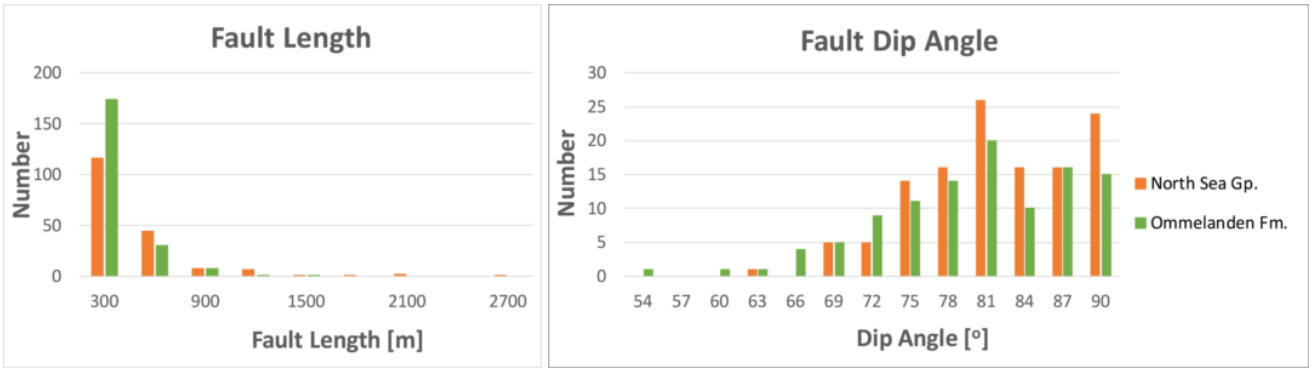

(a) (b)

Figure 6.7: *These images display Frequency Distribution diagrams extracted from the interpreted Z-Slices of Seismic Crop 3. Figure (a) displays a Frequency Distribution on Fault Length, whereas (b) displays a Frequency Distribution on Fault Dip Angle. Two Formations are shown: the North Sea Group in orange and the Ommelanden Formation in green.*

Z-Slice 2: Ommelanden Formation

Table 6.4 displays that in Z-Slice 2 a total of 216 faults have interpreted, which results in a P21 of 5.03km/km^2. When looking at figure 6.6d and its respective rose diagram it can be observed that, like in Z-Slice 1, there is one dominant orientation present in the fault network with a NW-SE orientation. Like in Z-Slice 1, a second, much less dominant orientation is found perpendicular to the NW-SE trend. These faults are observable SW of the NW-SE trending faults in the center, and have an orientation between 45° and 75°.The faulting that was interpreted in the area is directional, and consists of mostly short faults. When looking at the center of the antiform, the fracture patterns look similar to those of figures 6.4f and of 6.6b.

Figure 6.7 displays Frequency Distributions made from the extracted data of the interpreted fault model of Z-Slice 2 in green. The Fault Length Frequency Distribution of Figure

6.7a shows a normal distribution, where faults below 600m were interpreted the most. Figure 6.7b displays a Frequency Distribution on Dip Angle of the interpreted faults. Observable is that the area has a wide range of fault dips; between 51° and vertical dips. However most interpreted faults display very steep dips with angles above 69°.

6.2. P10

Two seismic crops, or steering-cubes, were generated from the P10 dataset. Figure 6.8 shows the locations of the two crops. Table 6.5 displays practical information regarding the two seismic crops, and the reasoning behind their positioning. The location of Seismic Crop 4 was chosen for it being away from major faulting and for the thickness of the Chalk Group at this position. As can be see in figure 6.8 there are almost no major faults surrounding this crop, making it easier to look at background structures, instead of looking at effects caused by regional extensional tectonics. The location of Seismic Crop 5 was chosen for the Chalk Group being thinnest at this position and the absence of major tectonic related faulting.

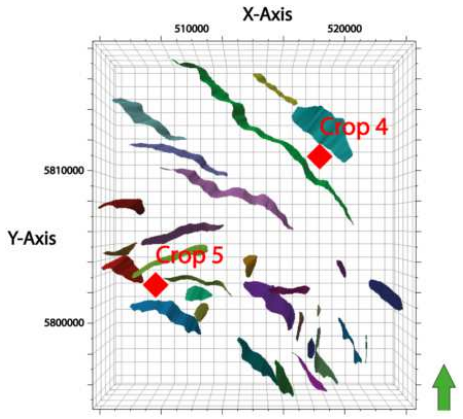

Figure 6.8: *An overview of the P10 dataset and fault model, with the displayed locations of the two seismic crops.*

	Seismic Crop 4	**Seismic Crop 5**
Area [km^2]	1.56	1.56
Avg. Thickness of Chalk Group [m]	485	261
Location	Located away from major faults, in an area where the Chalk Group is thickest.	Located away from major faults, in an area where the Chalk Group is thinnest.
Focus point	Background faulting, and influence of thickness	Background Faulting, and influence of thickness

Table 6.5: This table displays the practical information regarding the two seismic crops of the P10 dataset. It also shows on what basis the locations of the seismic crops were chosen and with what reasoning.

6.2.1. Seismic Crop 4

Figure 6.9 displays the 3 Z-Slices, with both the original image consisting of OpendTect's Similarity Attribute with a TFL overlay, and the interpreted fault networks as an overlay with

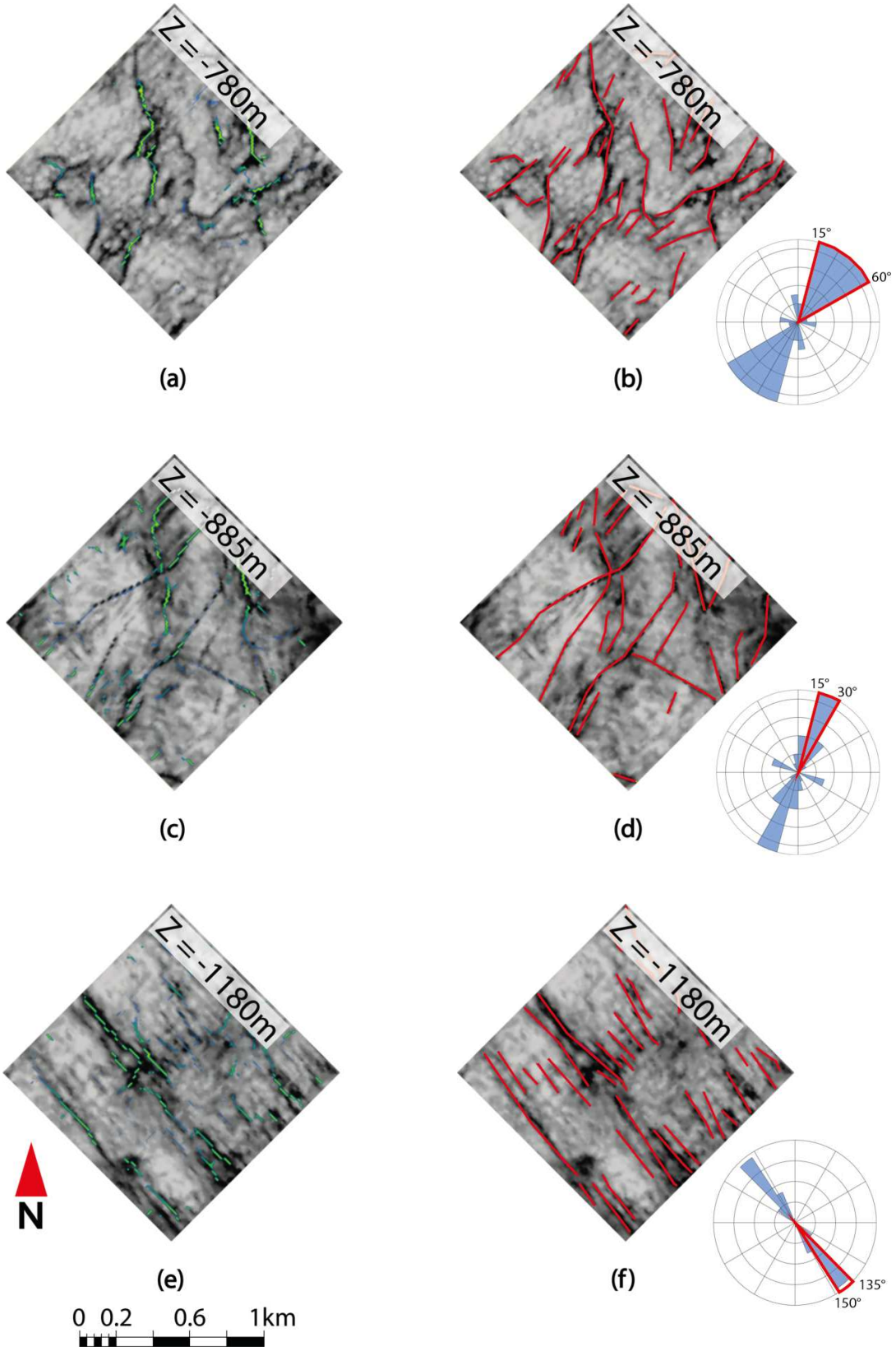

Figure 6.9: *These images display Frequency Distribution diagrams extracted from the interpreted Z-Slices of Seismic Crop 4. The left side displays the Frequency Distributions on Fault Length (a, c and e), and the right side displays the Frequency Distributions on Dip Angle (b, d and f).*

additional rose diagrams. As can be seen in figure 6.9 and table **??** the Z-Slices were taken at different depths. One at 780m depth, which is located within the sediments of the Lower North Sea Group. One is located within the Ekofisk Formation at a depth of 885m. And one Z-Slice was taken at a depth of 1180m in the Ommelanden Formation of the Chalk Group.

Z-Slice 1: Lower North Sea Group

Table 6.6 displays an overview of the results of Z-Slice 1. A total of 36 faults have been interpreted in this Z-Slice, resulting in a Fracture Density of 5.73km/km^2. Figure 6.9a displays the enhanced image from OpendTect and figure 6.4b displays the fault interpretation made using figure 6.4a as input. When looking at figure 6.4b and its respective rose diagram it can be observed that there is one dominant orientation present in the fault network with a NE-SW orientation between 15° and 60°. Only few other faults were interpreted with different orientations. When looking at the fault interpretation of figure 6.4b, the NE-SW trend is observable. The faulting that was interpreted in the area has a dominant orientation, and the faults in the fault network are mostly interconnected. The faulting pattern can be recognized to be slightly polygonal.

Figure 6.10 displays Frequency Distributions made from the extracted data of the interpreted fault model of Z-Slice 1 in orange. The Fault Length Frequency Distribution of Figure 6.10a, shows a normal distribution, where faults below 400m were interpreted the most. Out of a total of 36 faults, 31 interpreted faults have a length below 400m. Figure 6.10b displays a Frequency Distribution on Dip Angle of the interpreted faults. Observable is that the area has a wide range of fault dips; between 57° and vertical dips. However most interpreted faults display very steep dips with angles above 80°, which is very steep even for extensional faults.

	Z-Slice 1	**Z-Slice 2**	**Z-Slice 3**
Depth [m]	780	885	1180
Formation	North Sea Gp.	Ekofisk Fm.	Ommelanden Fm.
Nr. of Faults Interpreted	36	24	33
P21 (Fracture Density) [km/km^2]	5.73	5.11	4.98
Fault Orientation [°]	1 dominant orientation: 15° - 60°	1 dominant orientation: 15° - 30°	1 dominant orientation: 135° - 150°
Fault Length [m]	Almost all faults <400m	Almost all faults <400m	Almost all faults <400m
Fault Dip Angle [°]	Wide distribution: Most faults >80°	Narrow distribution: Most faults >80°	Wide distribution: Most faults >80°
Fault Geometry	Polygonal	Straight	Straight

Table 6.6: This table compares the various results of the three Z-Slices taken in Seismic Crop 4.

Z-Slice 2: Ekofisk Formation

An overview of the results of Z-Slice 2 are displayed in table 6.6. It shows that a total of 24 faults were interpreted, resulting in a P21 of 5.11km/km^2. When looking at figure 6.9c, it is observable that faults in this section are generally longer and present in smaller numbers when compared to a.o figures 6.2 and 6.6. Faults are generally straight, and cut almost

through the entire area. The rose diagram shows that there is one dominant orientation in this seismic crop, which is also highlighted in table 6.6.

Figure 6.10 displays Frequency Distributions made from the extracted data of the interpreted fault model of Z-Slice 2 in blue. The Fault Length Frequency Distribution of Figure 6.10a, shows a little bit skewed distribution, where faults below 400m were interpreted the most. Out of a total of 24 faults, 19 interpreted faults have a length below 400m. Figure 6.10b displays a Frequency Distribution on Dip Angle of the interpreted faults. Observable is that the area has a small range of fault dips; between 80° and vertical dips. Which is very steep for extensional faults.

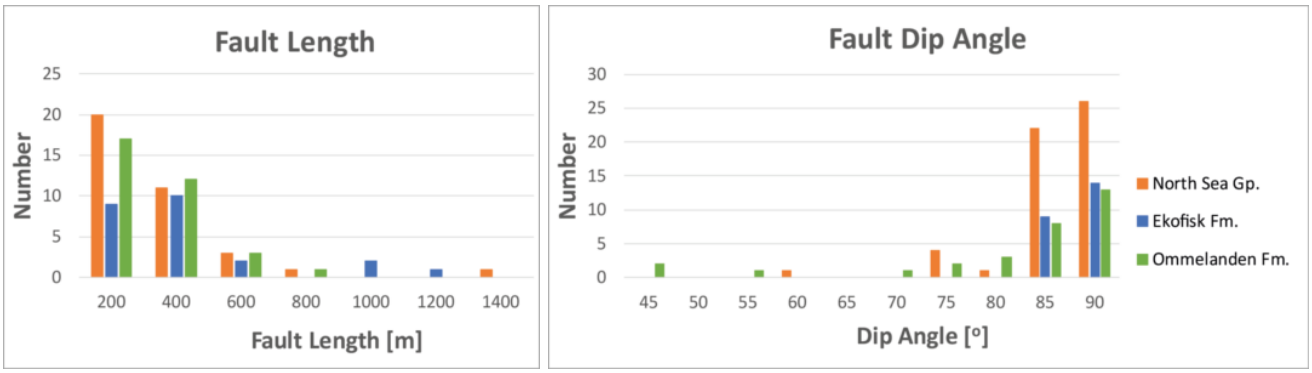

(a) (b)

Figure 6.10: *These images display Frequency Distribution diagrams extracted from the interpreted Z-Slices of Seismic Crop 4. Figure (a) displays a Frequency Distribution on Fault Length, whereas (b) displays a Frequency Distribution on Fault Dip Angle. All Formations are shown: the North Sea Group in orange, the Ekofisk Formation in blue and the Ommelanden Formation in green.*

Z-Slice 3: Ommelanden Formation

Table 6.6 displays that in Z-Slice 3 a total of 33 faults were interpreted, which resulted in a Fracture Density of 4.98km/km^2. Figure 6.9e displays the output consisting of the Similarity and TFL attributes, and figure 6.9f displays the fault interpretation based on the enhanced seismic image. Both the Similarity and TFL attributes interpret faults with a very dominant NW-SE orientation. The interpreted fault model of figure 6.9f and its respective rose diagram both show the same. The faults in this area have one clear dominant trend. Almost all faults have an orientation between 135° and 150°, as highlighted in table 6.6.

Figure 6.10 displays Frequency Distributions made from the extracted data of the interpreted fault model of Z-Slice 3 in green. The Fault Length Frequency Distribution of Figure 6.10a, shows a skewed distribution, where faults between 100m and 300m were interpreted the most. Figure 6.7b displays a Frequency Distribution on Dip Angle of the interpreted faults. Observable is that the area has a very wide range of fault dips; between 42° and vertical dips. However most faults were interpreted above a dip angle of 80°, which is very steep for extensional faults.

6.2.2. Seismic Crop 5

Figure 6.11 displays the 3 Z-Slices, with the original generated images from OpendTect on the left side, and the images with the interpreted faults as overlay on the right side. As can be seen in figure 6.11 and table 6.7 the Z-Slices were taken at different depths. One at 565m depth, which is located within the sediments of the Lower North Sea Group. One is located

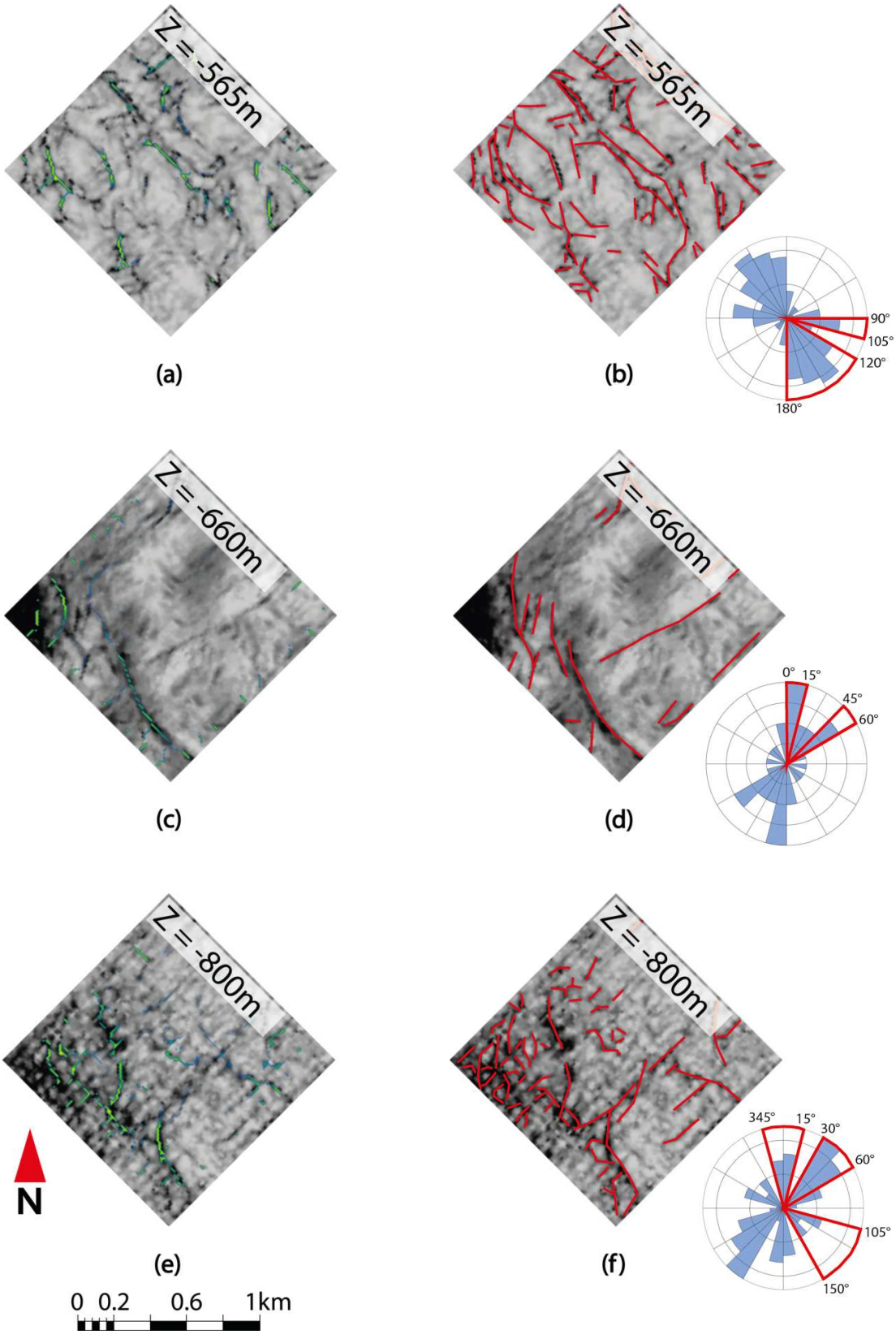

Figure 6.11: *These images display 3 Z-slices of seismic crop 5 extracted from the P10 dataset. The left side displays the original generated images (a, c and e), and the right side displays the images with interpreted faults and the corresponding rose diagrams (b, d and f).*

at a depth of 660m, which means its located within the Ekofisk Formation. And one Z-Slice was taken at a depth of 800m, within the Ommelanden Formation of the Chalk Group.

Z-Slice 1: Lower North Sea Group

Table 6.7 displays an overview of the results of Z-Slice 1. A total of 64 faults were interpreted, resulting in a P21 of 7.42km/km^2. When looking at figure 6.11b and its respective rose diagram it can be observed that there are two dominant orientations present in the fault network. One with a NNW-SSE orientation between 120° and 180°, and one with a WNW-ESE orientation between 90° and 105°, this is also displayed in table 6.7. When looking at the fault interpretation of figure 6.11b, the NW-SE trend is not clearly observable, as the interpreted faults are mostly short, and as interconnected as for example in figures 6.4 and 6.6. The faulting that was interpreted in the area has two dominant orientations, and can be interpreted as polygonal in some places. The fault network consists of short, mostly unconnected, faults.

	Z-Slice 1	**Z-Slice 2**	**Z-Slice 3**
Depth [m]	565	660	800
Formation	North Sea Gp.	Ekofisk Fm.	Ommelanden Fm.
Nr. of Faults Interpreted	64	17	62
P21 (Fracture Density) [km/km^2]	7.42	3.02	4.97
Fault Orientation [°]	2 dominant orientations: 90° - 105° 120° - 180°	2 dominant orientations: 0° - 15° 45° - 60°	3 dominant orientations: 345° - 15° 30° - 60° 105° - 150°
Fault Length [m]	Almost all faults <300m	Almost all faults 100m - 800m	Almost all faults <300m
Fault Dip Angle [°]	Wide distribution: Most faults >78°	Narrow distribution: Most faults >84°	Wide distribution: Most faults >81°
Fault Geometry	Polygonal	Straight	Polygonal

Table 6.7: This table compares the various results of the three Z-Slices taken in Seismic Crop 5.

Figure 6.12 displays Frequency Distributions made from the extracted data of the interpreted fault model of Z-Slice 1 in orange. The Fault Length Frequency Distribution of Figure 6.12a, shows a normal distribution, where faults below 300m were interpreted the most. Figure 6.12b displays a Frequency Distribution on Dip Angle of the interpreted faults. Observable is that the area has a wide range of fault dips; between 60° and vertical dips. However most faults were interpreted above a dip angle of 80°, which is very steep for extensional faults.

Z-Slice 2: Ekofisk Formation

An overview of the results of Z-Slice 2 are displayed in table 6.7. It shows that a total of 17 faults were interpreted, resulting in a Fracture Density of 3.02km/km^2. When looking at figure 6.11c, it is observable only a few faults were interpreted in this area, and that orientations of these faults can not immediately be distinguished from figure 6.11c. Image quality is similar to figure 6.2c and 6.9e. Faults are generally straight, and individual; only

3 faults show signs of interconnection. The rose diagram shows that there are two dominant orientations in this seismic crop between 0° and 15°, and between 45° and 60°.

Figure 6.12 displays Frequency Distributions made from the extracted data of the interpreted fault model of Z-Slice 2 in blue. The Fault Length Frequency Distribution of Figure 6.12a, shows a slightly skewed distribution, where faults between 100m and 200m were interpreted the most. Figure 6.12b displays a Frequency Distribution on Dip Angle of the interpreted faults. Observable is that the area has a narrow range of fault dips; with one interpretation between 70° and 75°, whereas all the other faults have dips above a dip angle of 84°, which is very steep for extensional faults.

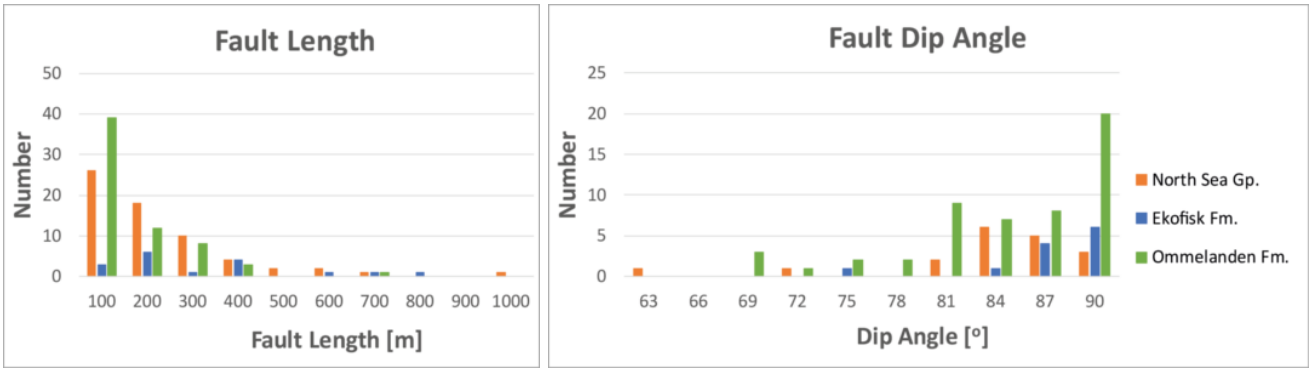

(a) (b)

Figure 6.12: *These images display Frequency Distribution diagrams extracted from the interpreted Z-Slices of Seismic Crop 5. Figure (a) displays a Frequency Distribution on Fault Length, whereas (b) displays a Frequency Distribution on Fault Dip Angle. All Formations are shown: the North Sea Group in orange, the Ekofisk Formation in blue and the Ommelanden Formation in green.*

Z-Slice 3: Ommelanden Formation

Table 6.7 displays that in Z-Slice 3 a total of 62 faults have been interpreted, which results in a P21 of 4.97km/km^2. Like in figure 6.11c, image quality was relatively poor, and the interpretation of faults was relatively challenging. Both the Similarity and TFL attributes interpreted few faults. The interpreted fault model of figure 6.11f and its respective rose diagram both show the same; many short, unconnected faults with many different orientation. In the South and Southwest of this area faults display polygonal faulting patterns. The faults in this area have one dominant trend between 30° and 60°. However there are two other directions that have been interpreted many times; between 345° and 15°, and between 105° and 150°.

Figure 6.12 displays Frequency Distributions made from the extracted data of the interpreted fault model of Z-Slice 3 in green. The Fault Length Frequency Distribution of Figure 6.12a, shows a normal distribution, where faults below 300m were interpreted the most. Figure 6.12b displays a Frequency Distribution on Dip Angle of the interpreted faults. Observable is that the area has a wide range of fault dips; between 66° and vertical dips. However most faults were interpreted above a dip angle of 78°, which is very steep for extensional faults.

6.3. Discussion

To determine what are the main drivers behind deformation on a local level, five seismic crops, or steering-cubes, were generated out of both the P10 dataset and the TEPNL dataset. The results of this chapter show that within the five seismic crops fracture geometries vary between seismic crops and even between Z-Slice within seismic crops. Based on geometric properties the different Z-Slices have been grouped together.

Table 6.8 displays a comparison of 7 Z-Slices out of all seismic crops, except for seismic crop 3. As displayed all fault models of the Z-Slices have either more than one dominant fault orientation, or have one very wide dominant orientation such as Z-Slice 1 of Seismic Crop 4. On that basis these Z-Slices were grouped together.

When comparing other properties of these Z-Slices it is observable that fault lengths are generally short (<300m), and fault dip angles are generally steep (>70°). The combination of these geometric properties show that these Z-Slices do in fact display polygonal fracture patterns. Cartwright et al. (2003) and Lonergan et al. (1998a) state that ”Polygonal Fault Systems are marked by normal faults with lengths between 100-1000m, that are organized in a characteristic polygonal pattern without a regionally consistent preferred strike orientation”. ”Polygonal faults are generally planar with dips between 30° and 70°” (Goulty, 2008). Both citations describe the geometric properties of the Z-Slices of table 6.8. A comparison showing first order similarities between research done by Cartwright (2011) and this research is displayed in figure 6.13.

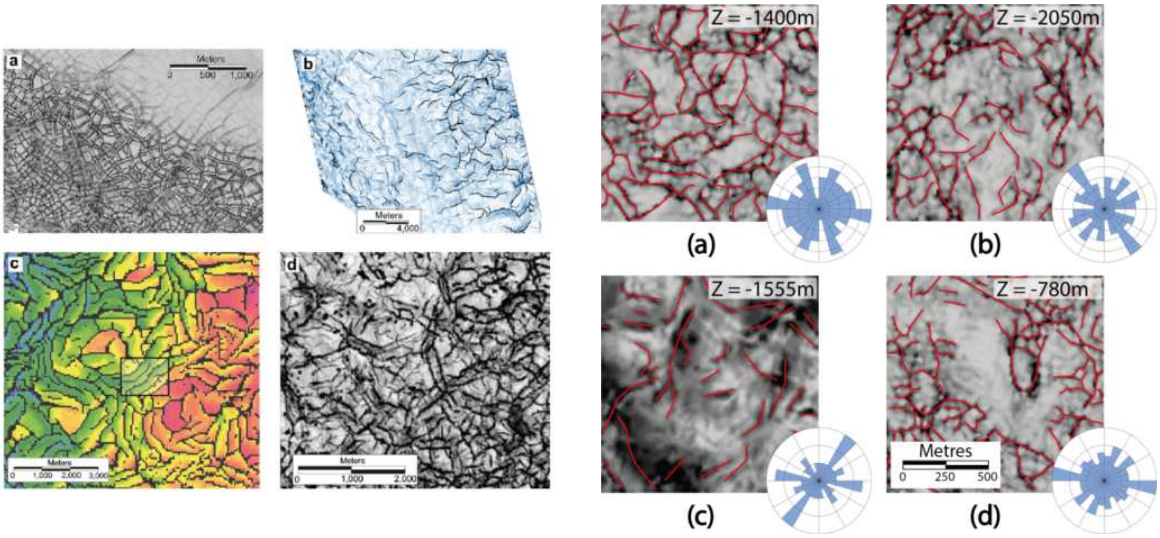

Figure 6.13: *This image displays the results of research done by Cartwright (2011), showing polygonal fault systems of various scales on the left side. And results from this study on the right. Observable is that the polygonal fault systems of this research show first order similarities to the ones of Cartwright (2011).*

Observable is that almost all polygonal fracture patterns are located in the North Sea Group, as 4 out of 7 Z-Slices are located in that lithological group. Also it is observable that generally polygonal fracture patterns are absent in the Ekofisk Formation, as only in Seismic Crop 1 polygonal faulting is present. Apparently polygonal faulting has a preference for lithology. This is substantiated by Cartwright and Lonergan (1996) and Lonergan et al. (1998a), who state that polygonal faulting patterns are believed to form due to fluid expulsion during early compaction stages. Eventual failure can be achieved in three ways: by an increase in pore fluid pressure, through tensile stresses generated by pore fluid loss, or by a combination of the two processes. According to Cartwright and Lonergan (1996) fluid expulsion are the most plausible theories as far-field tectonic stresses are generally not considered

to be of influence. Cartwright and Dewhurst (1996 have identified over 28 basins worldwide in which polygonal fault systems are present in both siliciclastic sediments and carbonates.

Crop	Z-Slice	*Formation*	*Orientation [°]*	*Fault Length [m]*	*Fault Dip Angle [°]*	*P21 [km/km^2]*
Seismic Crop 1	**Z-Slice 1**	North Sea Gp.	15° - 30° 90° - 105° 150° - 165°	<300m	78° - 84°	9.69
	Z-Slice 2	Ekofisk Fm.	30° - 45° 90° - 105°	<300m	>75°	4.04
	Z-Slice 3	Ommelanden Fm.	135° - 150° other orientations interpreted evenly	<300m	>69°	7.08
Seismic Crop 2	**Z-Slice 1**	North Sea Gp.	90° - 105° other orientations interpreted evenly	<300m	>78°	9.23
Seismic Crop 4	**Z-Slice 1**	North Sea Gp.	15° - 60°	<400m	>80°	5.73
Seismic Crop 5	**Z-Slice 1**	North Sea Gp.	90° - 105° 120° - 180°	<300m	>78°	7.42
	Z-Slice 3	Ommelanden Fm.	345° - 15° 30° - 60° 105° - 150°	<300m	>81°	4.97

Table 6.8: This table displays a comparison made between all seismic crops displaying polygonal fracture patterns.

Table 6.9 displays a comparison of 4 Z-Slices out of all seismic crops, except for seismic crops 1 and 3. As displayed all fault models of the Z-Slices have either one dominant fault orientation, or have two dominant orientation close together.

When comparing other properties of these Z-Slices it is observable that fault lengths are generally slightly longer (<400m) and more widespread (Z-Slice 2 of Seismic Crops 2 and 5), and fault dip angles are generally very steep (>80°). Observable is that these fracture patterns are mostly observable in the Ekofisk Formation, with the exception of Seismic Crop 4 in which this pattern is also present in the Ommelanden Formation.

Based on the locations of these crops it is observable that these fracture patterns are mostly present in the P10 dataset. As implied in chapter 5, the P10 dataset is mostly affected by regional extensional tectonics. However implied that the main driver behind deformation would be extensional far field tectonics, roughly NW-SE orientations would be expected. The case however is that most faults are roughly perpendicular to this orientation. However according to Duffy et al. (2015), it is possible in multiphase rifts for non-colinear faults to develop (figure 6.14). These can be cause by either along-strike displacement variations, or due to stress-perturbations. In both cases it would be expected that the orientations would be perpendicular to the major extensional faults as is the case.

For Z-Slice 2 of Seismic Crop 2 on the other side above explanation does not suffice, as the orientations in this Z-Slice are parallel to the expected regional NW-SE orientation present in the Dutch subsurface. In this case the driving force behind deformation is most likely halokinesis of the underlying salt. At the location of Seismic Crop 2 the salt has formed a NW-SE trending ridge, which forced overlying sediments in an anticlinal shape. Due to flexure of the antiform, the lowest layers experience mostly compression, whereas higher up this becomes extension. This compression is something we witness in the Ommelanden Formation of Seismic Crop 2 (table 6.10). As mentioned above, due to the flexure of the anticline

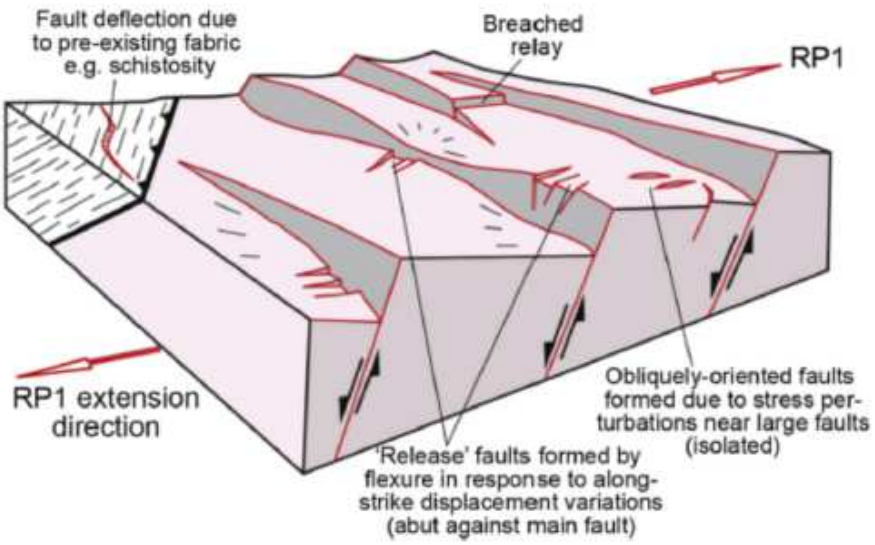

Figure 6.14: *Schematic drawing showing simple large-scale co-linear faults developed during a single-phase of rifting as well as the typical locations of any non-colinear faults that may develop. These non-colinear structures consist of Release Faults, Breached Relays and Isolated Obliquely-oriented Faults formed by stress perturbations near large faults (Duffy et al., 2015).*

the lowest layers experience most deformation, likely in the form of compression. Whereas to the top this deformation becomes extensional in nature. The Z-Slice of the Ommelanden Formation displays a fracture pattern resembling a fracture zone. This is also noticeable in the P21 as it has the highest value per square kilometer of 11.27. However when we travel up we notice in the Ekofisk Formation that the deformation gets less when traveling away from the center of the antiform, as the P21 is only 4.24 km/km^2. When traveling up even more the North Sea Group, we see that there is no influence of halokinesis anymore as the Z-Slice displays a polygonal fracture pattern.

Crop	***Z-Slice***	*Formation*	*Orientation [°]*	*Fault Length [m]*	*Fault Dip Angle [°]*	*P21 [km/km^2]*
Seismic Crop 2	**Z-Slice 2**	Ekofisk Fm.	105° - 120° 135° - 150°	100m - 900m	>78°	4.24
Seismic Crop 4	**Z-Slice 2**	Ekofisk Fm.	15° - 30°	<400m	>80°	5.11
	Z-Slice 3	Ommelanden Fm.	0° - 15° 45° - 60°	<400m	>80°	4.98
Seismic Crop 5	**Z-Slice 2**	Ekofisk Fm.	0° - 15° 45° - 60°	100m - 800m	>78°	3.02

Table 6.9: This table displays a comparison made between all seismic crops displaying straight, elongated faults.

Table 6.10 displays a comparison of 3 Z-Slices of Seismic Crops 2 and 3. As displayed all fault models of the Z-Slices have only one dominant fault orientation, with a NW-SE strike.

When comparing other properties of these Z-Slices it is observable that fault lengths are generally slightly longer (<600m), and fault dip angles are generally steep (>70°). Observable is that these fracture patterns are mostly observable in the Ommelanden Formation, with the exception of Seismic Crop 3 in which this pattern is also present in the North Sea Group.

Based on the locations of these crops it is observable that these fracture patterns are only present in the TEPNL dataset. As implied in chapter 5, the TEPNL dataset is mostly affected by salt tectonics, and not so much by regional extensional tectonics. This is also visible in

both Seismic Crops 2 and 3, which are located on NW-SE trending salt ridges. The difference between these two is that there are multiple major faults present in Seismic Crop 3. Above Z-Slice 3 of Seismic Crop 2 was already mentioned, being driven by the flexure of the antiform on which it is located.

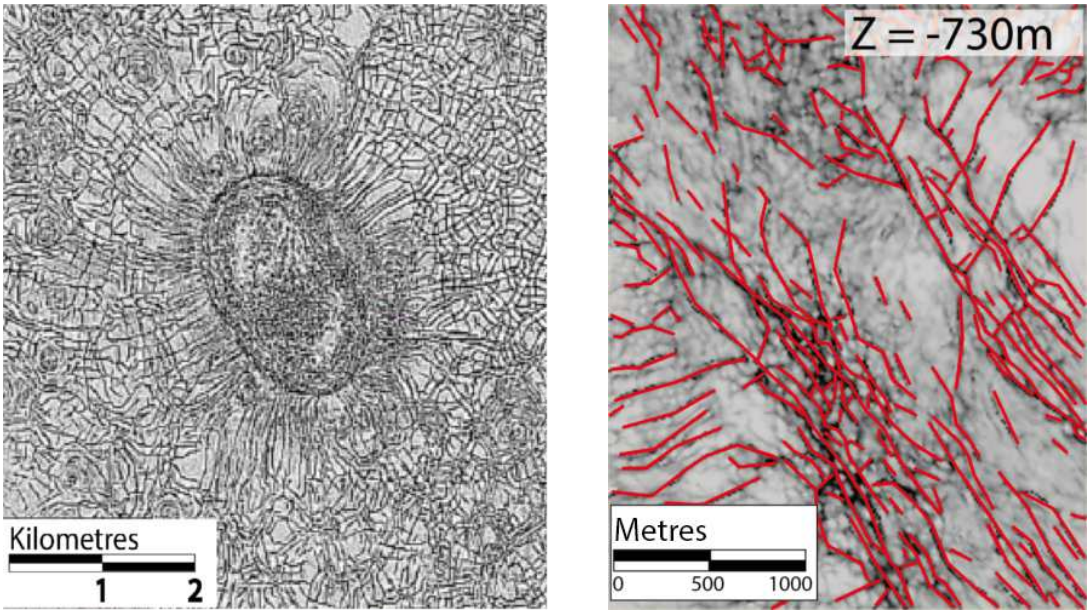

Figure 6.15: *A comparison is shown between results of a study by Cartwright (2011 and on the right side an image of Z-Slice 1 of Seismic Crop 3, displaying similar structures despite being located on top of a salt-ridge instead of a diapir. The research done by Cartwright (2011) displays structures proposed by Carruthers et al. (2013).*

The Z-Slices of Seismic Crop 3 display very similar fracture patterns, and observable in table 6.10 they also display very similar geometric properties. Like in Seismic Crop 2, the main driving mechanism behind deformation is salt tectonics. Halokinesis formed the NW-SE trending salt-ridge on which the crop is located, forcing the overlying layers in an anticlinal shape. The major faults present in Seismic Crop 3 however are related to collapse of the layers overlying the salt. However observable in both Z-Slices of Seismic Crop 3 is that many faults are located perpendicularly to the main NW-SE fault zone. Carruthers et al. (2013) researched radial faulting of salt diapirs in the North Sea. The sediments overlying the diapirs consisted of polygonal faulted mudrocks, similar to our area and to the one Cartwright (2011) did research on (figure 6.15). Carruthers et al. (2013) also witnessed the perpendicular faults to the “master fault”, and suggested that these perpendicular faults form due to hoop extension, caused by the rising of the salt. Carruthers et al. (2013 also suggest that a distance of at least 1km is needed in order to transition the halokinesis related faulting back to the polygonal faulting.

Crop	**Z-Slice**	*Formation*	*Orientation [°]*	*Fault Length [m]*	*Fault Dip Angle [°]*	*P21 [km/km^2]*
Seismic Crop 2	**Z-Slice 3**	Ommelanden Fm.	120° - 135°	<300m	69° - 75° >81°	11.27
Seismic Crop 3	**Z-Slice 1**	North Sea Gp.	135° - 150°	<600m	>72°	7.26
	Z-Slice 2	Ommelanden Fm.	135° - 165°	<600m	>69°	5.03

Table 6.10: This table displays a comparison made between all seismic crops displaying fracture zones.

6.3.1. Software Limitations

As can be observed in this research OpendTect is able to generate clear, noise-free images out of seismic datasets. The combination of OpendTect's capabilities to Dip-Steer seismic data, and to apply fracture enhancing attributes and filters to the dip-steered cubes, allows one to extract even the smallest faults above seismic resolution. This is substantiated through research done by for example Qayyum et al. (2010), Alai et al. (2014), Zhang et al. (2014) and Jaglan et al. (2015). However during this research still certain limitations were observed.

1. There is hardly distinction between fractured chalks or salt.

When focusing on the chalks that overlie the multiple salt-domes/diapirs in the TEPNL dataset, it was observed that there is no real distinction in OpendTect between faulted chalks or salt. This is observable in figure 6.16a. The Inline of figure 6.16a shows the absence of observable difference between both lithologies. Figure 6.16a displays a more or less homogeneous, fractured medium in both lithologies (chalk in green, salt in pink). In both the vertical and the horizontal directions no clear boundary can be observed between the chalks and the salts.

2. When interpreting Z-slices through steeply dipping layers it is hard to distinct between fault or layer/lithology change.

Another observation that was made when analyzing the Z-slice of the salt-ridge in Seismic Crop 3 (Figure 6.16), was the fact that surrounding the salt, no distinction could be made between NW-SE trending faults or dipping layers to either the NE or SW. Since these attributes are using the continuity of seismic reflectors, you expect to find clear boundaries where faults cut through layers; you would not expect clear boundaries where a Z-slice would cut a dipping layer. However the contrary was observed. The red oval in figure 6.16 displays on both an inline and Z-Slice the area where steeply eastward dipping layers are imaged as NW-SE trending faults. The solution to this problem is to use geological knowledge of faults, and to compare in-/crosslines to Z-Slices, as the comparison generally eliminates uncertainty.

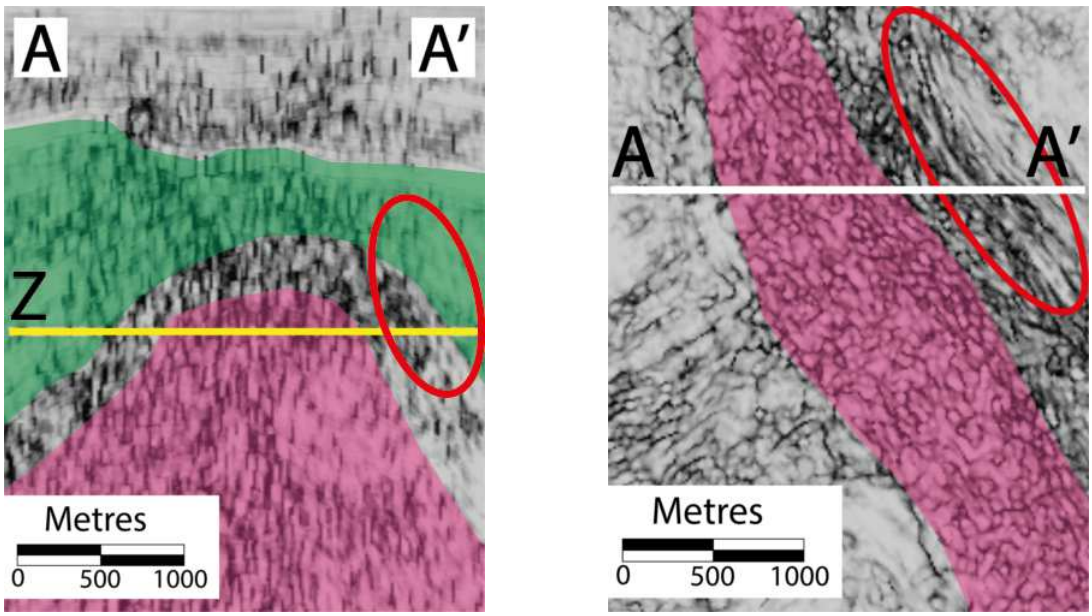

(a) (b)

Figure 6.16: *This image displays Inline 7173 and Z-Slice 1802 of Seismic Crop 3. Both images display poor distinction between salt and other lithologies. The red oval displays the steeply eastward dipping layers that OpendTect recognizes as being faults.*

7

Conclusion & Recommendations

7.1. Conclusion

Enhanced Fracture Characterization in OpendTect was done to gain new insights behind the trigger mechanisms behind fracturing in the Chalks of the Cretaceous Chalk Group in the Dutch subsurface. OpendTect's Fracture Enhancing Attributes and Filters were used to 'zoom' into two seismic datasets of two different areas of the Dutch offshore. Out of these two seismic datasets, five fundamentally different Seismic Crops were generated, to look at the different trigger mechanisms and origins of stress.

This research has shown that the deformation in the areas of this research is driven by two mechanisms on a regional scale. Regional extensional tectonics, and overprinting of older NW-SE faults in areas where salt is absent. And halokinesis in areas where salt is underlying the Chalk Group.

On a local level on the other hand things are less straightforward. Fluid expulsion is the driving force behind polygonal faulting, which is present almost everywhere in the North Sea Group. In the Chalk Group however this is not always the case. In areas far away from far field extensional tectonics and halokinesis structures, polygonal faulting is able to form in all formations. However when moving closer to salt-ridges or other halokinesis structures, these polygonal faulting patterns quickly transition into either fractures caused by the flexure of anticlinal structures cause by halokinesis, or due to structural collapse caused by underlying salts.

In areas where salt is absent structures might form influenced by regional extensional tectonics. These structures can take on both the form of extensional faults parallel to the surrounding major faults, or perpendicular to them.

Although research has shown that OpendTect's fault enhancing attributes, filters and its capability to Dip-Steer seismic data proves to be an important tool in enhanced fracture interpretation, it still shows that the software has its limits. First of all there is hardly any distinction between salts and fractured chalks. Secondly when interpreting faults on Z-Slices through steeply dipping layers, it is hard to distinct between fault or layer/lithology changes. However on layer cake models this problem is eliminated.

7.2. Recommendations

Further research on the subject of fracture characteristics on Chalks can be done by implementing the workflow used in this research on other areas with different tectonic regimes. The Chalks in the areas of this research show very wide results based on the extensional regime present. However Chalks in compressional regimes or near transform faults could deliver new insights in fracture patterns in Chalks.

When it comes to scaling, this research handles two scales: the Fault Network Scale and the Small Seismic Scale. The E&P industry for example often looks more to the reservoir scale, which usually falls below seismic resolution. For that reason a nice addition to this research would be to do outcrop studies of Chalks similar of for example the Hod and Tor Formations in England or Denmark. This could give insights in the fracture patterns present at those scales. Also the ability to then link that to the large scales such as in this research could give insights into the formation of fractures in Chalks on multiple scales.

Geomechanical Modelling is a tool to study the response of subsurface structures to different geological/geomechanical situations. Using Geomechanical Modelling tools could help better answer the question of why different fracture patterns occur in different places.

Bibliography

[1] R. Alai, A.A. Aqrawi, A.B. Mohamed, and M.T. A Taha. Fracture characterization in basement reservoirs through seismic attributes. *First Break*, 32:83–92, 2014.

[2] F. Brouwer and A. Huck. An integrated workflow to optimize discontinuity attributes for the imaging of faults. *Attributes: New Views on Seismic Imaging - Their Use in Exploration and Production*, pages 496–533, 2011.

[3] D. Carruthers, J.A. Cartwright, M.P.A. Jackson, and P. Schutjens. Origin and timing of layer-bound radial faulting around north sea salt stocks: New insights into the evolving stress state around rising diapirs. *Marine and Petroleum Geology*, 48:130–148, 2013.

[4] J.A. Cartwright. Diagenetically induced shear failure of fine-grained sediments and the development of polygonal fault systems. *Marine and Petroleum Geology*, 28:1593–1610, 2011.

[5] J.A. Cartwright and D.N. Dewhurst. Layer-bound compaction faults in fine-grained sediments. *Bulletin*, 110:1242–1257, 1996.

[6] J.A. Cartwright and L. Lonergan. Volumetric contraction during the compaction of mudrocks: A mechanism for the development of regional-scale polygonal fault systems. *Basin Research*, 8:183–193, 1996.

[7] J.A. Cartwright, D.M.D. James, and A. Bolton. The genesis of polygonal fault systems: A review. *Geological Society, London, Special Publications*, 216:223–243, 2003.

[8] T. Cox and K. Seitz. Ant-tracking seismic volumes for automated fault interpretation. *CSPG/CSPE GeoConvention*, 2007.

[9] P. de Groot, F. Aminzadeh, N. Hemstra, and G. de Bruin. Advanced seismic interpretation techniques in opendtect. *Drilling & Exploration World*, 17:42–46, 2008.

[10] J. de Jager. Inverted basins in the netherlands, similarities and differences. *Netherlands Journal of Geosciences*, 82:339–349, 2003.

[11] O.B. Duffy, R.E. Bell, C.A-L. Jackson, R.L. Gawthorpe, and P.S. Whipp. Fault growth and interactions in a multiphase rift fault network: Horda platform, norwegian north sea. *Journal of Structural Geology*, 80:99–119, 2015.

[12] N.R. Goulty. Geomechanics of polygonal fault systems: A review. *Petroleum Geoscience*, 14:389–397, 2008.

[13] C. Hibsch, J.A. Cartwright, D.M. Hansen, P. Gaviglio, G. André, M. Cushing, P. Bracq, P. Juignet, P. Benoit, and J. Allouc. Normal faulting in chalk: Tectonic stresses vs. compaction-related polygonal faulting. *Geological Society, London, Special Publications*, 216:291–308, 2003.

[14] R. Hill. Elastic properties of reinforced solids: some theoretical principles. *Journal of the Mechanics and Physics of Solids*, 11:357–372, 1963.

[15] H. Jaglan, F. Qayyum, and H. Huck. Unconventional seismic attributes for fracture characterization. *First Break*, 33:101–109, 2015.

[16] L. Lonergan, J.A. Cartwright, and R. Jolly. The geometry of polygonal fault systems in tertiary mudrocks of the north sea. *Journal of Structural Geology*, 20:529–548, 1998a.

[17] L. Lonergan, J.A. Cartwright, R. Laver, and J. Staffurth. Polygonal faulting in the tertiary of the central north sea: Implications for reservoir geology. *Geological Society, London, Special Publications*, 127:191–207, 1998b.

[18] R.N. Mortimore, C.J. Wood, and R.W. Gallois. British upper cretaceous stratigraphy. *Geological Conservation Review Series*, 23:558, 2001.

[19] NAM. *Stratigraphic Nomenclature of the Netherlands*. Geological Survey of the Netherlands, 1980.

[20] R. Oppermann. Finding sweet spots through seismic fracture extraction - unconventional case studies from around the world. *Society of Petroleum Engineers*, 2012a.

[21] R. Oppermann. New method for seismic identification of fluid conduits or barriers challenges several industry paradigms. *AAPG/SPE/SEG Hedberg Research Conference*, 2012b.

[22] P. Pharaoh, R. England, and M. Lee. The concealed caledonide basement of eastern england and the southern north sea - a review. *Studia Geophysica et Geodaetica*, 39: 330–346, 1995.

[23] F. Qayyum, S. Yousaf, D. Malik, R. Zaheer, and M.H. Manzoor. Superimposed geologic features in seismic interpretation. *PAPG/SPE Annual Technical Conference*, 2010.

[24] S.R. Tubb, A. Soulsby, and S.R. Lawrence. Palaeozoic prospects on the northern flanks of the london-brabant massif. *Geological Society, London, Special Publications*, 23:55–72, 1986.

[25] H.A. van Adrichem Boogaert. *Stratigraphic Nomenclature of the Netherlands: Revision and Update by RGD and NOGEPA*. Geological Survey of the Netherlands, 1993.

[26] H.A. van Adrichem Boogaert and W.F. Kouwe. *Stratigraphic Nomenclature of the Netherlands, Revision and Update by RGD and NOGEPA*. Geological Survey of the Netherlands, 1997.

[27] A.S. van der Molen and Th.E. Wong. Towards an improved lithostratigraphic subdivision of the chalk group in the netherlands north sea area – a seismic stratigraphic approach. *Geologie en Mijnbouw*, 86:131–143, 2007.

[28] H. van Gent, S. Back, J.L. Urai, and P. Kukla. Small-scale faulting in the upper cretaceous of the groningen block (the netherlands): 3d seismic interpretation, fault plane analysis and regional paleostress. *Journal of Structural Geology*, 32:537–553, 2010.

[29] J.D. van Wees, R.A. Stephenson, P.A. Ziegler, U. Bayer, T. McCann, R. Dadlez, R. Gaupp, M. Narkiewicz, F. Bitzer, and M. Scheck. On the origin of the southern permian basin, central europe. *Marine and Petroleum Geology*, 17:43–59, 2000.

[30] N. Vandenberghe. The subsurface geology of the meer area in north belgium, and its significance for the occurrence of hydrocarbons. *Journal of Petroleum Geology*, 7:55–66, 1984.

[31] M.J. Welch, C. Souque, R.K. Davies, and R.J. Knipe. Using mechanical models to investigate the controls on fracture geometry and distribution in chalk. *Geological Society, London, Special Publications*, 406:281–309, 2015.

[32] Th.E. Wong, D.A.J. Batjes, and J. de Jager. *Geology of the Netherlands*. Royal Netherlands Academy of Arts and Sciences, 2007.

[33] B. Zhang, Y. Liu, M. Pelissier, and N. Hemstra. Semiautomated fault interpretation based on seismic attributes. *Interpretation*, 2:11–19, 2014.

[34] P.A. Ziegler. *Evolution of the Arctic-North Atlantic and the Western Tethys*. American Association of Petroleum Geologists, 1988.

[35] P.A. Ziegler. *Geological Atlas of Western and Central Europe*. Geological Society of London, 1990.

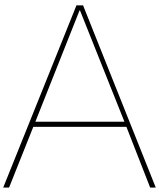

Well Data

A.1. TEPNL 2012 Data

Well Nr.	X	Y	Well Datum	Well Datum to SS [m]	TVD [m]	MD [m]	Logs				Check-shot Data
							GR	DT	RHOB	NPHI	
J03-02	499270	5970153	RT	39.6	3973.6	3975.0	x	x	x		x
J06-A-01	496394	5964072	RT	41.0	3635.8	3769.0	x	x	x		x
K01-01	515815	5973267	RT	30.0	1849.7	1850.0	x	x	x		x
K01-02	513888	5973416	RT	30.1	4580.9	4586.1	x	x	x	x	x
K03-02	549363	5965944	RT	39.0	4442.9	4444.9	x	x	x	x	x
K04-01	504569	5953630	KB	32.3	3065.1	3069.5	x	x		x	
K04-03	506743	5952035	RT	41.1	3978.3	3980.0	x	x	x	x	x
K04-04	505751	5953093	RT	33.0	3699.6	3710.0	x	x	x	x	x
K04-D-01	502541	5960505	RT	38.6	3739.7	3750.0	x	x	x	x	x
K05-01	533414	5957669	KB	27.5	3872.1	3872.5	x	x	x	x	x
K05-02	527110	5961405	RT	31.8	4118.9	4122.0	x	x	x	x	x
K05-11	540784	5955091	KB	40.5	4129.4	4140.0	x	x	x	x	x
K05-B-02	532572	5963563	RT	44.0	3775.3	4080.0	x	x	x	x	x

Continued:

Well Nr.	X	Y	Well Datum	Well Datum to SS [m]	TVD [m]	MD [m]	Logs				Check-shot Data
							GR	DT	RHOB	NPHI	
K05-D-01	532266	5949455	RT	36.0	4278.8	4280.0	x	x	x	x	x
K05-ENC-01	533818	5951672	RT	35.0	3932.4	3955.0	x	x	x	x	x
K06-01	564853	5963608	RT	31.7	3717.2	3718.5	x	x	x	x	x
K06-02	565951	5948463	RT	25.5	3491.5	3500.0	x	x	x	x	x
K06-06	559654	5960563	RT	35.8	4131.5	4135.0	x	x	x	x	x
K06-07	553168	5953514	RT	36.0	4019.4	4426.0	x	x	x	x	x
K06-08	557383	5957418	RT	36.0	4038.7	4040.0	x	x	x	x	x
K06-C-01	557453	5950531	RT	33.5	3958.0	3960.0	x	x	x	x	x
K06-D-01	554804	5947891	RT	31.0	4051.7	4060.0	x	x	x	x	x
K06-GT-01	560419	5956617	RT	39.0	4195.2	4300.0	x	x	x	x	x
K06-N-01	549467	5950471	KB	39.0	4193.9	4200.0	x	x	x	x	x
K09-02	565679	5946277	RT	31.0	3640.3	3642.0	x	x	x	x	x
K09-07	545922	5944939	RT	39.6	4145.6	4148.3	x	x	x	x	x
L01-02	580244	5973208	RT	34.9	3067.5	3070.0	x	x	x	x	x
L01-06	572549	5974559	RT	39.0	4441.5	4459.0	x	x	x	x	x
L04-01	570877	5956460	RT	28.4	3987.2	3991.0	x	x	x	x	x
L04-03	567473	5953668	RT	35.1	3822.0	3830.0	x	x	x	x	x
L04-04	575390	5958169	RT	35.5	3961.5	3975.0	x	x	x	x	x
L04-05	583844	5960545	RT	39.7	4148.0	4155.0	x	x	x	x	x
L04-06	573062	5965151	RT	36.0	4320.5	4335.0	x	x	x	x	x

Continued:

Well Nr.	X	Y	Well Datum	Well Datum to SS [m]	TVD [m]	MD [m]	Logs				Check-shot Data
							GR	DT	RHOB	NPHI	
L04-07	570132	5961694	RT	36.0	4087.4	4124.0	x	x	x	x	x
L07-01	571092	5940328	RT	26.0	3932.4	3934.0	x	x	x	x	x
L07-04	579785	5942882	RT	30.5	4183.5	4186.0	x	x	x	x	x
L07-05	572355	5932054	RT	31.4	3875.9	3886.0	x	x	x	x	x
L07-06	587298	5930269	RT	28.6	4143.7	4150.0	x	x	x	x	x
L08-07	589791	5945953	KB	36.0	4592.4	4593.0	x	x	x	x	x
L10-01	578922	5927393	RT	31.6	4120.6	4122.0	x	x	x	x	x
L10-17	583780	5927176	RT	31.4	3891.5	3978.0	x	x	x	x	x
L10-29	570341	5928044	RT	34.0	4186.4	4187.0	x	x	x	x	x
L10-K-01A	584286	5928104	RT	38.1	3903.2	3909.1	x	x	x	x	x

A.2. P10 Data

Well Nr.	X	Y	Well Datum	Well Datum to SS [m]	TVD [m]	MD [m]	Logs				Check-shot Data
							GR	DT	RHOB	NPHI	
P10-01	510112	5812715	RT	31.7	2692.7	2696.0	x	x	x		x
P10-02	507273	5803642	RT	30.5	1834.7	1834.9	x	x	x	x	x
P10-03	518235	5803739	RT	41.0	1803.9	1804.0	x	x	x	x	x
P10-04	512634	5812139	RT	40.0	1728.5	1832.0	x	x	x	x	x
P10-05	520622	5804180	RT	40.0	1638.4	2520.0	x	x	x	x	x
P11-03	523469	5802826	RT	36.6	1905.7	1974.0	x	x	x	x	x
P11-04	522933	5802269	RT	36.9	1721.0	1760.0	x	x	x	x	
P11-05	524395	5809137	RT	40.0	2088.2	2093.0	x	x	x	x	x